The Handbook
of Dielectric Analysis and
Cure Monitoring

Huan L. Lee

tech·nol·o·gy

noun \tek-   nä-lə-jē\

1) The use of science in industry, engineering, etc., to invent useful things or to solve problems.

2) A machine, piece of equipment, method, etc., that is created by technology.

plural tech·nol·o·gies

About Lambient Technologies

Lambient Technologies LLC develops instruments, sensors and software for monitoring the properties of curing polymers. Lambient Technologies was founded by members of the team that developed products for Micromet Instruments, which commercialized dielectric cure monitoring technology developed at the Massachusetts Institute of Technology.

Address   :   Lambient Technologies LLC
               649 Massachusetts Avenue
               Cambridge, MA 02139

Telephone: 857-242-3963
E-mail   :   info@lambient.com

URL   :   www.lambient.com

Acknowledgements

Table of Contents

Terms and Definitions

$e = 2.71828$	Base of natural logarithm
$i = \sqrt{-1}$	Square root of -1
$\pi = 3.14159$	Pi
$\varepsilon_0 = 8.854 \times 10^{-14}$ F/cm	Permittivity of free space
$k = 8.61733 \times 10^{-5}$ eV/K	Boltzmann's constant
$q = 1.602 \times 10^{-19}$ C	Magnitude of electronic charge
f	Frequency (cycles/s or Hz)
$\omega = 2\pi f$	Angular frequency (radians/s)
q	Charge (coulomb)
t	Time (s)
σ	Conductivity (ohm^{-1} – cm^{-1})
$\rho = 1/\sigma$	Resistivity, or ion viscosity (ohm-cm)
ε	Permittivity (F/cm)
$\varepsilon^* = \varepsilon_0\,(\varepsilon' - i\varepsilon'')$	Permittivity as a complex quantity (F/cm)
$\kappa = \varepsilon' - i\varepsilon''$	Relative permittivity* or dielectric constant (unitless)
$\varepsilon' = Re(\varepsilon^*/\varepsilon_0)$	Relative permittivity* or dielectric constant (unitless)
$\varepsilon'' = Im(\varepsilon^*/\varepsilon_0) = \sigma/\omega\varepsilon_0$	Loss factor or loss index (unitless)
$D = \tan\delta = \varepsilon''/\varepsilon'$	Dissipation factor or loss tangent (unitless)
$\delta = \tan^{-1}(\varepsilon''/\varepsilon')$	Delta (unitless)
$\delta \sim \varepsilon''/\varepsilon'$	Delta for small $\varepsilon''/\varepsilon'$ (unitless)
A/D	Ratio of electrode area to distance between parallel plate electrodes (cm)
V	Voltage (volt)
$I = q/t$	Current (amp)
$C = q/V$	Capacitance (farad)
$G = V/I$	Conductance (ohm^{-1})
$R = 1/G$	Resistance (ohm)
$C = \varepsilon_0\,\varepsilon' A/D$	Capacitance (farad)
$G = \sigma A/D$	Conductance (siemen or ohm^{-1})
$R = \rho/(A/D)$	Resistance (ohm)
$Y = G + i\omega C$	Admittance (siemen or ohm^{-1})
$Z = 1/Y = 1/(G + i\omega C)$	Impedence (ohm)

* There is inconsistency in use of the term *relative permittivity*. In some literature it is the complex quantity $\varepsilon/\varepsilon_0 = (\varepsilon' - i\varepsilon'')/\varepsilon_0$ and in others it is the real part of permittivity $Re(\varepsilon/\varepsilon_0) = \varepsilon'$.

α	Degree of cure (unitless, between 0 and 1)
α_{max}	Maximum degree of cure at cure temperature
M_w	Molecular weight (gm/mole)
M_{w0}	Molecular weight at $\alpha = 0$ (uncured)
$M_{w\infty}$	Molecular weight at $\alpha = 1$ (fully cured)
T_{Cure}	Cure or process temperature (K or °C)
T_g	Glass transition temperature (K or °C)

$\mathcal{E}'$ (free space)	$= 1.0$	Relative permittivity of free space
$\mathcal{E}'$ (air)	$= 1.0$	Relative permittivity of air
$\mathcal{E}'$ (teflon)	~ 2.2	Relative permittivity of teflon
$\mathcal{E}'$ (mineral oil)	~ 2.2	Relative permittivity of mineral oil
$\mathcal{E}'$ (polimide)	~ 3.6	Relative permittivity of polyimide
$\mathcal{E}'$ (aluminia)	~ 9.8	Relative permittivity of alumina

DiBenedetto T_g model:

$$\frac{(T_g - T_{g0})}{(T_{g\infty} - T_{g0})} = \frac{\lambda\,\alpha}{(1 - (1 - \lambda)\,\alpha)}$$

Where:
T_g = Glass transition temperature (K or °C)
T_{g0} = Glass transition temperature at $\alpha = 0$ (uncured)
T_{gmax} = Maximum glass transition at T_{Cure}
$T_{g\infty}$ = Glass transition temperature at $\alpha = 1$ (fully cured)
λ = Adjustable parameter

Debye relaxation for relative permittivity and loss factor:

$$\mathcal{E}' = \mathcal{E}'_u + \frac{\mathcal{E}'_r - \mathcal{E}'_u}{1 + (\omega\tau)^2}$$

$$\mathcal{E}'' = \sigma/\omega\varepsilon_0 + (\mathcal{E}'_r - \mathcal{E}'_u)\,\frac{\omega\tau}{1 + (\omega\tau)^2}$$

Where:
$\mathcal{E}'_u$ = Unrelaxed (high frequency) relative permittivity
$\mathcal{E}'_r$ = Relaxed (low frequency) relative permittivity
ω = $2\pi f$ (radians/s)
τ = Dipole relaxation time (s)

Havriliak-Negami relaxation for relative permittivity and loss factor:

$$\varepsilon' = \varepsilon'_u + (\varepsilon'_r - \varepsilon'_u)\,(1 + 2(\omega\tau)^{\alpha}\cos(\pi\alpha/2) + (\omega\tau)^{2\alpha})^{-\beta/2}\cos(\beta\theta)$$

$$\varepsilon'' = (\varepsilon'_r - \varepsilon'_u)\,(1 + 2(\omega\tau)^{\alpha}\cos(\pi\alpha/2) + (\omega\tau)^{2\alpha})^{-\beta/2}\sin(\beta\theta)$$

Where: $\theta = \tan^{-1}[(\omega\tau)^{\alpha}\sin(\pi\alpha/2)\,/\,(1 + (\omega\tau)^{\alpha}\cos(\pi\alpha/2))]$
                α = Empirical "broadness" parameter
                β = Empirical "asymmetry" parameter
                ε'_u = Unrelaxed (high frequency) relative permittivity
                ε'_r = Relaxed (low frequency) relative permittivity
                ω = $2\pi f$ (radians/s)
                τ = Dipole relaxation time (s)

Apparent relative permittivity and loss factor due to electrode polarization:

$$\varepsilon'_x = \varepsilon'\,(D/2t_b)\,\frac{(\varepsilon''/\varepsilon')^2 + (D/2t_b)}{(\varepsilon''/\varepsilon')^2 + (D/2t_b)^2}\qquad\text{Apparent relative permittivity}$$

$$\varepsilon''_x = \varepsilon''\,(D/2t_b)\,\frac{(D/2t_b) - 1}{(\varepsilon''/\varepsilon')^2 + (D/2t_b)^2}\qquad\text{Apparent loss factor}$$

Where: t_b = boundary layer thickness
                D = distance between electrodes or plate separation
                ε'_x = uncorrected permittivity
                ε''_x = uncorrected loss factor
                ε' = actual permittivity
                ε'' = actual loss factor

Introduction

Thermoset and composite materials, with their formability, high strength and low weight, have revolutionized the design of structures such as automobile bodies, aerospace components and wind turbine blades. While irreplaceable for these high performance applications, thermosets also find use in a range of industries: adhesive, sheet molding compound (SMC), bulk molding compound (BMC), glass and carbon fiber prepreg, automotive, aerospace, electronics, consumer goods and many others.

Manufacturers, however, are often hindered by limited understanding of how these materials cure and harden. As a result the integrity of the end product often can't be determined until after the process has ended—too late to make necessary improvements. For mission-critical applications such as the heat shield of a spacecraft or the wing of an airplane, failure is not an option.

Many researchers are studying the chemistry of cure as well as improving manufacturing methods. Laboratory tests, including differential scanning calorimetry (DSC), dynamic mechanical analysis (DMA) and dielectric analysis (DEA) yield valuable information. Only DEA provides critical insights into thermoset processing in real time and across the fields of research and development; quality control/quality assurance; and manufacturing.

The intent of this handbook is to provide the background for making dielectric measurements as well as practical information for using and understanding dielectric cure monitoring. We present data from actual cures and discuss how to interpret them, with the goal of assisting all who use these advanced materials.

The following chapters cover dielectric measurements and cure monitoring. While the development of these subjects proceeds from basic concepts to practical results then theory, each chapter is relatively self-contained and users can read them alone or in any order. Those interested in carbon fiber reinforced prepreg or sheet molding compound, in particular, may wish to start with those topics, to see results of actual tests and gain an immediate understanding of dielectric cure monitoring of those materials.

Chapter 1—Frequently Asked Questions

Q1. What is Dielectric Analysis (also known as DEA) or dielectric cure monitoring?

- Dielectric Analysis (DEA) or dielectric cure monitoring is a thermal analysis technique for determining cure state.
    - DEA tracks the cure state of a material by measuring the electrical properties of permittivity and resistivity.
    - Permittivity (ε) is related to energy storage in a material.
    - Resistivity (ρ) is related to energy loss in a material.
    - Frequency independent resistivity, or DC resistivity, (ρ_{DC}) is also called ion viscosity.
    - Ion viscosity is proportional to mechanical viscosity for significant portions of cure. See Figure 1-1.
    - Ion viscosity tracks cure state throughout cure, even after ion viscosity deviates from mechanical viscosity.

Q2. What are the benefits of dielectric cure monitoring?

- Dielectric cure monitoring provides insight into cure state.
    - DEA can determine the effects of chemistry and formulation,
    - DEA can determine the effects of time, temperature and other process parameters.
- Dielectric cure monitoring saves time, effort and expense.
    - Electrical measurements are simple.
        - Instruments and software are easy to set up and use.
    - Sample preparation is simple.
        - Sensors are rugged and can be used in presses, molds or ovens.
        - Samples can be applied to sensors in any form.
    - Materials can be tested with production process configurations.
    - Materials can be tested under production process conditions.
- The same measurement can be used in R&D, QA/QC and manufacturing.
    - Data from Research and Development are the same as data from Quality Assurance/Quality Control and manufacturing.

Q3. What materials can dielectric cure monitoring study?

- Thermosets
- Epoxies
- Acrylics
- Silicones
- Polyesters/polyurethanes/polystyrenes/polyimides/polyamides
- Composites and laminates
- Bulk Molding Compounds (BMC)/Sheet Molding Compounds (SMC)
- Paints, coatings and adhesives
- Oils
- Pharmaceuticals

Q4. What applications can use dielectric cure monitoring?

- Formulation, reaction rate, cure and process development/monitoring
- Water and solvent diffusion
- UV curing
    - Dental and optical adhesives
    - Photoresist
- Nondestructive materials testing
- Rheology
- Research & Development
- Quality Assurance/Quality Control
- Manufacturing

Q5. What processing environments can use dielectric cure monitoring?

- Ovens
- Presses and molds
- Autoclaves
- Pultruders and extruders
- Batch reaction vessels
- Injection molding

Q6. What types of companies use dielectric cure monitoring?

- Raw resin/materials manufacturers
    - Suppliers of monomers, resins and catalysts
    - Suppliers of adhesives, paints and coatings
- Suppliers of pre-impregnated (pre-preg) composites
    - Bulk Molding Compound (BMC)/Sheet Molding Compound (SMC)
    - Epoxy-fiber/Polyester-fiber/Polystyrene-fiber thread, sheet or laminates
- Manufacturers of composite end products
    - Aircraft
    - Automobile
    - Electronic components
    - Consumer products
- Government agencies with R&D—Army, Navy, NASA, etc.

Q7. What are thermosets?

- Thermosets are materials that solidify ("cure") with an irreversible reaction.
    - Monomers link into a network and form a polymer.
    - Catalysts often facilitate the curing reaction.
    - The reaction rate increases as temperature increases.
    - Thermosets cannot melt and be reformed.
    - Ion viscosity is a measure of the state of cure and network formation.
    - **Dielectric cure monitoring provides information about thermoset viscosity, rigidity and cure state.**

Q8. What are thermoplastics?

- Thermoplastics are materials that melt and can be reformed multiple times.
    - Thermoplastics do not cure and ion viscosity is usually a function of temperature.
    - **Dielectric cure monitoring provides information about thermoplastic viscosity and rigidity.**

Q9. What does dielectric cure monitoring data look like?

- As shown in Figure 1-1, four Critical Points characterize the dielectric cure curve:

    o CP(1)—A user defined level of ion viscosity, which can identify the onset of material flow at the beginning of cure.

    o CP(2)—Ion viscosity minimum, which typically also corresponds to the mechanical viscosity minimum. This Critical Point indicates the time the accelerating crosslinking reaction dominates the behavior of the system.

    o CP(3)—Inflection point, which identifies when the crosslinking reaction begins to slow. CP(3) is often used as a signpost that can be associated with gelation.

    o CP(4)—A user defined slope that can define the end of cure. The decreasing slope corresponds to the decreasing reaction rate. Note that dielectric cure monitoring continues to reveal changes in the evolving material past the point when mechanical measurement of viscosity is not possible.
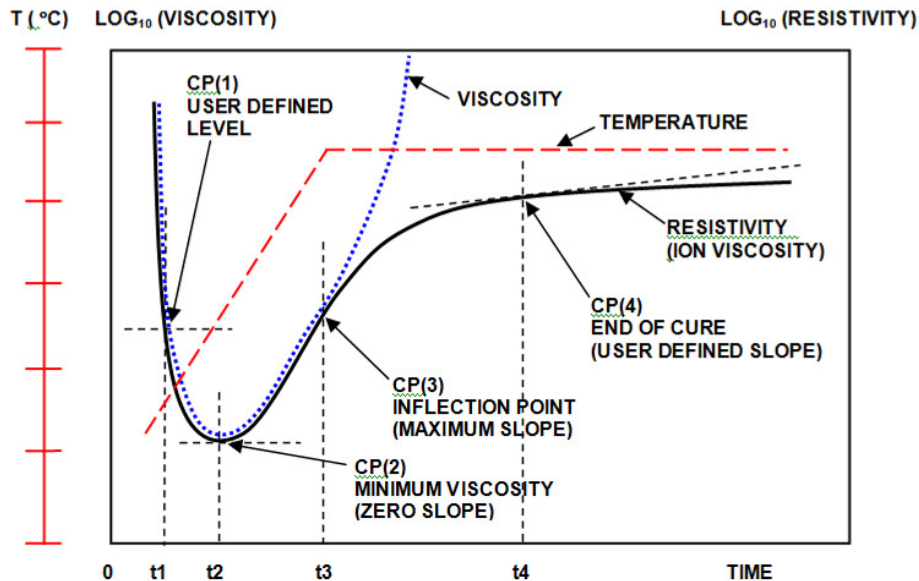

Figure 1-1
Comparison of ion viscosity (DC resistivity) and mechanical viscosity during cure

Q10. How does the user prepare samples for dielectric cure monitoring?

Dielectric cure monitoring requires only a small sample, weighing no more than a few grams in most cases, and a simple setup. The user places the sample on a sensor, applies heat and/or pressure then starts the data acquisition software.

Q11. How does sample preparation for dielectric cure monitoring compare to other types of cure tests?

It is very common for manufacturers to test cure times by having a technician measure a known quantity of raw resin and then stir it on a hot plate. The technician then starts a stopwatch and notes the time when the material stiffens enough to draw a string. This method is very subjective and suffers from considerable variation with different technicians.

With semi-solid materials, such SMC or BMC, such stir tests are not possible. An alternative, such as a spiral flow test, forces uncured material through a heated spiral channel. As the material flows, it cures, becomes more viscous and eventually stops. Someone then measures the length at which the material has stopped flowing. At best this method crudely indicates the time to cure, but requires considerable apparatus, is labor intensive and—like the stir test—gives no information at all about the reaction during entire cure process.

Q12. How do end-users use dielectric cure monitoring to manage quality control during manufacturing of thermoset materials?

Because sample preparation for dielectric cure monitoring is simple, the cost of testing decreases, allowing companies to be more vigilant about product quality. Some sheet molding compound (SMC) or bulk molding compound (BMC) manufacturers test their materials very frequently—sometimes daily—to confirm and document curing behavior. When their fresh product is processed at 150 °C, for example, they want to know that the cure time is what they expect, or else they want to see problems immediately.

Q13. How does dielectric cure monitoring assist in the quality assurance of products?

Consistent quality of a thermoset product results in a consistent cure profile. Aged material, deviant processing conditions or different formulations can change the cure curve, so monitoring Critical Points is a way to quickly and easily identify problems.

Q14. How is dielectric cure monitoring used in manufacturing and for what applications?

In the development of raw resins and thermosets, dielectric cure monitoring allows a researcher to see how the material cures, how fast it cures in response to different formulations, how the reaction responds to the additions of catalysts or additives, and how the reaction rate changes at different temperatures.

For the manufacturers of SMC/BMC and prepregs, dielectric cure monitoring is largely used to check consistency of the product, as assurance to *their* customers that these products will cure as expected.

In aerospace applications, different sections of single, large composite parts can cure at different rates because of varying thicknesses and thermal conditions. Several current aerospace projects around the world use dielectric cure monitoring to control the manufacture of large components. Dielectric cure monitoring provides information for adjusting the process temperature, therefore ensuring that a large part cures uniformly.

Q15. What future applications can use dielectric cure monitoring

The growing field of commercial space ventures has many opportunities for dielectric cure monitoring. Spacecraft components such as fuselages and heat shields use composites because of their unique combination of high strength and low weight. Even more than for aircraft, the safety requirements for spacecraft are paramount and dielectric cure monitoring can document that a life and mission critical component was manufactured to specification.

Other growing applications:

- o   Wind turbines
- o   Construction materials

Q16. How does dielectric cure monitoring work?

Dielectric cure monitoring works by measuring the conductivity of a curing material. Under the influence of the electric field of across a dielectric sensor, ions flow through the resin under test. As the material cures, more and more of the molecules within it bond to each other, growing a crosslinked network that increases mechanical viscosity and at the same time restricts the flow of these ions, which in turn decreases conductivity, or conversely increases resistivity (the inverse of conductivity).

It is more common to consider the frequency independent (DC) resistivity when discussing cure monitoring. During the early part of cure, DC resistivity tracks viscosity. This correspondence has given rise to the term *ion viscosity*, which is simply another name for DC resistivity.

Even after the resin has become rigid and viscosity is infinite, DC resistivity and ion viscosity continue to increase and dielectric measurements can still observe the advancing cure.

Q17. How does dielectric cure monitoring measure material properties?

The dielectric properties of conductivity (σ), and permittivity (ε), arise from ionic current and dipole rotation in the material. For polymers, mobile ions are typically due to impurities and additives, while dipoles result from the separation of charge in the monomers making up the material. When analyzing dielectric properties, it is possible to separate the influence of ions from dipoles, as shown in Figure 1-2, to consider their individual effects.
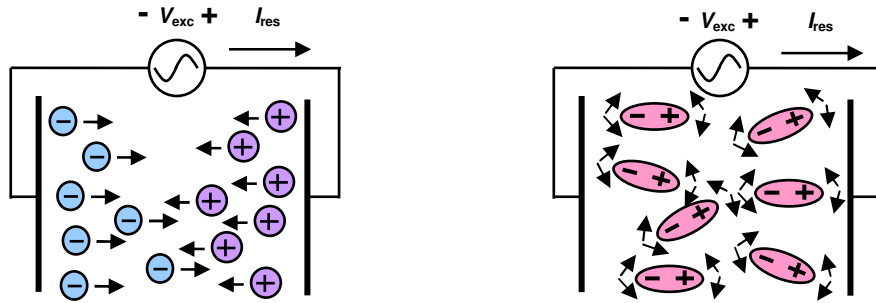
Figure 1-2
Mobile ions and dipole rotation in a material

The flow of ions under the influence of an electric field is responsible for conductive current, and therefore for conductivity (σ) and its inverse, resistivity (ρ). Consequently, the effect of mobile ions can be modeled as a conductance, as shown in Figure 1-3. This conductance may be frequency dependent, and changes as the bulk material changes. The mobility of ions highly depends on the nature of the medium—ions flow more easily through a material with low viscosity and with greater difficulty as the viscosity increases.

Ion current   Dipole rotation
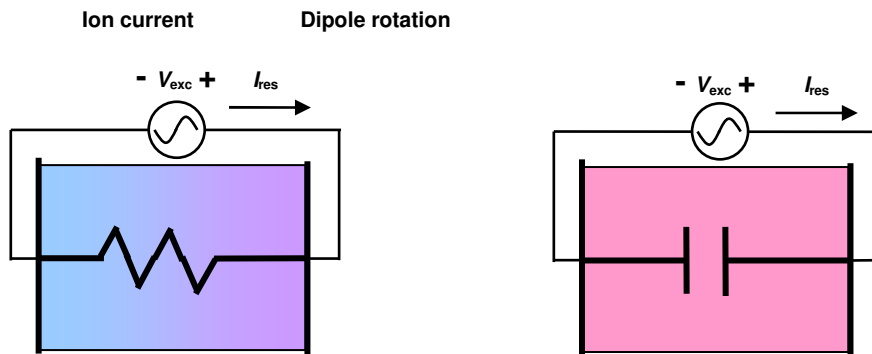
Figure 1-3
Electrical circuit equivalent to mobile ions and dipole rot ation

For dielectric cure monitoring, it is convenient to observe the ***ion viscosity***, which is simply the frequency independent, or DC, resistivity (ρ)—i.e the inverse of the frequency independent conductivity. As the physical viscosity of a curing polymer increases, the ion viscosity presented to ion current also increases. This relationship is the principle behind the usefulness of dielectric cure monitoring, and makes possible the observation of cure state.

Q18. How are parallel plate sensors different from interdigitated sensors?

Researchers studying dielectric properties often use parallel plate electrodes, for which plate separation sometimes cannot be accurately controlled. The distance between the plates may change upon the application of pressure, or as the material between them expands or contracts. For such situations tan δ is used to characterize dielectric properties because $\varepsilon'/\varepsilon'$ does not vary with plate spacing. However, tan δ alone cannot provide information about either permittivity or loss factor, and therefore has limited

usefulness—especially because permittivity and loss factor are themselves complicated functions of several factors.

Interdigitated electrodes on a substrate can be used instead of parallel plate electrodes, as shown in Figure 1-4. The planar structure of interdigitated electrodes has a geometry that does not change with pressure or expansion or contraction of the material under test, and therefore can accurately measure both permittivity and loss factor.
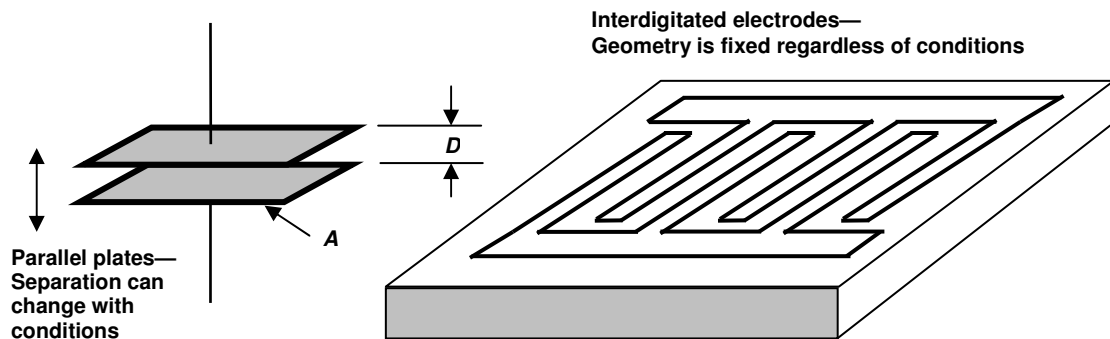

Figure 1-4
Parallel plate and interdigitated electrode geometries

Chapter 2—Basics of Thermoset Cure and Dielectric Measurements

The thermoset cure process

Thermosets are an important class of materials used for adhesives, coatings and composites. They include epoxies, (poly)urethanes, acrylics, phenolics, vinyl esters, silicones and many other compounds. Uncured thermosets, or *A-stage* materials, are composed of small molecules called monomers, as shown in Figure 2-1.
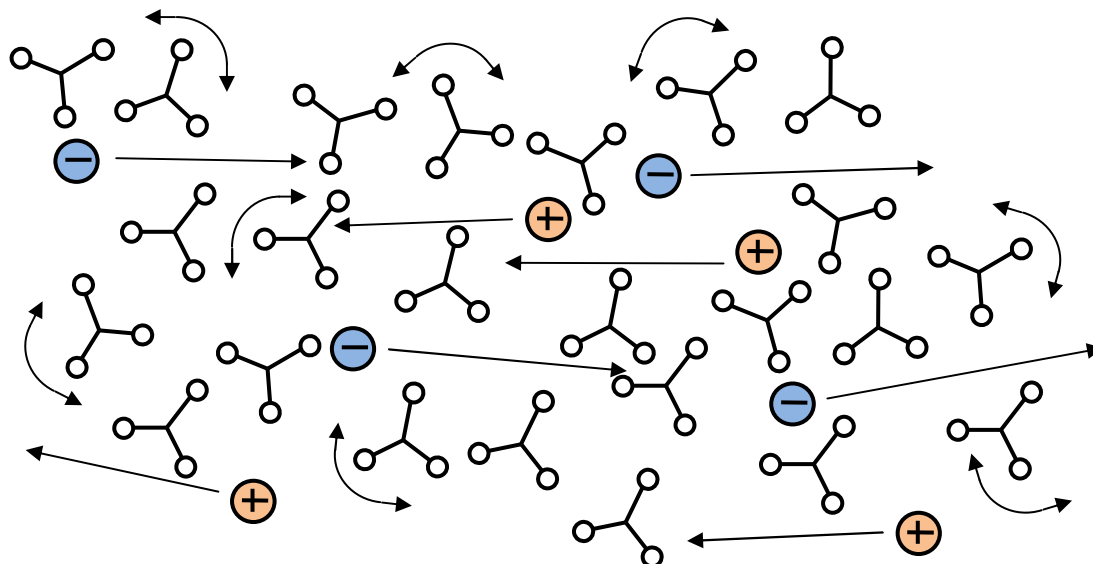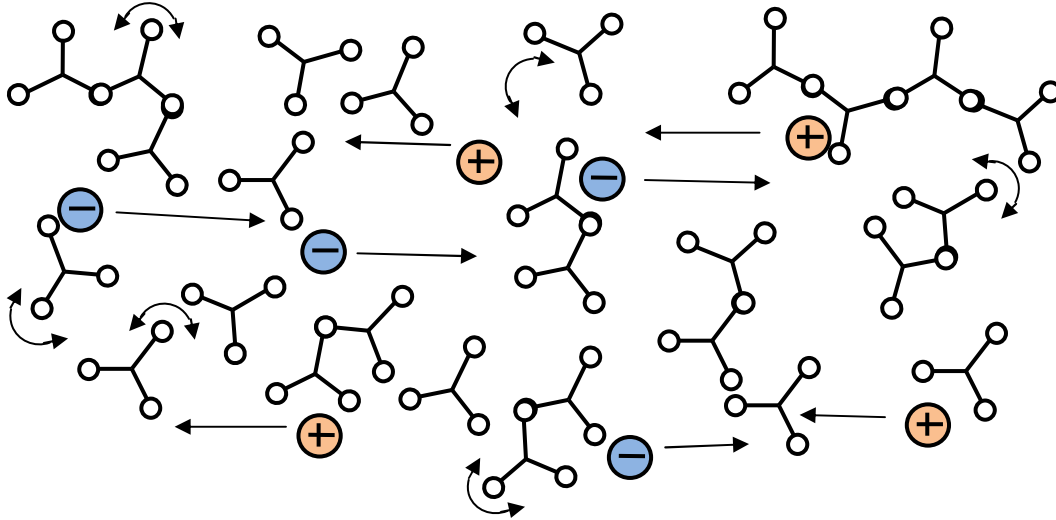
Characteristics of A-Stage thermoset:

- Chemical
  - Monomers unreacted
  - Molecular weight low
  - Degree of cure $\alpha = 0$
  - No network formation
- Physical
  - Fluidity measured by viscosity
  - Viscosity at minimum
  - Glass transition temperature T_g low
  - Mean free path long
  - Diffusion coefficient large
  - Free ion mobility high
  - Dipole rotation large
- Electrical
  - Conductivity at maximum (resistivity at minimum)
  - Dielectric constant at maximum

Figure 2-1
A-Stage thermoset (uncured)

   With the application of a catalyst, hardener, or energy such as heat or light, these monomers react and bond to one another to form longer and longer chains called polymers. Once curing begins, but while still fluid, the thermoset is a *B-Stage* material, represented in Figure 2-2. During this period the number of molecules decreases while their molecular weight increases. The thermoset's viscosity also increases, as does its resistance to the flow of mobile ions in an electric field. Dipoles in the polymer can rotate in response to an oscillating electric field, and this ability to rotate also decreases as cure advances.

Characteristics of B-Stage thermoset:

- Chemical
  - Monomers reacting and molecular chains lengthening
  - Molecular weight increasing
  - Degree of cure α increasing
  - Little network formation
- Physical
  - Fluidity measured by viscosity
  - Viscosity increasing
  - Glass transition temperature T_g increasing
  - Mean free path shortening
  - Diffusion coefficient decreasing
  - Free ion mobility decreasing
  - Dipole rotation decreasing
- Electrical
  - Conductivity decreasing (resistivity increasing)
  - Dielectric constant decreasing

Figure 2-2
B-Stage thermoset (partial curing, before gel point)

Through the process of crosslinking, which is the formation of bonds that link one polymer chain to another, an extended branching network appears as shown in Figure 2-3. Crosslinks limit the movement of polymer chains and the thermoset's viscosity increases rapidly.
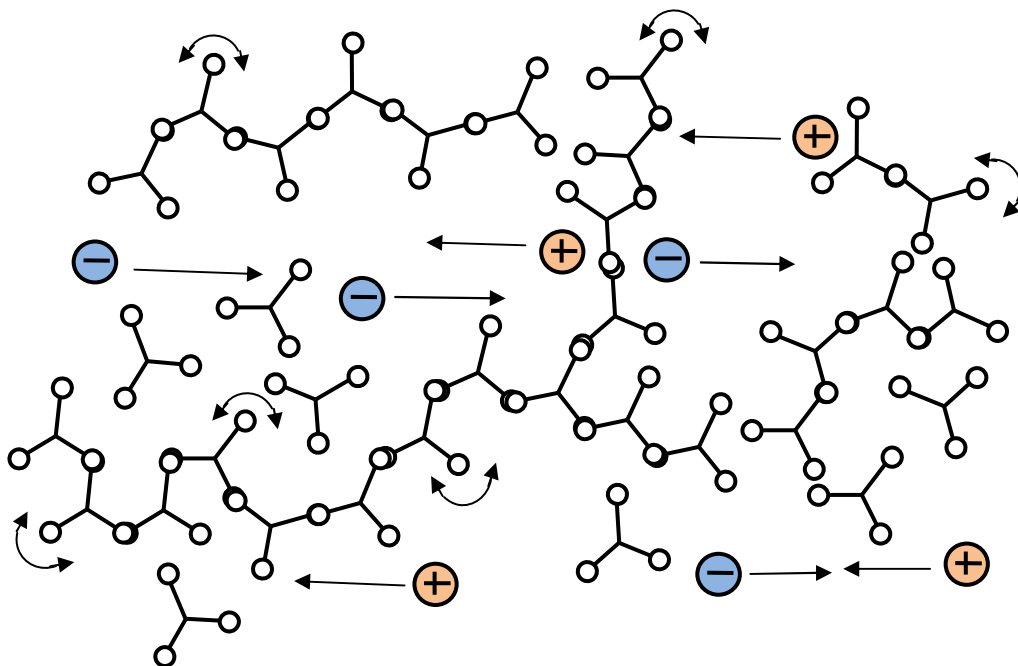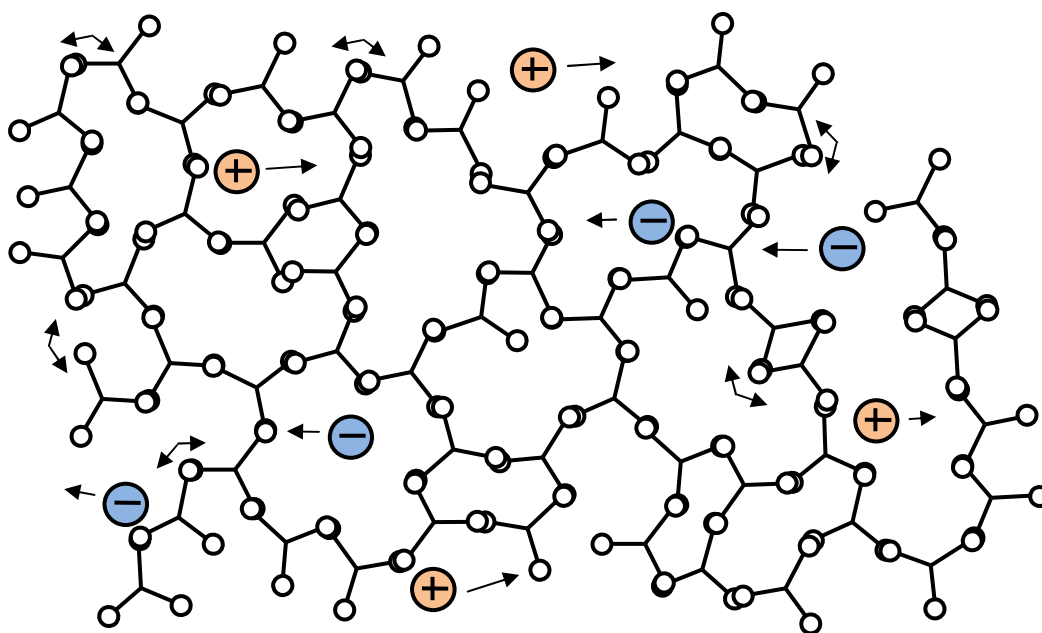

Characteristics of thermoset at gel point:

- Chemical
  - Monomers reacting, molecular chains lengthening and branching
  - Molecular weight increasing
  - Degree of cure α increasing
  - Beginning of infinite network formation
- Physical
  - Viscosity increasing rapidly to infinity
  - Rigidity measured by modulus
  - Modulus at minimum
  - Glass temperature T_g increasing
  - Mean free path shortening
  - Diffusion coefficient decreasing
  - Free ion mobility decreasing
  - Dipole rotation decreasing
- Electrical
  - Conductivity decreasing (resistivity increasing)
  - Dielectric constant decreasing
  - No sudden change in dielectric properties

Figure 2-3
Gel point (start of infinite network)

At some point the network essentially becomes a single molecule of infinite molecular weight, and the moment of its appearance is called *gelation* or the *gel* point—the material changes from a viscous liquid that can flow to a gel or rubber that cannot. Note that gelation is a mechanical condition that does not cause a corresponding sudden change in electrical properties.

After gelation the thermoset hardens into a solid. Upon full cure the thermoset is a *C-Stage* material as shown in Figure 2-4.

Characteristics of C-Stage thermoset:

- Chemical
  - Reaction approaching end of cure
  - Molecular chains lengthening and branching
  - Molecular weight approaching infinity
  - Degree of cure α approaching maximum for cure temperature
  - Infinite network approaching maximum
- Physical
  - Rigidity measured by modulus
  - Modulus increasing to maximum for cure temperature
  - Glass transition temperature T_g reaching maximum for cure temperature
  - Mean free path shortening
  - Diffusion coefficient decreasing
  - Free ion mobility decreasing
  - Dipole rotation decreasing
- Electrical
  - Conductivity reaching minimum (resistivity reaching maximum)
  - Dielectric constant reaching minimum

Figure 2-4
C-Stage resin (end of cure)

Throughout the cure, from A-Stage to B-Stage to C-Stage, both free ion mobility and the amount of dipole rotation decrease continuously. Resistivity depends on free ion mobility and permittivity depends on dipole rotation. As a result these dielectric properties vary with viscosity before gelation, and with rigidity or modulus after gelation.

The degree of cure α is a measure of the amount of reaction for the thermoset. Each bond releases a fixed amount of heat, and the degree of cure is defined as:

(eq. 2-1) $$\alpha = \Delta H \,/\, \Delta H_R$$

where:

ΔH = Total heat released
ΔH_R = Heat of reaction

The degree of cure also correlates with *crosslink density* and α therefore is useful for indicating physical state.

A material undergoes a glass transition when it changes from a glassy and relatively brittle solid to one that is rubbery and relatively soft. Above the glass transition temperature T_g (actually a range of temperature) a polymer is rubbery because sufficient thermal energy is available to increase the flexibility of crosslinks. Below T_g the polymer vitrifies and is rigid. Like degree of cure, glass transition temperature increases with crosslink density, increases as cure progresses and is a measure of cure state. The DiBenedetto model, below, is often used to relate degree of cure to glass transition temperature.

(eq. 2-2) $$\frac{(T_g - T_{g0})}{(T_{g\infty} - T_{g0})} = \frac{\lambda\,\alpha}{(1 - (1 - \lambda)\,\alpha)}$$

where:
T_g = Glass transition temperature (K or °C)
T_{g0} = Glass transition temperature at $\alpha = 0$ (uncured)
$T_{g\infty}$ = Glass transition temperature at $\alpha = 1$ (fully cured)
λ = Adjustable parameter

The relationships among degree of cure, glass transition temperature and electrical properties of the thermoset are the basis for dielectric cure monitoring, which uses electrical measurements to measure cure.

ASTM standard for dielectric measurements

The ASTM standard E 2039-04 **Standard Test Methods for Determining and Reporting Dynamic Dielectric Properties** describes general configurations of sensors, circuits and instruments. Although withdrawn in 2009 without replacement, this standard still provides useful background and guidance for making dielectric measurements.

Section 4.1 of E 2039-04, cited below, recognizes that the dielectric properties of material between two electrodes are determined by measuring the current passing through the material along with the voltage driving that current between the electrodes.

4. Summary of Practice

4.1 An oscillatory electric potential (voltage) is applied to a test specimen by means of an electrode of known geometry. An electric current is measured at a sensing electrode separated from the transmitting electrode by the specimen under test. From the amplitude and phase shift of the measured current relative to the applied voltage and from known geometrical constants, such as electrode spacing and electrode arrangement, desired dielectric properties of the specimen under test may be obtained. Such properties include conductivity, dielectric constant, dielectric dissipation factor, dielectric loss angle, dipole relaxation time, dissipation factor, relative permittivity, loss factor, and tangent delta. The desired dielectric properties may be obtained as a function of frequency, temperature, or time by varying and measuring these independent parameters during the course of the experiment.

NOTE 1—The particular method for measurement of amplitude and phase shift depends upon the operating principle of the instrument used.

(From ASTM 2039-04, withdrawn without replacement in 2009)

Electrical model of Material Under Test (MUT)

Dielectric instrumentation measures the conductance G (or resistance R) and capacitance C between a pair of electrodes at a given frequency. The Material Under Test (MUT) between these electrodes can be modeled as a conductance in parallel with a capacitance, as shown in Figure 2-5.
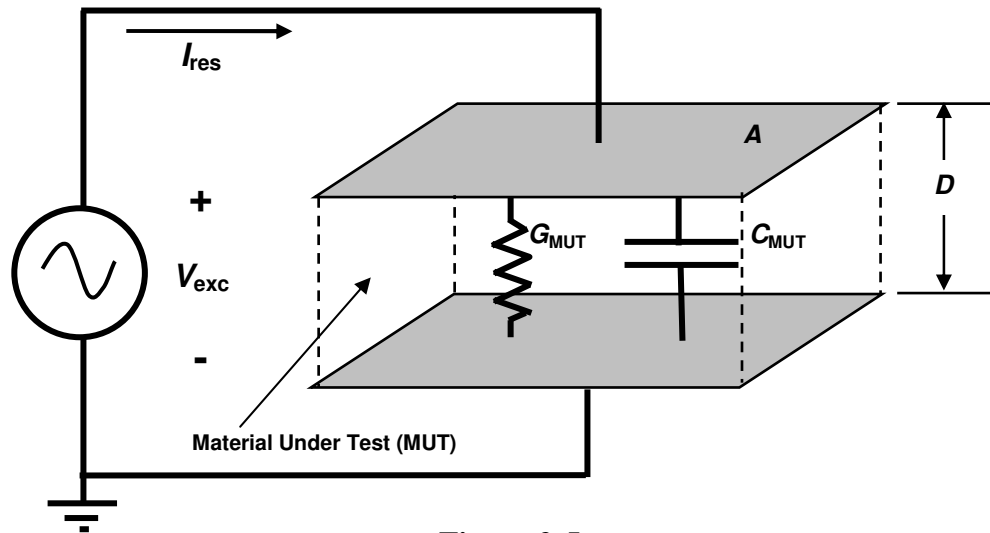
Figure 2-5
Electrical model of dielectric Material Under Test

An AC excitation voltage V_{exc}, applied between a pair of parallel plate electrodes, drives response current I_{res} through the MUT. The amplitude of this current and the phase relationship between V_{exc} and I_{res} provide the information to calculate admittance Y, as shown in Figure 2-6.
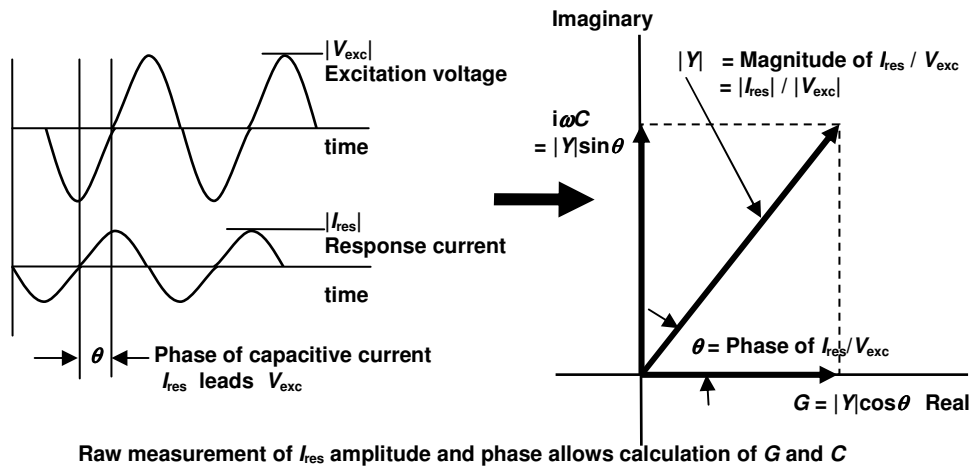

Raw measurement of I_{res} amplitude and phase allows calculation of G and C

Figure 2-6
Signal relationships for the admittance of Material Under Test

Admittance Y, and therefore conductance G and capacitance C, of the MUT are defined by equation 2-3:

(eq. 2-3) $$Y_{MUT} = G_{MUT} + i\omega C_{MUT} = I_{res} / V_{exc}$$

where:

I_{res}	= AC current through MUT	(a complex number, amps)
V_{exc}	= AC voltage across MUT	(a complex number, volts)
C_{MUT}	= Capacitance of MUT	(a real number, Farads)
G_{MUT}	= Conductance of MUT	(a real number, ohms^{-1})
f	= Excitation frequency	(Hz)
ω	= $2\pi f$	(angular frequency, radians/sec)

The material properties of relative conductivity σ', and relative permittivity ε'**,** can be calculated from equations 2-4 and 2-5, as shown in Figure 2-7.

(eq. 2-4) σ' = $G / (\varepsilon_o A/D)$ (relative conductivity)
(eq. 2-5) ε' = $C / (\varepsilon_o A/D)$ (relative permittivity)

where:

ε_0 = 8.85 x 10^{-14} F/cm
A = Electrode area (cm^2)
D = Distance between electrodes (cm)

After factoring *A/D* ratio and ε_0, *G* and *C* reduce to relative conductivity σ' and relative permittivity ε'
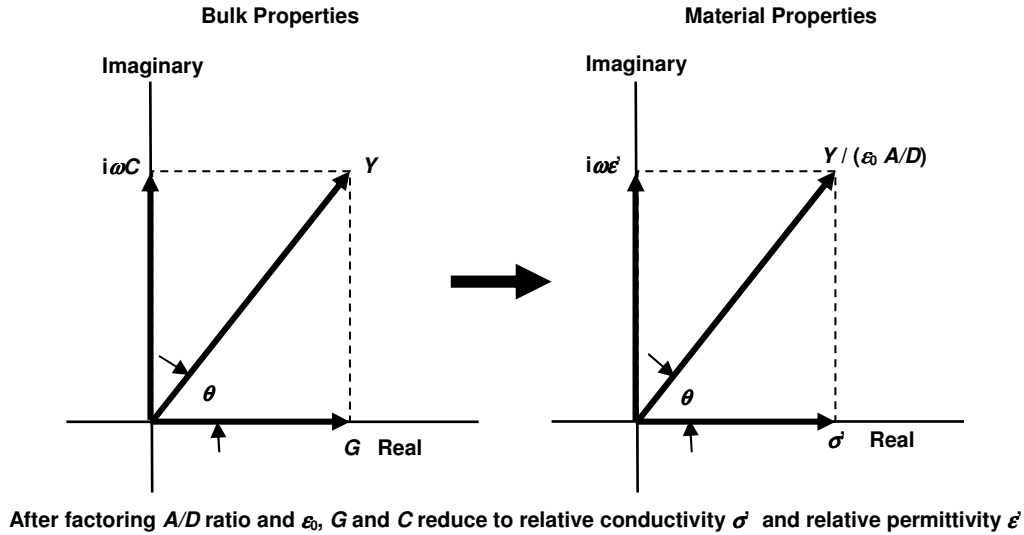
Figure 2-7
Converting bulk properties to material properties

It is preferable to obtain relative permittivity ε'$_r$ and relative conductivity σ' (or conductivity σ) because they are fundamental material properties, which do not depend on the quantity of material being measured.

Chapter 3—Linear vs. Logarithmic Scales: Seeing All the Information

Introduction

During cure the conductance G_{MUT} of a thermoset between the electrodes of a sensor changes by several orders of magnitude. Before processing starts, conductance is normally low because the material is either in a solid state or is at a temperature too low for significant crosslinking. Typically the thermoset is cured by heating to an elevated temperature. As the material becomes warm and softens, the conductance increases. The rate of crosslinking increases with temperature, also, and at some point its influence dominates and the material begins to harden—conductance reaches a maximum at this time then decreases as the material becomes more viscous then rigid. By the end of cure the conductance may have decreased by a factor of 100 or more from its peak value.

Plotting conductance on a logarithmic scale is the optimum method for seeing all the information available from dielectric measurements.

Data plotted against linear scales

Figure 3-1 shows how conductance varied during cures of several samples from the same batch of sheet molding compound (SMC). The data are plotted against a linear scale and reveal considerable sample to sample variation, with a 140% difference between the maximum and minimum values of peak conductance .
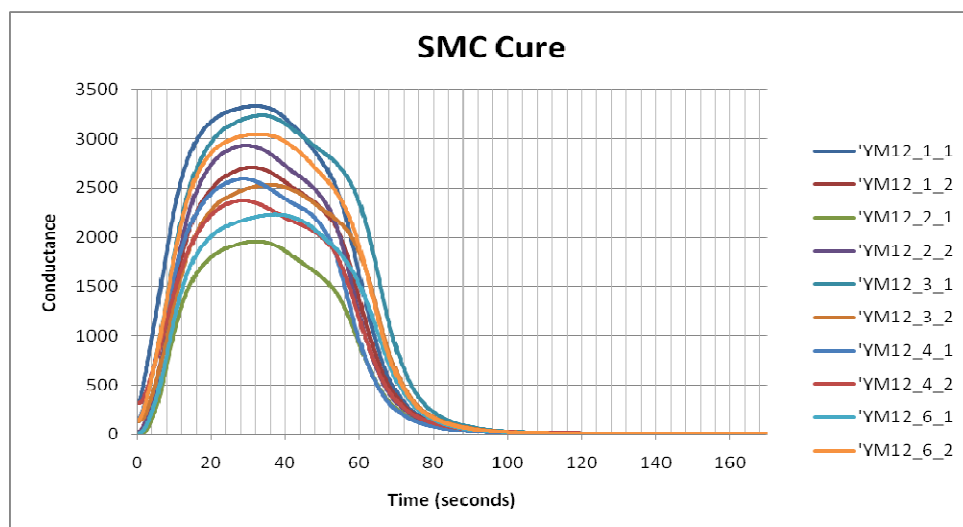
Figure 3-1
SMC conductance during cure on a linear scale

At first glance the lack of consistency casts doubt about the usefulness of dielectric cure monitoring; however, to avoid misinterpretation, it is necessary to understand the factors that determine conductance. Figure 3-2 shows a model of the

conductance and capacitance of a material under test (MUT) between parallel plate electrodes. Note that only conductance is relevant in this section.
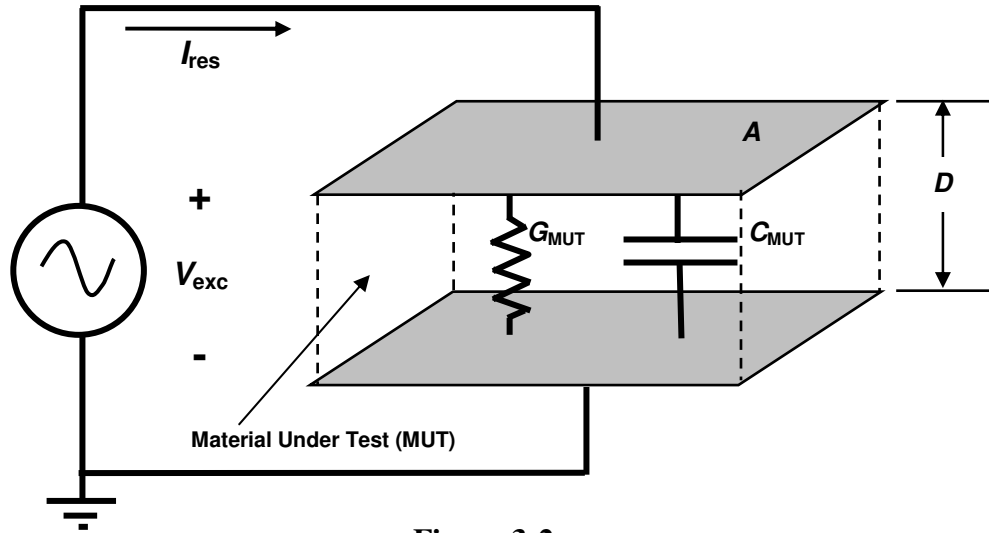

Figure 3-2
Electrical model of dielectric Material Under Test

Conductance and conductivity

Conductance is a bulk property that depends both on the geometry of the electrodes as well as on the *conductivity* of the material between them. Like density, conductivity is a property that is independent of the quantity of material. During cure this conductivity changes with time, and the measured conductance as a function of time, $G_{MUT}(t)$, is given by equation 3-1.

(eq. 3-1) $G_{MUT}(t) = \sigma(t)\,(A/D)$ (ohm^{-1})

Where: $\sigma(t)$ = time varying conductivity (ohm^{-1}-cm^{-1})
            A/D = ratio of electrode area to electrode separation (cm)

Several factors determine the time varying conductivity, which is given by equation 3-2.

(eq. 3-2) $\sigma(t) = n\,q\,\mu(t)$ (ohm^{-1}-cm^{-1})

Where: n = free ion concentration (cm^{-3})
            q = magnitude of electronic charge (coulombs)
            $\mu(t)$ = free ion mobility (cm^2 / (V-s))

Assuming the free ion concentration and the charge of the free ions do not change during cure, then only the change in free ion mobility, $\mu(t)$, affects conductivity and ultimately conductance. In a thermoset, perhaps the most significant factor determining mobility is

the crosslinking among monomers. As crosslink density increases, the growing molecular network impedes the flow of ions and reduces mobility.

Combining equations 3-1 and 3-2 produces the following expression:

$$(3\text{-}3) \qquad G_{MUT}(t) = [n \, (A/D) \, q] \, \mu(t)$$

In reality, the value of **[n (A/D) q]** may change from sample to sample and test to test. The free ion concentration, n, increases with conductive additives and decreases with non-conductive filler. The geometry (A/D) of the electrodes may differ from sensor to sensor because of variations in fabrication or set up. The free ion charge normally does not change but is included with the terms in brackets for simplicity. Equation 3-3 may then be reduced to:

$$(3\text{-}4) \qquad G_{MUT}(t) = [B] \, \mu(t)$$

Here $B = n$ (A/D) q, the variable terms unrelated to curing. Expressed logarithmically, equation 3-4 becomes:

$$(3\text{-}5) \qquad \log_{10}(G_{MUT}(t)) = \log_{10}(B) + \log_{10}(\mu(t))$$

From equation 3-5, plotting the measured conductance on a logarithmic scale captures the entire range of $G_{MUT}(t)$ caused by the mobility, which can change by several orders of magnitude during cure.

Plotting on a logarithmic scale also produces an offset, which is $\log_{10}(B)$, caused by the terms unrelated to curing. If the free ion concentration and the electrode geometry are constant for a particular sample and test, then *the result is a constant offset from the baseline behavior* of $\log_{10}(\mu(t))$.

Effect of mixing and fillers

For a single batch of liquid resin, good mixing can produce a homogeneous free ion concentration, and the measured conductance can be uniform from sample to sample. In contrast, a material like SMC has a high content of non-conductive chopped glass fibers mixed with polyester, vinyl ester or epoxy resin. This composite is semi-solid, is difficult to mix well, and as a result different samples may have different ratios of fiber to resin. The measured conductance of SMC is therefore likely to vary among samples from a single batch, as illustrated in Figure 3-3.
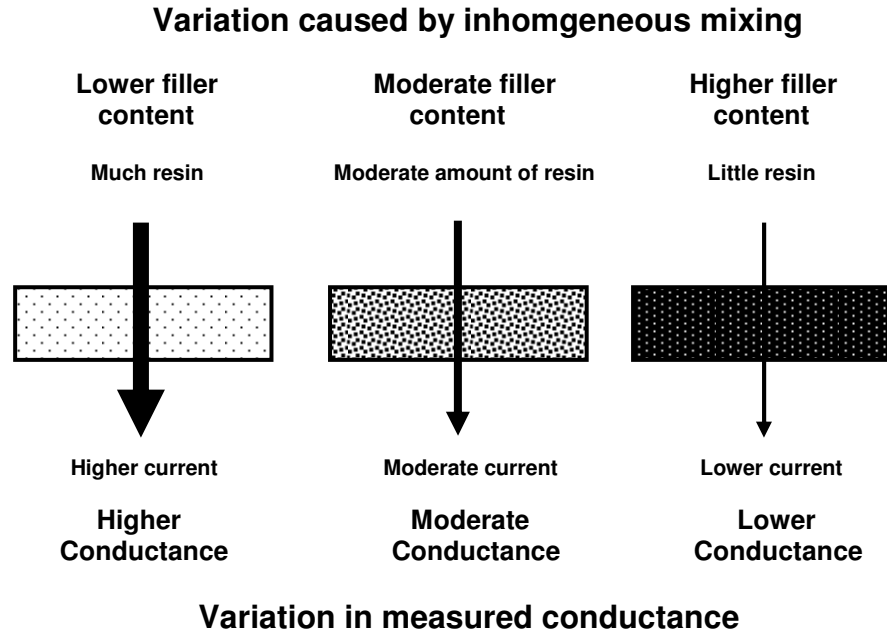
Variation caused by inhomgeneous mixing

Figure 3-3
Addition of non-conductive filler reduces amount of conductive resin

Data plotted against logarithmic scales

When the data of Figure 3-1 are plotted on the logarithmic scale, the curves are largely parallel to one another and differ by an offset in conductance. This offset is typically caused by sample-to-sample variation in filler content, which does not affect the cure rate.
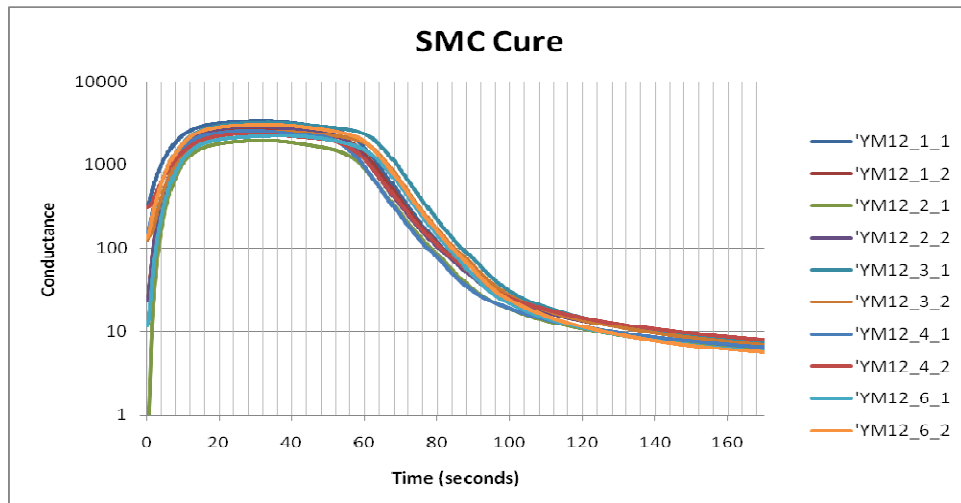

Figure 3-4
SMC conductance during cure on a logarithmic scale

Plotting conductance against logarithmic scales has significant advantages compared to linear scales:

- The entire range of conductance is visible

- Only factors that affect cure determine the shape of the conductance curve

- Factors that do not affect cure, such as variations in filler content or sensor geometry, determine offsets of the conductivity curve but not its shape

Chapter 4–Dielectric Measurements, Viscosity and Critical Points

Introduction

Dielectric cure monitoring measures the bulk conductance and capacitance of Material Under Test (MUT), which are used to calculate the material properties of conductivity and permittivity.

Conductivity (σ) has both frequency independent (σ_{DC}) and frequency dependent (σ_{AC}) components. In an oscillating electric field, σ_{DC} arises from the flow of mobile ions while σ_{AC} arises from the rotation of stationary dipoles. These two responses act like electrical elements in parallel and add together to produce the total measured conductivity:

(Eq. 4-1) $$\sigma = \sigma_{DC} + \sigma_{AC}$$

Resistivity (ρ) is the inverse of conductivity as shown below:

(Eq. 4-2) $$\rho = 1 / \sigma$$

Like conductivity, resistivity has both frequency independent (ρ_{DC}) and frequency dependent (ρ_{AC}) components.

Of particular interest for cure monitoring is the DC resistivity, $\rho_{DC,}$ because of its relationship to a fluid's mechanical viscosity. Crosslink density, which is a measure of cure state, affects both mechanical viscosity and the movement of ions, and therefore influences ρ_{DC}. The term *ion viscosity* was coined to emphasize this relationship between mechanical viscosity and ρ_{DC}. Ion viscosity (*IV*) is defined as:

(Eq. 4-3) $$IV = \rho_{DC} = 1 / \sigma_{DC}$$

Often differing by only a scaling factor, ρ_{DC} and mechanical viscosity are related to the cure state of thermosets such as epoxies, polyurethanes, polystyrenes, bulk molding compound (BMC) and sheet molding compound (SMC). The measurement of ρ_{DC} requires no mechanical components, and yet provides information about a mechanical property.

For convenience, unless otherwise indicated, this chapter will use the term *resistivity* to refer to ρ_{DC}. Similarly, the term *viscosity* will refer to *mechanical viscosity*.

Viscosity and resistivity

Viscosity is a measure of how easily the molecules of a fluid move past each other in response to shear forces, and in the case of polymeric materials is determined by

the motion of polymer chain segments. In contrast, resistivity is a measure of the mobility of free ions through a medium under the influence of an electric field. DC resistivity, ρ_{DC}, is given by equation 4-4.

(eq. 4-4) $\rho_{DC} = 1 / (q \, \mu \, n)$

Where: q = magnitude of electronic charge (coulombs)
               μ = free ion mobility ($cm^2 / (V\text{-}s)$)
               n = free ion concentration (cm^{-3})

Mobility determines the rate of ionic diffusion through a medium, and is given by the Einstein relationship of equation 4-5:

(eq. 4-5) $\mu = q \, D / (k \, T)$ ($cm^2 / (V\text{-}s)$)

Where: D = diffusion coefficient (cm^2 / s)
               k = Boltzmann's constant (eV / K)
               T = temperature in degrees Kelvin (K)

If mobile ions are modeled as spherical particles, then in the limit of low Reynold's numbers, by the Stokes-Einstein Relation of equation 4-6:

(eq. 4-6) $D = k \, T / (6\pi \, \eta \, r)$ (cm^2 / s)

Where: η = mechanical viscosity (g / (cm-s))
               r = radius of sphere (cm)

Combining equations 4-4, 4-5 and 4-6 yields the following relationship between resistivity and viscosity:

(eq. 4-7) $\rho_{DC} = (6\pi \, \eta \, r) / (q^2 \, n)$

$$\therefore \qquad \rho_{DC} \propto \eta$$

Consequently, resistivity is proportional to viscosity. Empirical results show that this relationship is valid in many cases, although some systems for poorly understood reasons obey a power law:

(eq. 4-8) $\rho \propto \eta^n$ where $n = 1, 2, 3 \ldots$

To emphasize the proportionality between resistivity and viscosity, the term *ion viscosity* was coined as a synonym for resistivity.

        Figure 4-1 compares ion viscosity and viscosity from the non-isothermal cure of an epoxy. Ion viscosity was measured with a dielectrometer and viscosity was measured with a Rheological Dynamic Spectrometer. The two curves show strong correlation from

the beginning of cure up to gelation at about 135 minutes. After gelation, viscosity increases rapidly and becomes immeasurable. Ion viscosity continues to change as the polymer network grows, and provides useful information about cure state until the end of cure.
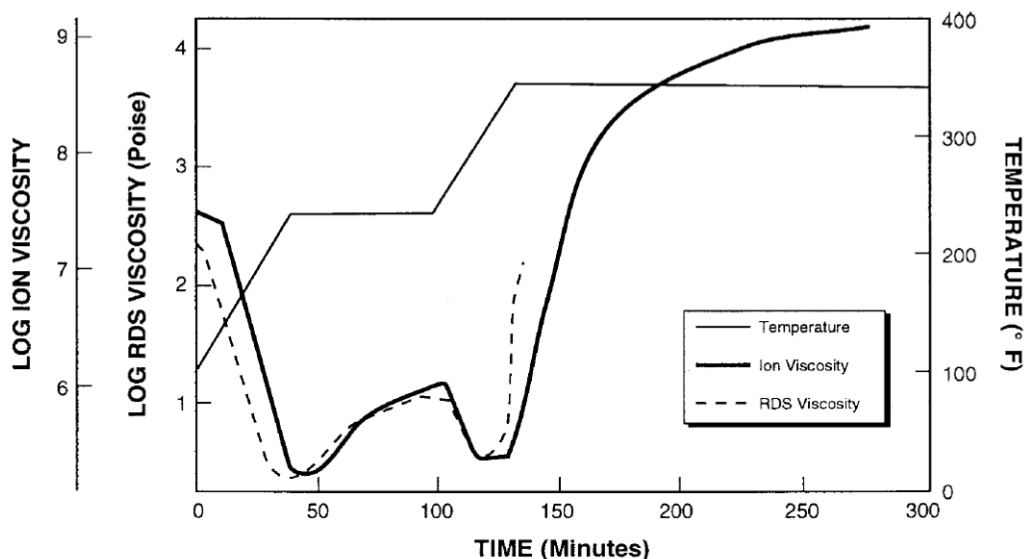

Figure 4-1
Correlation of ion viscosity and viscosity during epoxy cure[1]

Critical Points during cure

A thermoset cures because monomers crosslink to form a polymer network. Often this reaction is exothermic—generating heat—or is driven by the heat of a press or oven. Typically the viscosity initially decreases as temperature increases. The material responds by simply melting or becoming less rigid. Resistivity also decreases as mobile ions experience less resistance to movement. At this point the reaction is still slow but eventually accelerates until it dominates the system. Viscosity reaches a minimum—a point of zero slope—and then increases as the material becomes more viscous, gels then becomes more rigid. Resistivity similarly reaches a minimum and then increases due to the growing network, which presents a greater and greater impediment to the flow of ions.

Eventually the reaction slows and viscosity becomes unmeasurable. At this point the resistivity is no longer proportional to viscosity. Resistivity continues to change, but more and more slowly, approaching a limit at the end of cure. Viscosity and resistivity (ion viscosity) typically follow curves like those of Figures 4-2 and 4-3.
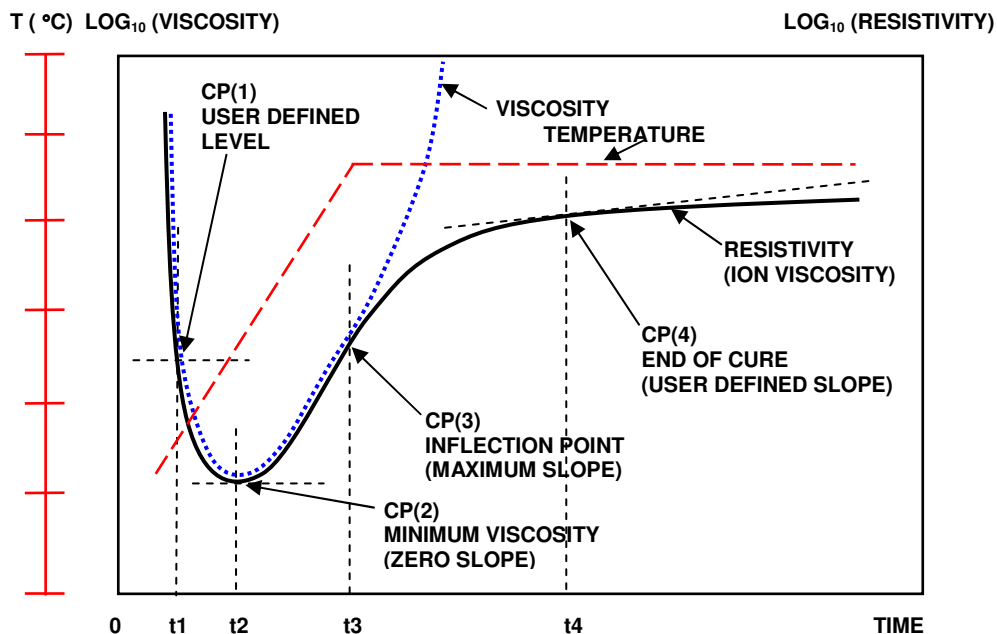
Figure 4-2
Viscosity and ion viscosity (resistivity) in a curing thermoset
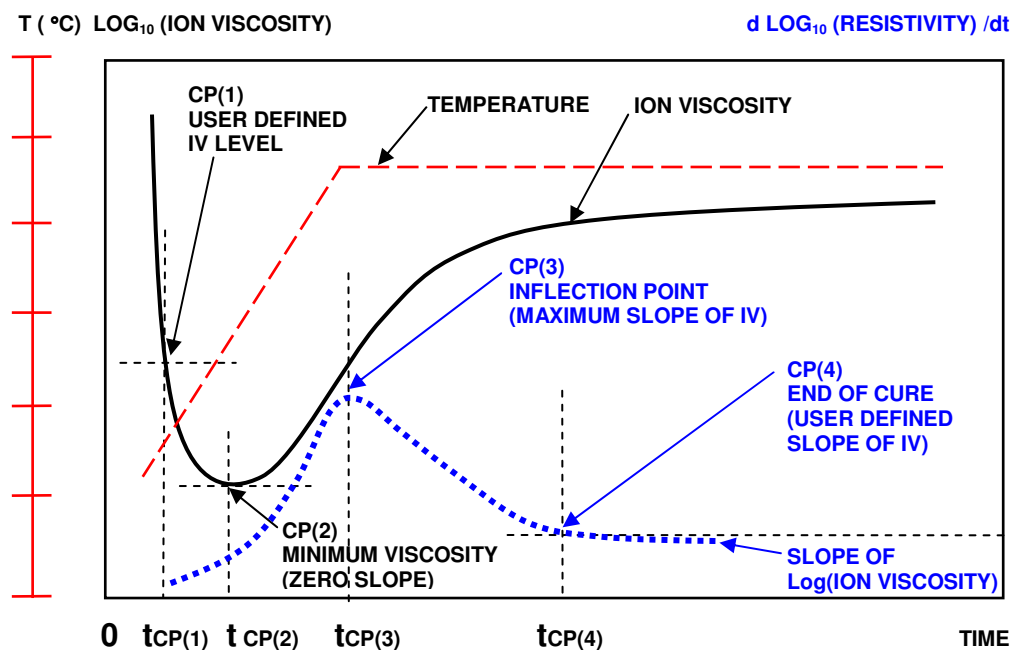
Figure 4-3
Ion viscosity, slope and Critical Points in a curing material

The dielectric cure curve is characterized by four Critical Points:

- CP(1)—A user defined level of ion viscosity, which can identify the onset of material flow at the beginning of cure.

- CP(2)—Ion viscosity minimum, which typically also corresponds to the mechanical viscosity minimum. This Critical Point indicates the time the accelerating crosslinking reaction dominates the behavior of the system.

- CP(3)—Inflection point, which identifies when the crosslinking reaction begins to slow. CP(3) is often used as a signpost that can be associated with gelation.

- CP(4)—A user defined slope that can define the end of cure. The decreasing slope corresponds to the decreasing reaction rate. Note that dielectric cure monitoring continues to reveal changes in the evolving material past the point when mechanical measurement of viscosity is not possible.

The proportionality between ion viscosity and viscosity has proven to be useful in thermoset processing. Knowing when a material has reached the viscosity minimum, for example, allows optimum application of pressure to compress a laminate or to extract air bubbles from a molded part. Even after ion viscosity diverges from viscosity, ion viscosity continues to indicate cure state until polymerization stops.

References

1. *Cure Monitoring of Thermosetting Resins Utilizing Dielectric Sensors*, David Shepard, Holometrix-Micromet

Chapter 5–Loss Factor and Ion Viscosity

Introduction

Dielectric permittivity ε is a quantity with real and imaginary parts:

(Eq. 5-1) $$\varepsilon^* = \varepsilon_0 (\varepsilon' + i\,\varepsilon'') = \varepsilon_0 [\varepsilon' + i\,\sigma / (\varepsilon_0\,\omega)]$$

Conductivity σ is the sum of frequency independent (σ_{DC}) and frequency dependent (σ_{AC}) components[1], as expressed below:

(Eq. 5-2) $$\sigma = \sigma_{DC} + \sigma_{AC}$$

In an oscillating electric field, σ_{DC} arises from the flow of mobile ions while σ_{AC} arises from the rotation of stationary dipoles. Loss factor ε'' is a measure of the dissipation, or loss, of electromagnetic energy as heat and is given by:

(Eq. 5-3) $$\varepsilon'' = \sigma / (\omega\,\varepsilon_0) = (\sigma_{DC} + \sigma_{AC}) / (\omega\,\varepsilon_0)$$

During thermoset cure, σ_{DC} tends to dominate in the early part of cure, when the material is most conductive. Frequency independent conductivity also may dominate throughout cure at low frequencies. During these times the loss factor may be approximated as:

(Eq. 5-4) $$\varepsilon'' \approx \sigma_{DC} / (\omega\,\varepsilon_0)$$

In this case, loss factor is inversely proportional to frequency. For example, if the excitation frequency decreases by a factor of 10, loss factor increases by the same factor of 10—this relationship identifies when σ_{DC} dominates the dielectric response and can indicate cure state.

During the latter part of cure, frequency *dependent* conductivity due to dipoles may dominate the dielectric response, especially at higher frequencies. It is important to identify these times and frequencies to avoid misinterpreting data for purposes of cure monitoring.

Cure monitoring with multiple frequencies

Figure 5-1 shows dielectric data at multiple frequencies during the cure of an epoxy resin. A plot of loss factor can reveal when frequency independent conductivity σ_{DC} dominates the dielectric response. In the early part of this cure, loss factors for 10 Hz, 100 Hz, 1 kHz, and 10 kHz all are inversely proportional to frequency.

---

1. The real part of relative permittivity, or relative dielectric constant, ε' also has frequency independent and frequency dependent components, but they will not be treated in this chapter.
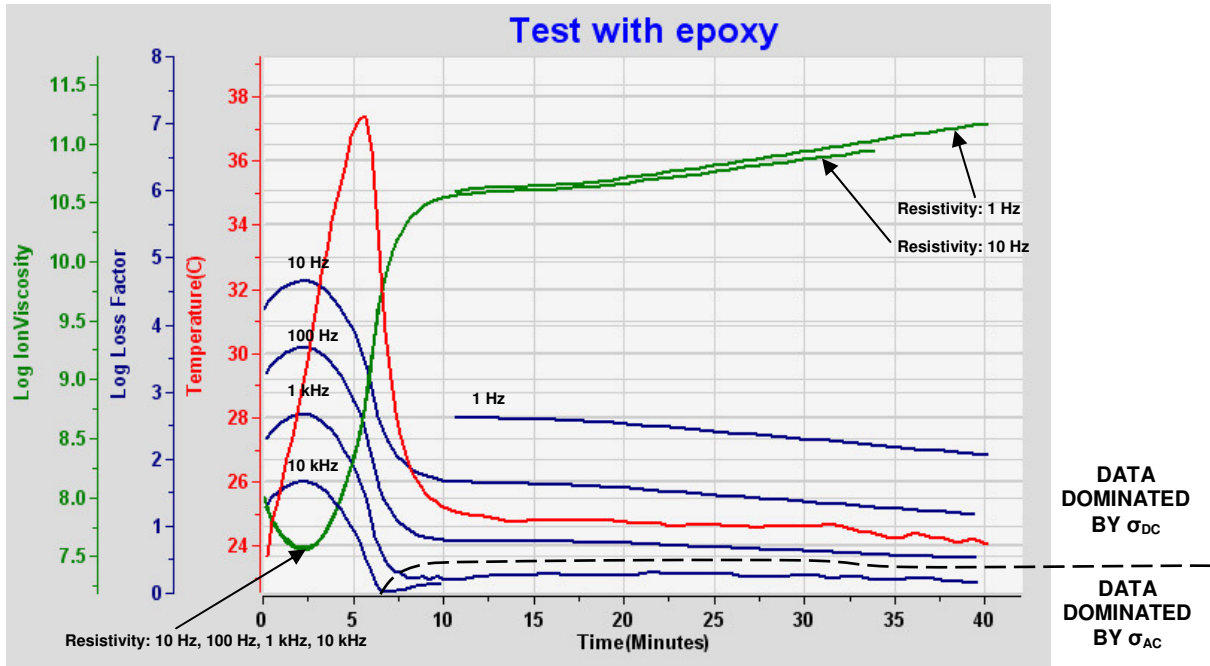
Figure 5-1
Multiple frequency data from epoxy cure

In the latter part, however, only loss factors for 1 Hz, 10 Hz and 100 Hz are inversely proportional to frequency.

Resistivity ρ is the inverse of conductivity, as expressed in equation 5-5:

(Eq. 5-5) $$\rho = 1 / (\sigma_{DC} + \sigma_{AC}) = 1/(\omega\, \varepsilon_0\, \varepsilon")$$

When frequency independent conductivity σ_{DC} dominates the data, then resistivity is also largely frequency independent. Frequency independent resistivity ρ_{DC} is called *ion viscosity*, and is characterized by the overlap of resistivity at multiple frequencies, as shown in Figure 5-1.

During thermoset cure, ion viscosity typically increases proportionately with mechanical viscosity until they diverge around the time of gelation (See Figure 4-2). Even after mechanical viscosity becomes infinite, however, the crosslinking reaction continues and the growing polymer network still presents greater and greater resistance to the flow of ions. Consequently, frequency independent resistivity ρ_{DC}—ion viscosity— can be used for determining cure state throughout the entire cure.

Chapter 6–Ion Viscosity and Temperature

Introduction

For the measurement of mechanical viscosity and cure state, ion viscosity (DC resistivity) provides valuable information from a simple electrical measurement. Ion viscosity depends on the mobility of free ions under the influence of an electric field, but also varies with temperature. Therefore, correct interpretation of ion viscosity requires knowledge of temperature at the time of measurement and an understanding of how temperature influences the data. For brevity, ion viscosity will alternatively be called *IV*.

Temperature dependence of ion viscosity

At a constant cure state, which is a fixed crosslink density in a thermoset, ion viscosity decreases as temperature rises because the mobility increases. Ion viscosity is another term for DC resistivity, ρ_{DC}, which is given by equation 6-1.

(eq. 6-1) $\qquad\qquad\qquad \rho_{DC} = 1 / (q\, \mu\, n\,)$

Where: $\quad q$ = magnitude of electronic charge (coulombs)
$\qquad\qquad \mu$ = free ion mobility $(cm^2 / (V\text{-s}))$
$\qquad\qquad n$ = free ion concentration (cm^{-3})

Free ion mobility determines the rate of ionic diffusion through a medium, and is given by the Einstein relationship of equation 6-2:

(eq. 6-2) $\qquad\qquad\qquad \mu = q\, D / (k\, T) \qquad (cm^2 / (V\text{-s}))$

Where: $\quad D$ = diffusion coefficient (cm^2 / s)
$\qquad\qquad k$ = Boltzmann's constant (eV / K)
$\qquad\qquad T$ = temperature in degrees Kelvin (K)

The diffusion coefficient itself is exponentially temperature dependent:

(eq. 6-3) $\qquad\qquad\qquad D = D_0\, e^{-Q/kT} \qquad (cm^2 / s)$

Where: $\quad D_0$ = Maximum value of diffusion coefficient (cm^2 / s)
$\qquad\qquad Q$ = Activation energy (eV)

The maximum value of the diffusion coefficient D_0 is constant with temperature, but decreases as cure progresses because greater crosslink densities reduce the mean free path of a mobile ion. Combining equations 6-1, 6-2 and 6-3 results in the following expression for DC resistivity:

(eq. 6-4) $$\rho_{DC} = (k / (q^2 \, n \, D_0)) \, T \, e^{Q/kT}$$

The logarithm of ion viscosity (DC resistivity) then becomes:

(eq. 6-5) $$\log_{10}(IV) = \log_{10}(k / (q^2 \, n \, D_0)) + \log_{10}(T) + (Q / (kT \ln(10)))$$

which may be expressed as:

(eq. 6-6) $$\log_{10}(IV) = A + \log_{10}(T) + B \, (1 / T)$$

Where: $A = \log_{10}[k / (q^2 \, n \, D_0)]$
$B = Q / (k \ln(10))$

At a given cure state, D_0 is constant and coefficients A and B are also both constants. The $1 / T$ term of equation 6-6 dominates the response because it varies more with temperature than $\log_{10}(T)$. As a result, for a fixed cure state, ion viscosity decreases as temperature increases.

Figure 6-1 shows how ion viscosity changes with temperature for an epoxy resin with catalyst. Figure 6-2 shows how ion viscosity changes for a thermoplastic polyimide.[1] Overlaid on the data are results from equation 6-6, where coefficients A and B are determined for best fit. The good correspondence between equation 6-6 and the data validates this model of ion viscosity temperature response. As the cure state advances, D_0 decreases, causing the offset between calculated lines for 0% and 100% cure.

As seen in Figures 6-1 and 6-2, the activation energy Q, which largely determines the slope of each calculated line, may vary with degree of cure.
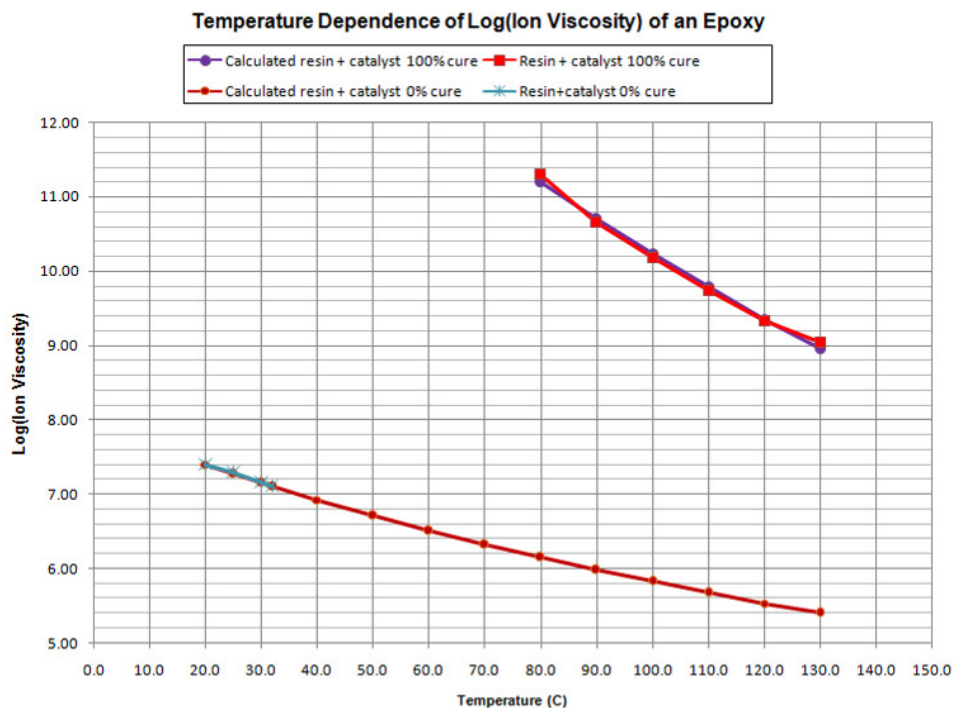
Figure 6-1
Variation in log(*IV*) with temperature for an epoxy resin
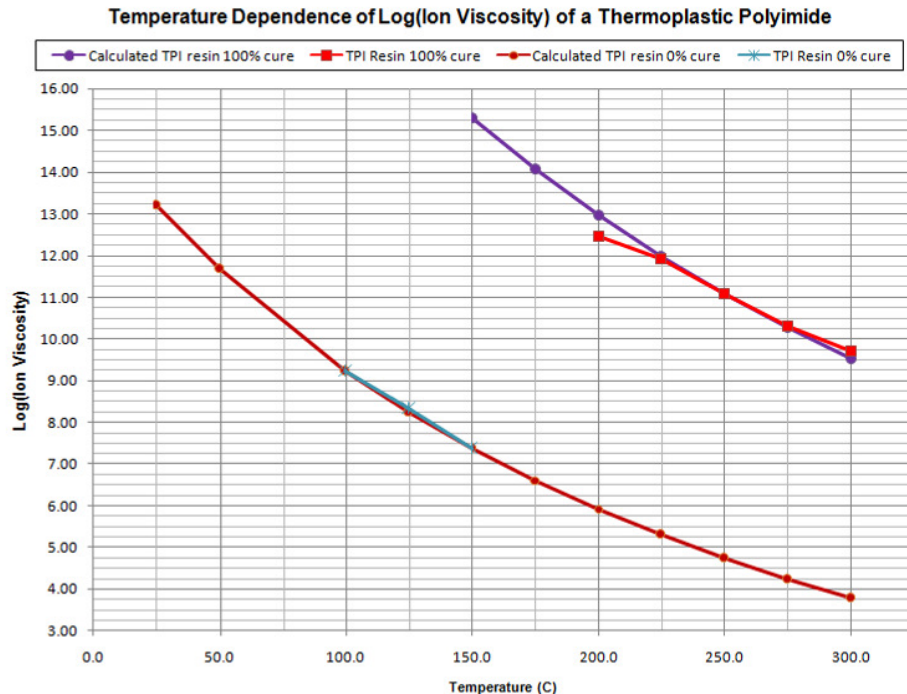
Figure 6-2
Variation in log(*IV*) with temperature for a thermoplastic polyimide[1]

Prepreg processing

A common temperature schedule for vacuum bag curing of prepregs begins with an initial ramp-and-hold step, called the *B-Stage*. During the B-Stage, volatiles and reaction by-products are free to escape as the resin heats and melts. After the B-Stage a second ramp-and-hold heats the prepreg to high temperature for final curing. Pressure is applied during this second step to compress together the laminates of prepreg and consolidate the part. At this time any residual volatiles are unable to escape.

Figure 6-3 shows dielectric and viscosity data from the cure of an epoxy resin with two ramp-and-hold steps. Here the first minimum in ion viscosity (*IV*) occurs at 50 minutes. At this time the increase in *IV* due to the accelerating reaction dominates the decrease in *IV* caused by the temperature rise. After the second temperature ramp begins, *IV* again decreases as temperature increases. In this case the second decrease in mechanical viscosity may cause resin to flow excessively under the application of pressure, causing undesirable loss of resin and producing dry fibers and voids in the laminate. Eventually the thermally driven cure dominates once more and ion viscosity rises again.
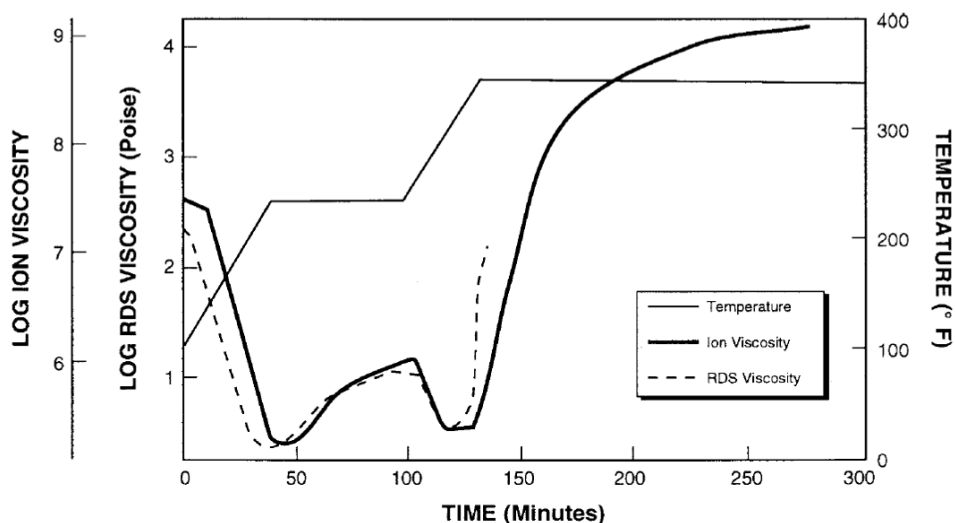
Figure 6-3
Ion viscosity for an epoxy resin cure with two ramp-and-hold steps[2]

Dielectric cure monitoring is uniquely able to observe thermoset material state in real time, and can provide valuable information for process development and process control. The ability of dielectric cure monitoring to infer mechanical viscosity during a process allows adjustment of temperature and pressure to avoid excessive flow of resin and reduce the occurrence of voids that can cause delamination of the finished part.

References

1. Proprietary thermoplastic polyimide adhesive, derived from its FM901 polyamic-acid polymer solution, provided by Fraivillig Technologies Company.

2. *Cure Monitoring of Thermosetting Resins Utilizing Dielectric Sensors*, David Shepard, Holometrix-Micromet

Chapter 7–Sensors, A/D Ratio and Base Capacitance

Introduction

Measurements of dielectric properties often involve the use of simple parallel plate electrodes. However, their separation can change with pressure, or expansion and contraction of the material between them. The ratio of electrode area A and the distance D between them—the A/D ratio—therefore may not be well known. As the scaling factor between conductance and conductivity, or capacitance and permittivity, uncertainty in A/D causes inaccuracies in determining dielectric material properties.

A common alternative is the interdigitated electrode shown in Figure 7-1. A rigid substrate supports the electrodes and resulting the planar structure does not change with pressure, or expansion and contraction of the MUT.

The A/D ratio of parallel plate electrodes may be generalized for application to interdigitated electrodes. In this case, A is not simply the area of the electrodes and D is not simply the distance between them. For interdigitated electrodes, the A/D ratio also accounts for fringing electric fields and other factors and as a result can also act as the scaling factor between conductance and conductivity, and capacitance and permittivity.

Two-dimensional numerical simulations and experimental results have validated this generalization across a wide range of conductivity. The benefit of using interdigitated electrodes is an A/D ratio that is not affected by pressure, or expansion and contraction.
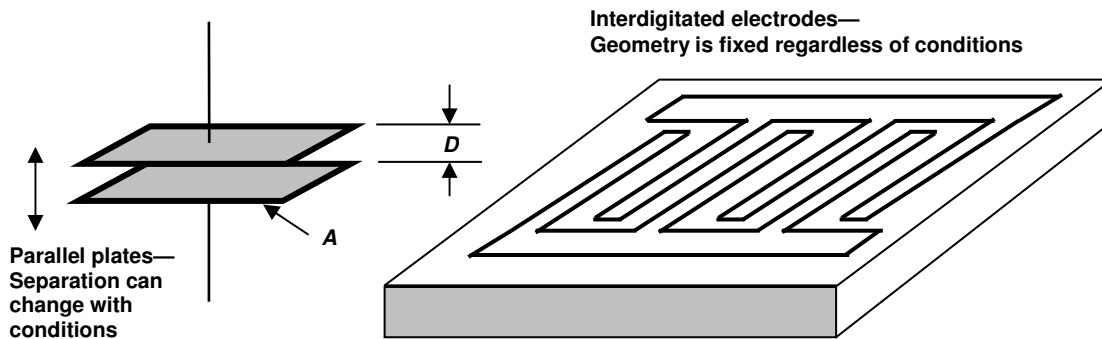
Figure 7-1
Comparison of parallel plate and interdigitated electrodes

Base capacitance

The substrate supporting interdigitated electrodes introduces an additional component into the system being measured. The cross section of Figure 7-2 shows that capacitance C_{tot} has a contribution C_{MUT} from the Material Under Test above electrodes. However, there is also a contribution C_{base} from the substrate beneath the electrodes. This second component is called the base capacitance.
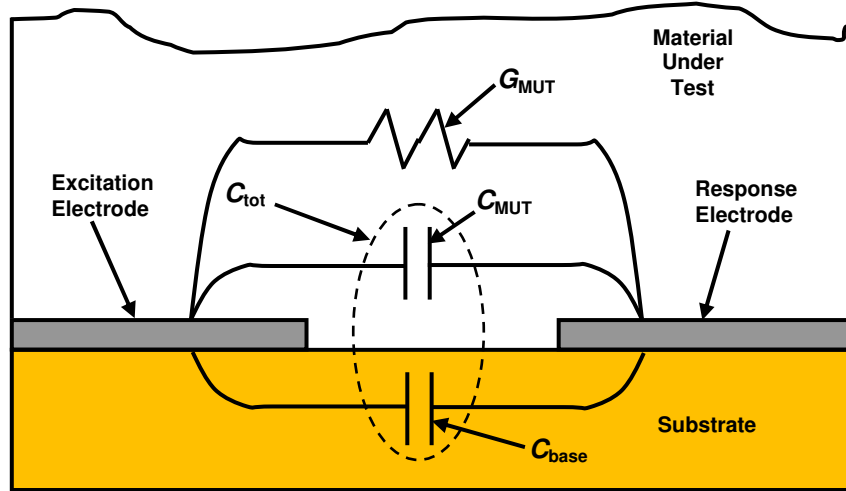
Figure 7-2
Cross section of interdigitated electrode structure

The total capacitance between the interdigitated electrodes is:

(eq. 7-1) $C_{tot} = C_{MUT} + C_{base}$

The capacitance of the MUT is:

(eq. 7-2) $C_{MUT} = C_{tot} - C_{base} = \varepsilon_0 \, \varepsilon'_{MUT} \, A/D$

Finally, the conductivity, ion viscosity (*IV*) and permittivity of the MUT are:

(eq. 7-3) $\sigma_{MUT} = G_{MUT} / (A/D)$

(eq. 7-4) $IV = \rho_{MUT} = (A/D) / G_{MUT}$

(eq. 7-5) $\varepsilon'_{MUT} = C_{MUT} / [\varepsilon_0 \, (A/D)] = (C_{tot} - C_{base}) / [\varepsilon_0 \, (A/D)]$

Comparison of measurements with different sensors

  To compare results from different sensors, a Ceramicomb-1"[1] sensor measured dielectric properties during cure on the surface of a graphite-epoxy prepreg and a Mini-Varicon[2] sensor measured dielectric properties between two layers of the same prepreg, as shown in Figure 7-4.

---

1. P/N CCR-250-J-300-1 manufactured by Lambient Technologies, LLC, Boston, MA USA
2. P/N VC-400-X-40 manufactured by Lambient Technologies, LLC, Boston, MA USA

a.   b.

Figure 7-3
Ceramicomb-1" sensor (a.) and Mini-Varicon sensor (b.)
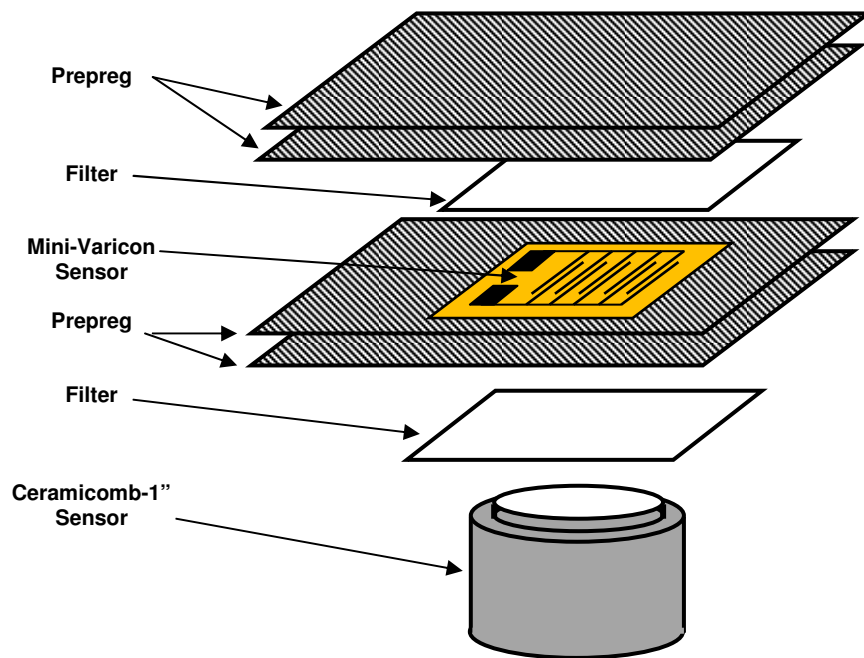
Figure 7-4
Lay-up of Ceramicomb-1" and Mini-Varicon sensors

The Ceramicomb-1" and Mini-Varicon sensors have very different constructions and geometries. In particular, the Ceramicomb-1" has an A/D = 10 cm and 1/8th the

sensitivity of the Mini-Varicon, which has an A/D = 80 cm. Specifications of the Ceramicomb-1" and Mini-Varicon sensors are listed in Table 7-1:

Table 7-1
Comparison of Ceramicomb-1" and Mini-Varicon sensors

Sensor	Ceramicomb-1"	Mini-Varicon
Electrode Width	0.020"	0.004"
Electrode Spacing	0.020"	0.004"
Substrate	Alumina (ε_r = 9.8)	Polyimide (ε_r = 3.6)
A/D	10 cm	80 cm
Base Capacitance	≈25 pF	≈25 pF

Figure 7-5 shows the log(ion viscosity) and slope of log(ion viscosity) data obtained with a frequency of 100 Hz from the two sensors during a single test. For brevity, log(ion viscosity) will be called *log(IV)* and the slope of log(ion viscosity) will simply be called *slope*.

Ch:1 – Temperature(C)	—
Ch:2 – Temperature(C)	—
Ch:1 – 100 Hz Log Ion Viscosity	—
Ch:2 – 100 Hz Log Ion Viscosity	—
Ch:1 – 100 Hz dLog Ion Visc/dt	—
Ch:2 – 100 Hz dLog Ion Visc/dt	—
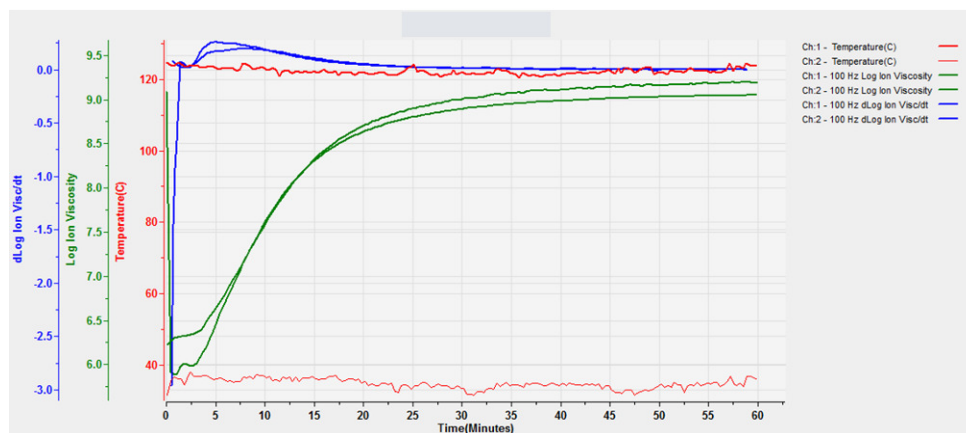
Figure 7-5
Cure of prepreg, two sensors simultaneously
(Ceramicomb-1" sensor on surface, Mini-Varicon sensor between plies)

The curves for slope overlap almost completely after the time of maximum slope (CP(3)), indicating that cure rates are essentially identical on the surface and within the laminate. For clarity, only the log(*IV*) curves are displayed in Figure 7-6 and only the slope curves are displayed in Figure 7-7.
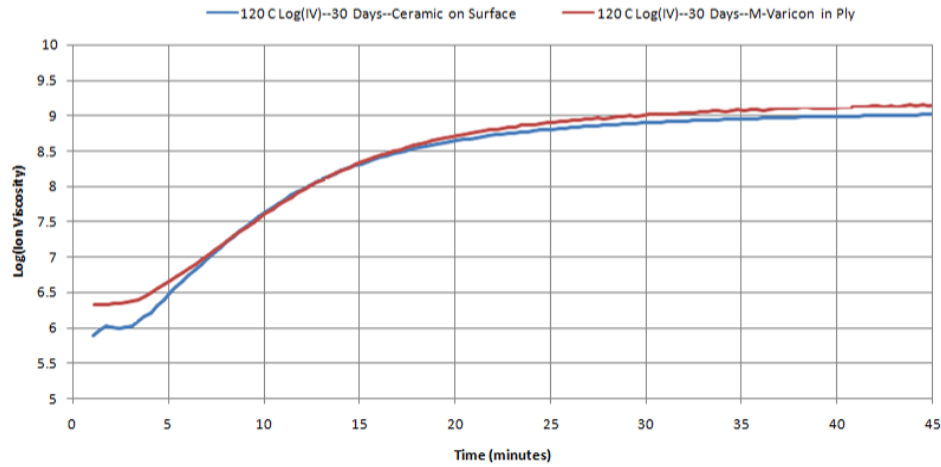
Figure 7-6
Log(*IV*) data for Ceramicomb-1" and Mini-Varicon sensors
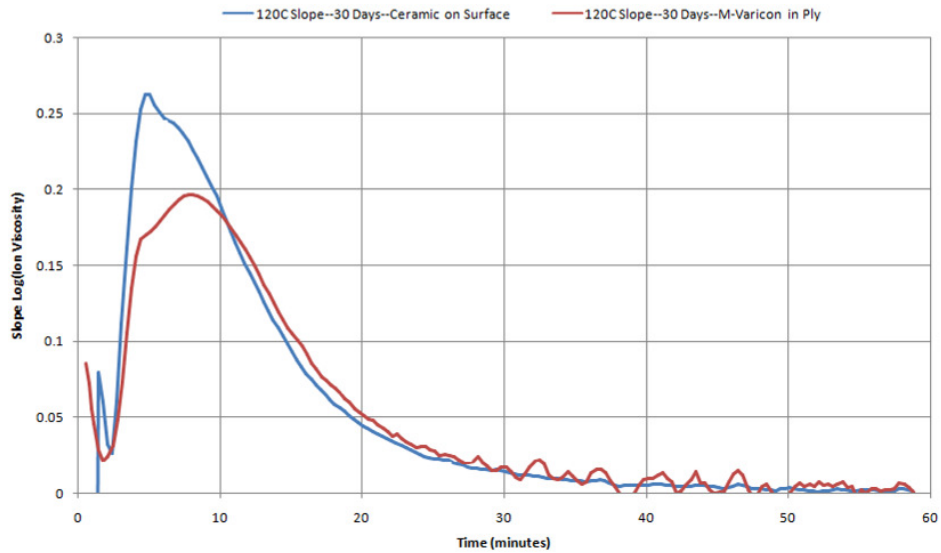
Figure 7-7
Slope data for Ceramicomb-1" and Mini-Varicon sensors

Figures 7-6 and 7-7 illustrate that with the correct *A/D* ratio, different sensors provide the same cure data and are interchangeable for measuring ion viscosity. Note that equation 7-4 indicates that *only A/D ratio is used to obtain ion viscosity* from measurements of the conductance between the electrodes, G_{MUT}. Equation 7-5, however, shows that the base capacitance must be subtracted from measurements of the capacitance between the electrodes, C_{tot}, to obtain the capacitance of the Material Under Test, C_{MUT}.

Chapter 8—Sample Preparation for Dielectric Measurements

Sensor cleaning

Clean sensors with acetone, alcohol or other solvent to remove oils and contaminants. Solvent or water adsorbed onto the surface of the sensor normally will not interfere with cure monitoring because it is released at elevated temperatures and would not be present at typical process temperatures.

At room temperature, however, adsorbed solvent or water may appear as an additional conductance that can produce erroneous dielectric measurements.

- Heating the sensor above 100 °C for a short time should remove adsorbed solvents.

Sample lay-up

1. To prevent adhering of sample material to a sensor, apply mold release to molds and to the face of ceramic sensors.

- Use silicone based or non-conductive mold release.

2. To prevent a short circuit between the bond pads, sensors with attached leads should not contact electrically conductive surfaces.

- Prevent short circuits of the sensor by covering the bond pads with Kapton® or polyimide tape, as shown in Figure 8-1.

To prevent short circuit of bond pads
—Avoid electrically conductive surfaces in this area
—Insulate above and below bond pad area
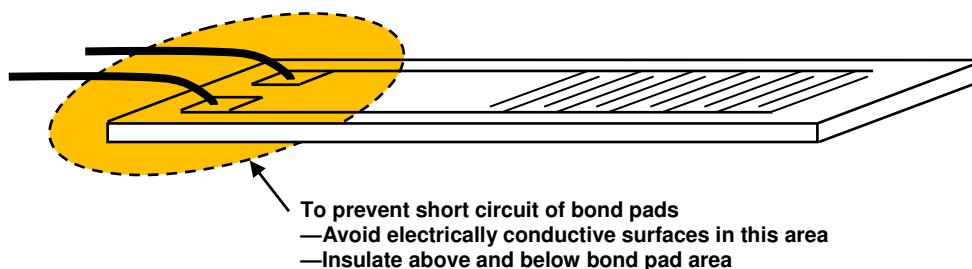
**Figure 8-1
Insulating bond pad area**

3. To reduce lead capacitance, avoid twisting the leads together; instead, let leads run parallel to each other.

4. Place a sample on the sensor so it has good contact with the electrodes. Cover electrodes completely as shown in Figure 8-2.
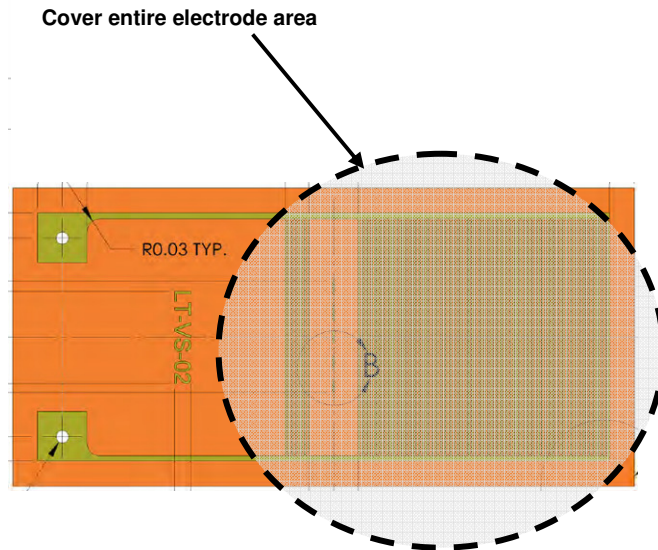
Figure 8-2
Sample application area on sensor

5. Solid samples, or solid samples that melt during processing, require applied pressure.

6. For planar interdigitated electrodes, the thickness of the sample should be greater than the separation between electrodes, otherwise the sensor will also detect air or material on the top side of the sample.

7. To ensure enough resin for good measurements with prepreg, stack at least two or three layers of prepreg on top of a sensor, as shown in Figure 8-3.

8. To prevent shorting of the electrodes, composite materials containing graphite or other conductive fibers require a filter between the sensor and sample, as shown in Figure 8-3.

*   Glass cloth with small pore size, fiberglass felt or laboratory filter paper are recommended filter materials.

9. To prevent the sample from adhering to press platens or mold surfaces, use a sheet of aluminum foil above and below the lay-up, as shown in Figure 8-3.

Pressure from press or mold

Aluminum foil

**Prepreg sample
(2 or 3 Layers)**

**Use filter when
testing carbon fiber
prepreg**

Aluminum foil

**To prevent short circuit of bond pads,
wrap Kapton® or other insulating tape
around bond pad area**
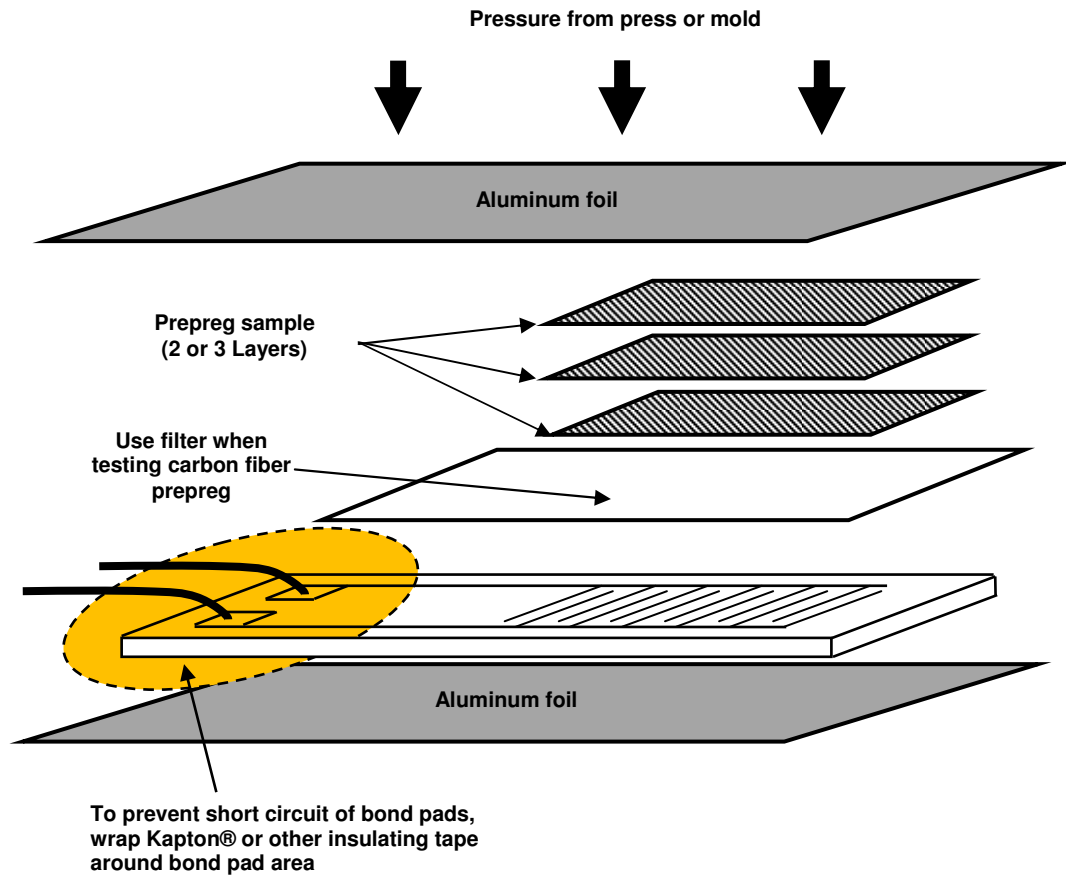
**Figure 8-3
Suggested lay-up for prepregs**

Reducing noise in leads, extension cables and sensors

Long, unshielded leads can pick up electrical interference and produce noisy data, especially at the end of cure when signal levels are low. For best results, use coaxial cable with shields that are guarded or grounded.

If an instrument measures a response voltage from the dielectric sensor, then a guarded cable is usually more suitable. Figure 8-4 shows a typical configuration for guarded cables. Note that the shields around the leads connect to a x1 amplifier that outputs the guard signal. This guard signal drives the shields with a reproduction of the response, reducing capacitive interaction between the sensitive response line and the outside world.
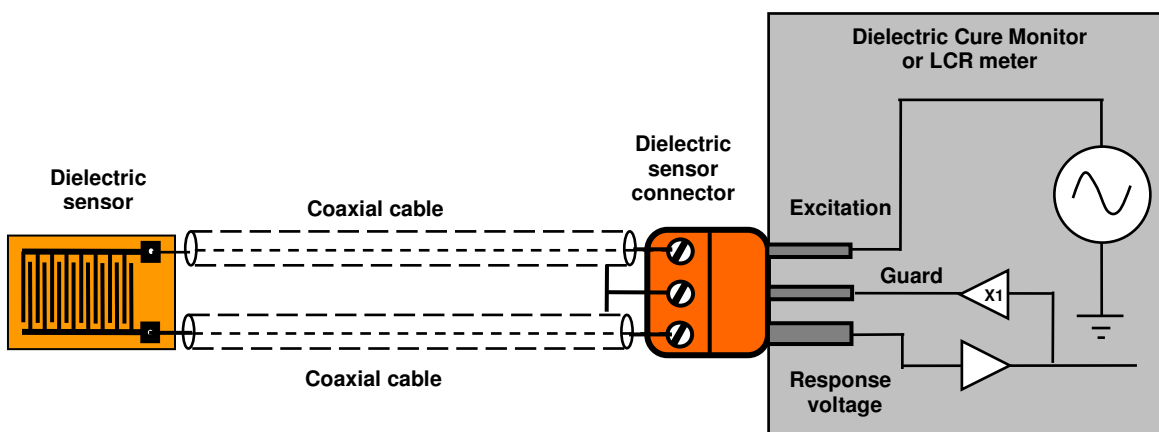
Figure 8-4
Connecting a dielectric sensor using coaxial cable with guarded shields

If an instrument measures a response current from the dielectric sensor, then this current typically goes into a virtual ground. In this case a grounded shield is more suitable, as shown in Figure 8-5.
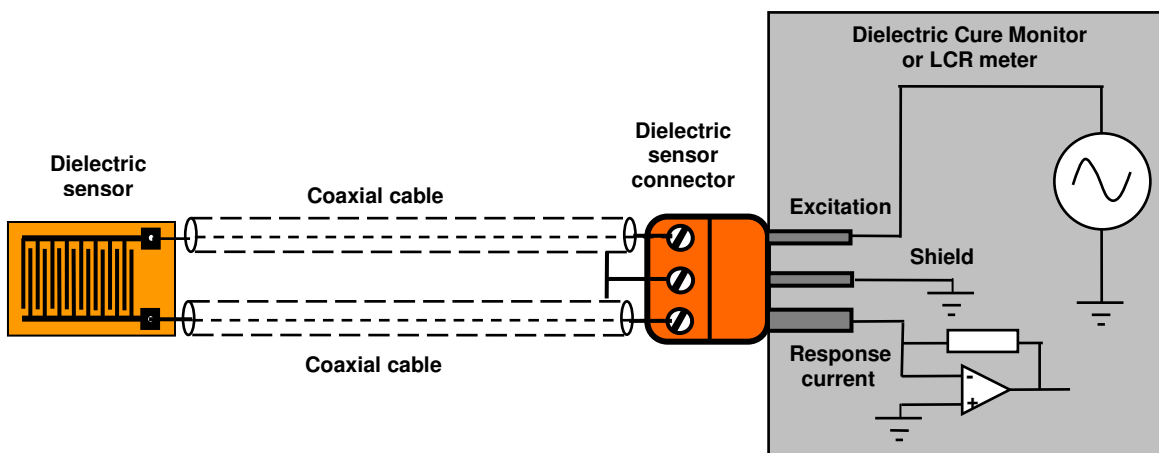
Figure 8-5
Connecting a dielectric sensor using coaxial cable with grounded shields

Even with guarded or shielded leads, the sensor itself picks up electrical noise from the environment. The amplitude of the sensor's voltage signal may be only 10 mV, and the current may be measured in microamps. Nearby power cords, which can carry 120 VAC or 240 VAC, or ungrounded metal surfaces, which can act as antennas, both are common sources of noise.
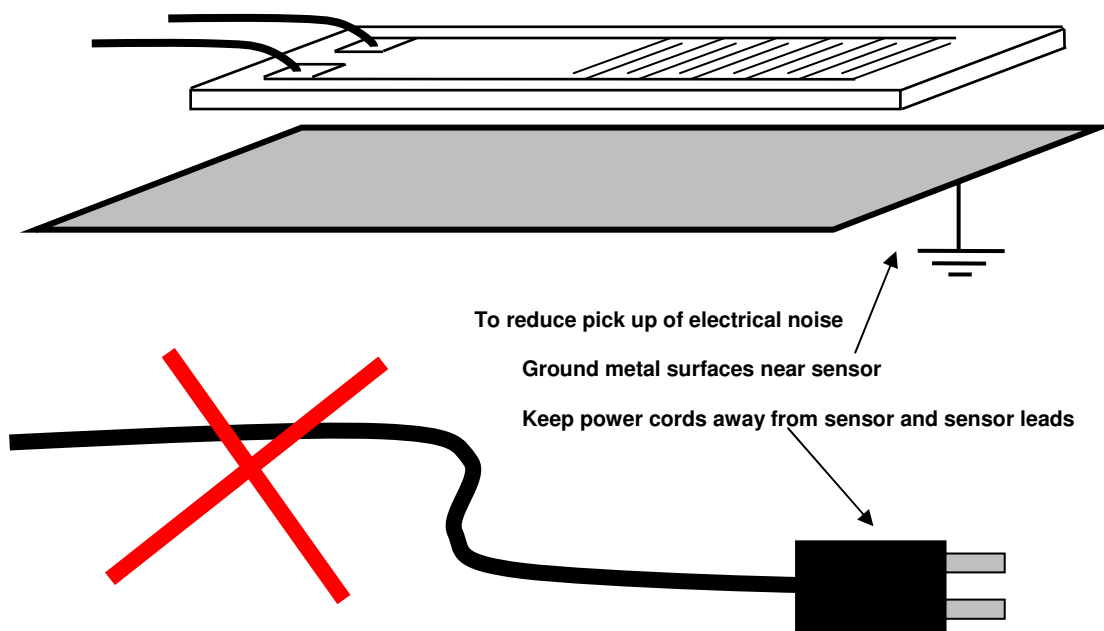
Figure 8-6
Methods to reduce pick up of electrical noise

With proper sample preparation, lay-up and shielding of leads, and attention to the electrical environment it is possible to make good, reproducible measurements of dielectric properties for monitoring the cure of thermoset and composite materials.

Chapter 9—Cure Monitoring of SMC/BMC

Introduction

The curing behavior of Sheet Molding Compound (SMC) was observed using the LT-451 Dielectric Cure Monitor.[1] Bulk Molding Compound (BMC) is the generally the same material as SMC but in bulk form, so the analysis of results apply to BMC as well. The data from dielectric cure monitoring clearly show:

- Critical Points identify characteristic features of the cure such as minimum ion viscosity, maximum slope of log(ion viscosity) and the time to a chosen end of cure.

- Cure time decreases as cure temperature increases, as expected for a reaction that is thermally driven.

This chapter presents and discusses data for *log(ion viscosity)* and *slope of log(ion viscosity)*, which indicate the state of cure. The plots show characteristic features such as minimum ion viscosity, maximum slope of log(ion viscosity) and the time to a chosen end of cure. For brevity, log(ion viscosity) will be called *log(IV)* and slope of log(ion viscosity) will simply be called *slope*.

Procedure

Samples of SMC were applied to Mini-Varicon[2] sensors and cured in a laboratory press at 135 °C, 145 °C and 155 °C. Previous tests had identified 10 Hz as an optimum excitation frequency for cure monitoring. An LT-451 Dielectric Cure Monitor measured the dielectric properties of each sample at 10 Hz for the duration of each test. Lambient Technology's CureView software acquired and stored the data, and performed post-analysis and presentation of the results.

Results

Figures 9-1, 9-2 and 9-3 show data from the cures of SMC at 135 °C, 145 °C and 155 °C, respectively. The data are averaged and filtered to reduce noise.[3]

---

1. LT-451 Dielectric Cure Monitor manufactured by Lambient Technologies.
2. Mini-Varicon sensor manufactured by Lambient Technologies.
3. CureView data processing parameters: Data Averaging = 1, Slope Span = 3, Data Filtering = 0, Slope Filtering = 1, Slope Filtering Start Time = 0 minutes.
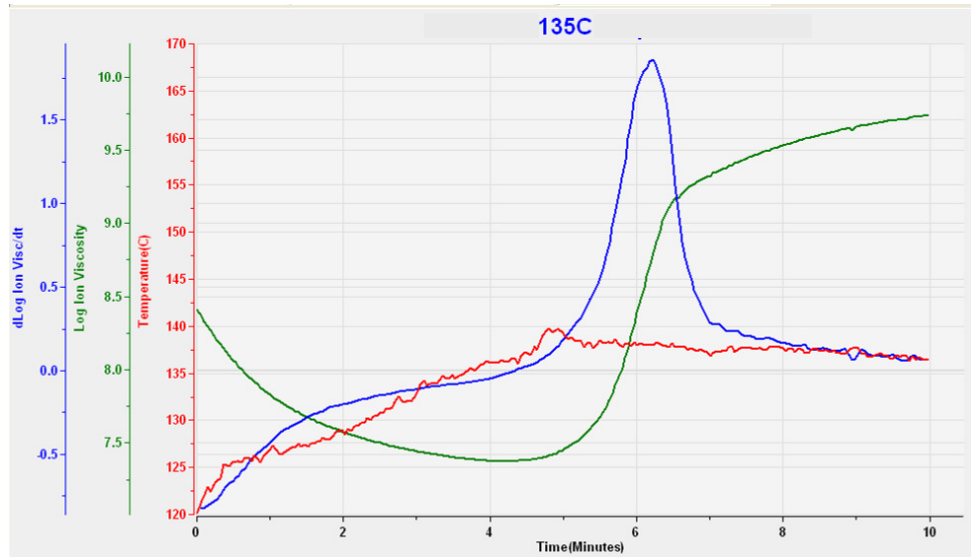
Figure 9-1
135 °C SMC cure data at 10 Hz
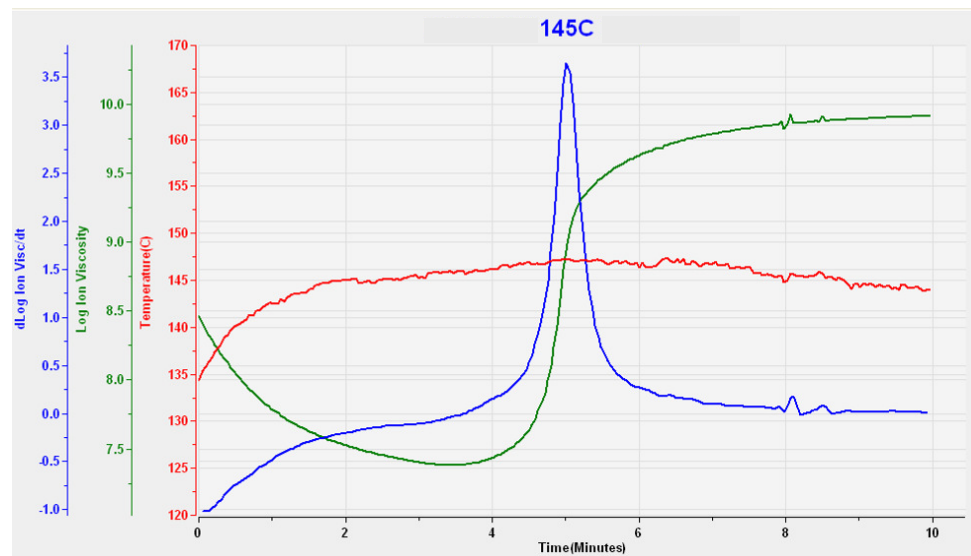
Figure 9-2
145 °C SMC cure data at 10 Hz
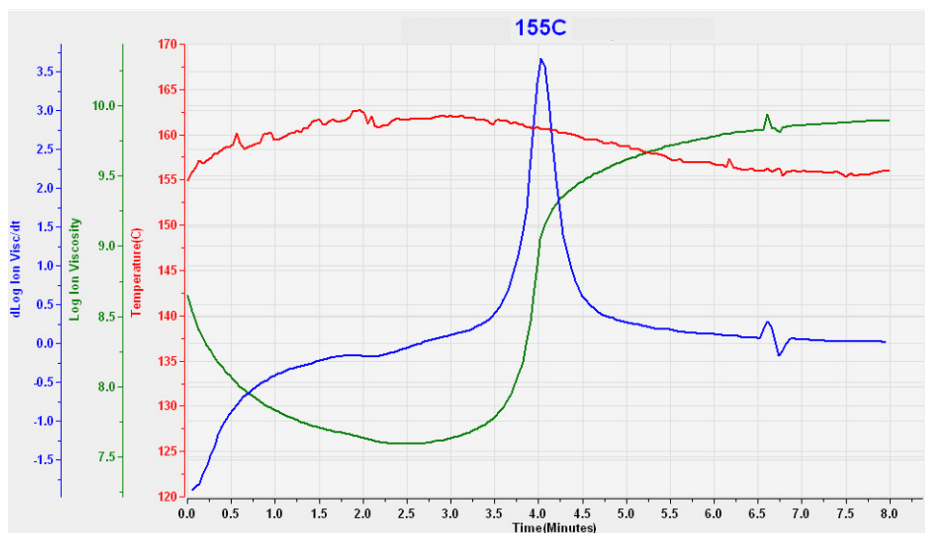
Figure 9-3
155 °C SMC cure data at 10 Hz

The Critical Points that characterize each cure are shown in Table 9-1. **Note that the slope of 0.25 to define CP(4), the end of cure, was chosen arbitrarily.** In actuality a user must determine the appropriate slope to indicate end of cure for the application.

Table 9-1
Critical Points from SMC cure monitoring

Cure Temp. (°C)	CP(1) Crit. Visc.		CP(2) Min. Visc.		CP(3) Max Slope		CP(4) Crit. Slope	
	Value	Time	Value	Time	Value	Time	Value	Time
135	8.0	0.65 min (39 s)	7.38	4.17 min (250 s)	1.86	6.23 min (374 s)	0.25	7.21 min (433 s)
145	8.0	0.60 min (36 s)	7.39	3.42 min (205 s)	3.65	5.01 min (301 s)	0.25	6.13 min (368 s)
155	8.0	0.65 min (39 s)	7.60	2.48 min (149 s)	3.67	4.03 min (242 s)	0.25	5.14 min (308 s)

As plotted in Figure 9-4, the times to reach each Critical Point are shorter for cures at higher temperatures, which is expected for thermally driven reactions. Furthermore, the relationship between the time to a Critical Point and the temperature of cure follow a well defined line.
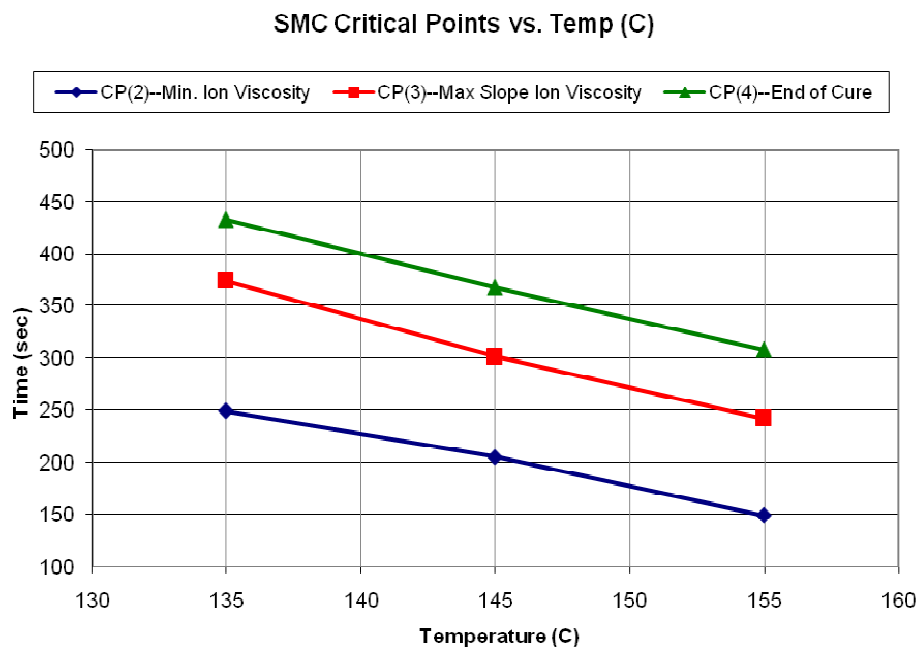
Figure 9-4
Critical Point time vs. cure temperature for SMC

Note that the time to Critical Point 1—CP(1)—is not plotted in Figure 9-4. CP(1) determines when the ion viscosity of the SMC has decreased the user selected value of 8.0, which was chosen to indicate the onset of flow. The time to flow is a measure of heating time and not of curing, consequently CP(1) has been omitted for clarity.

Within the 20 °C range of the plot of Figure 9-4, the time to reach CP(2)—the ion viscosity minimum—decreases by approximately 50 seconds for each 10 °C increase in processing temperature. The times to reach CP(3) and CP(4) vary by a similar amount with temperature. Over a wider temperature range this relationship typically follows an Arrhenius function.

Chapter 10– Cure Monitoring of Carbon Fiber Reinforced Prepreg (CFRP)

Introduction

Samples from a single batch of carbon fiber reinforced prepreg (CFRP) were tested for repeatability and effect of temperature on cure rate. The data from dielectric cure monitoring clearly show:

- Critical Points identify characteristic features of the cure such as minimum ion viscosity, maximum slope of log(ion viscosity) and the time to a chosen end of cure.

- Cure time decreases as cure temperature increases, as expected for a reaction that is thermally driven.

This chapter presents and discusses data for *log(ion viscosity)* and *slope of log(ion viscosity)*, which indicate the state of cure. The plots show characteristic features such as minimum ion viscosity, maximum slope of log(ion viscosity) and the time to a chosen end of cure. For brevity, log(ion viscosity) will be called *log(IV)* and slope of log(ion viscosity) will simply be called *slope*.

Procedure

Samples were tested using the Ceramicomb-1"[1] sensor, which was embedded into the lower heater platen of a press as shown in Figure 10-1. A sheet of laboratory grade filter paper was placed on top of the sensor to allow flow of resin to the sensor while preventing carbon fibers from short circuiting the electrodes. Two layers of CFRP approximately 1" x 1" were then placed on top of the filter paper. During each test the press applied heat and pressure to the lay-up.

An LT-451 Dielectric Cure Monitor[2] measured dielectric properties at 100 Hz and 1.0 KHz excitation frequencies. CureView[3] software acquired and stored the data, and performed post-analysis and presentation of the data.

CureView can extract Critical Points only for data obtained at a single frequency; therefore the first tests on a material require measurement with multiple frequencies to determine an optimum single frequency. During subsequent tests CureView can extract Critical Points automatically and characterize the cure.

1. Ceramicomb-1" sensor manufactured by Lambient Technologies.
2. LT-451 Dielectric Cure Monitor manufactured by Lambient Technologies.
3. CureView software manufactured by Lambient Technologies.

Figure 10-1
Ceramicomb-1" reusable sensor embedded in press platen

Repeatibility of measurements

Figure 10-2 shows the results from one of five tests of fresh CFRP under identical conditions: temperature was 120 °C and pressure was approximately 10 psi. The minimum of the log(*IV*) curve, also the time of minimum mechanical viscosity, occurs at the start of the test. This point is called Critical Point 2 (CP(2)). Minimum viscosity occurs when the thermally driven reaction dominates the decreasing viscosity caused by "melting." At 120 °C, the reaction dominates from the very start.

Maximum slope occurs at approximately 15 minutes, indicating the time of maximum reaction rate. This point is called Critical Point 3 (CP(3)). After this time the reaction slows and the cure is in its end stage. Although some users identify CP(3) with gelation, gelation is actually a mechanical event that has no dielectric indicator. At best CP(3) may be used as a signpost *associated* with gelation but not *identifying* gelation

By the end of the test the material is still slowly curing, as indicated by the non-zero slope of log(*IV*). To define the end of cure, the user may choose a particular slope, also called Critical Point 4 (CP(4)), according to the needs of the application.
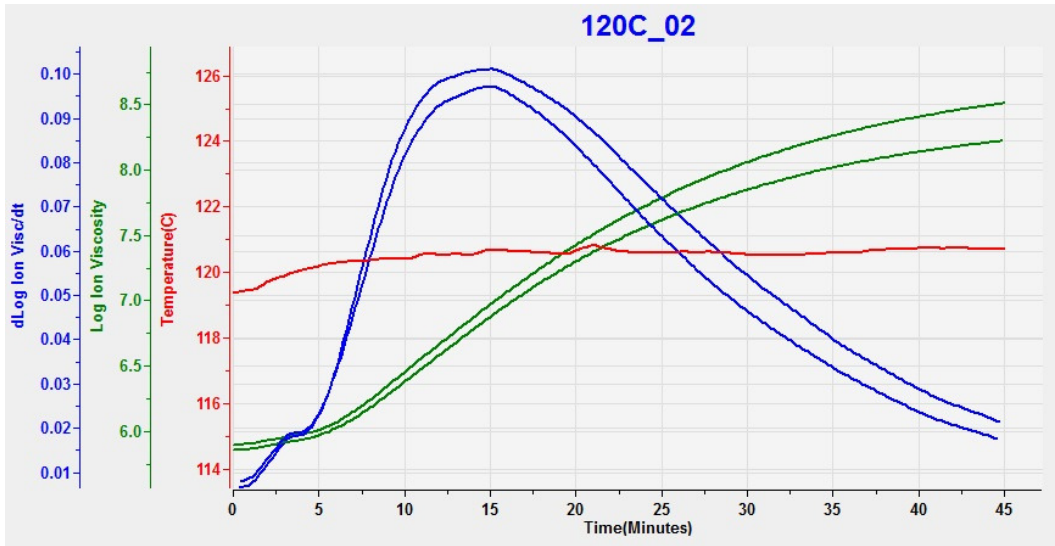
Figure 10-2
CFRP cure at 120 °C, 100 Hz and 1 kHz data

Figures 10-3 and 10-4 show log(*IV*) and slope curves for the 100 Hz data from six tests. The data are overlaid on top of each other to reveal typical reproducibility and range of variation.
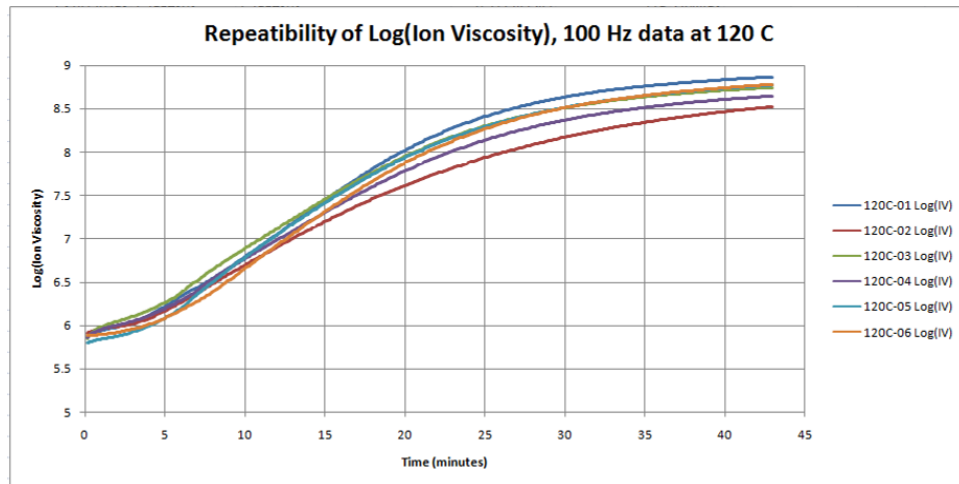
Figure 10-3
Log(IV) from cures of six samples of CFRP
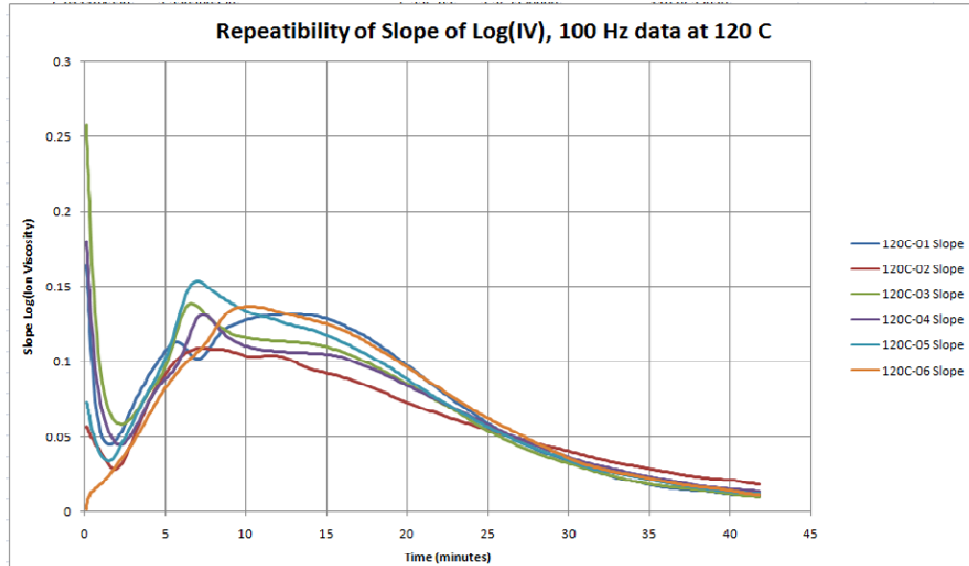
Figure 10-4
Slope from cures of six samples of CFRP

Effect of process temperature on cure rate

Figures 10-5 through 10-8 show results from samples of the same fresh CFRP tested at 120 °C, 135 °C, 150 °C and 165 °C.
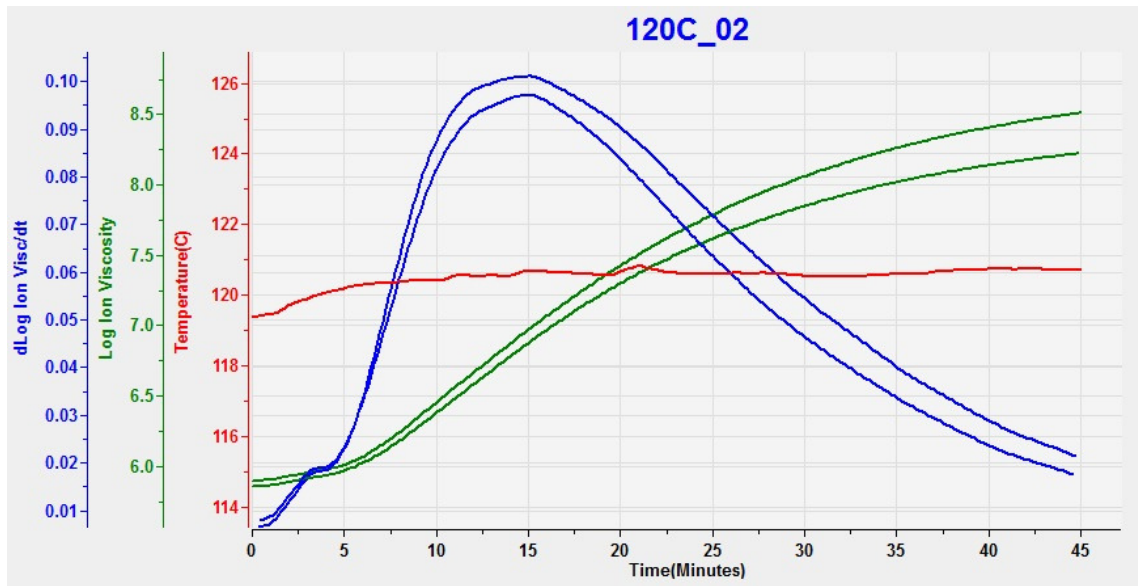
Figure 10-5
CFRP cure at 120 °C, 100 Hz and 1 kHz data
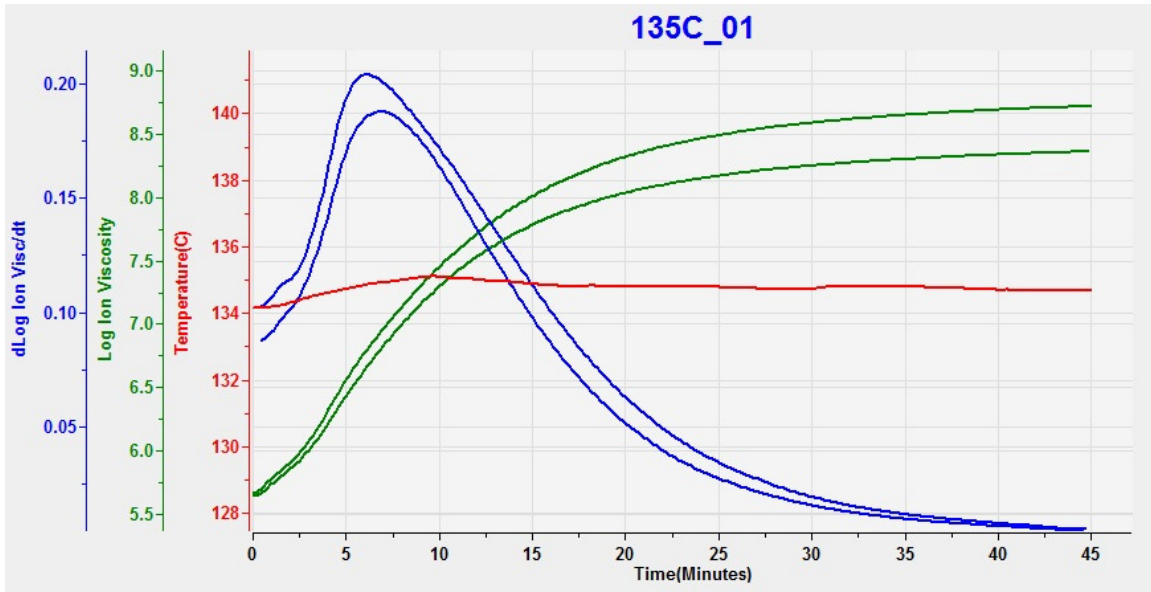
Figure 10-6
CFRP cure at 135 °C, 100 Hz and 1 kHz data
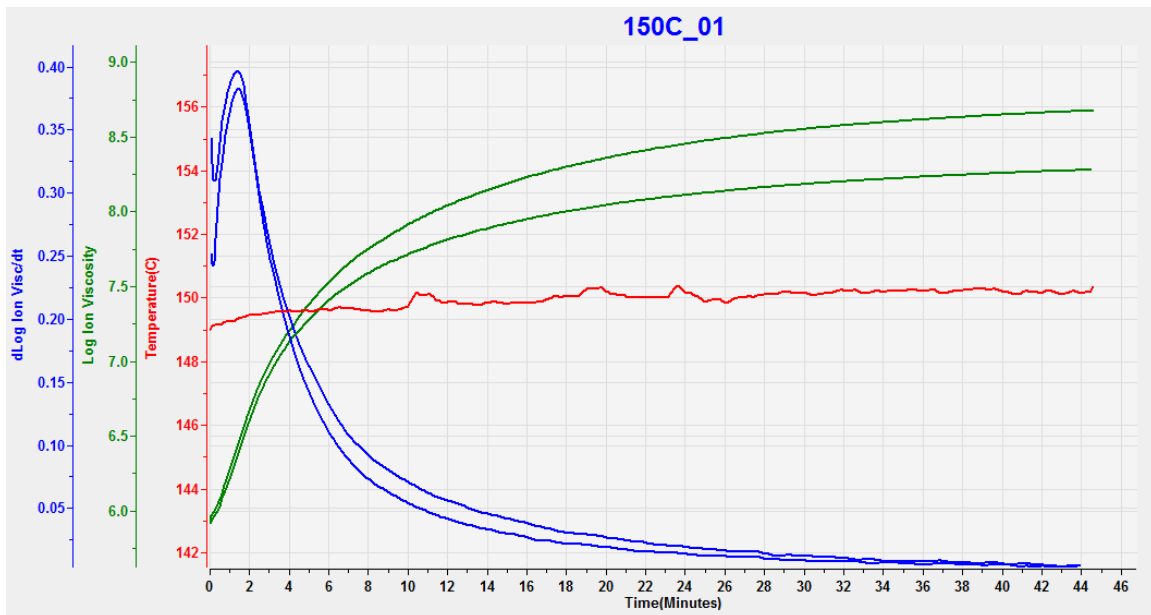
Figure 10-7
CFRP cure at 150 °C, 100 Hz and 1 kHz data
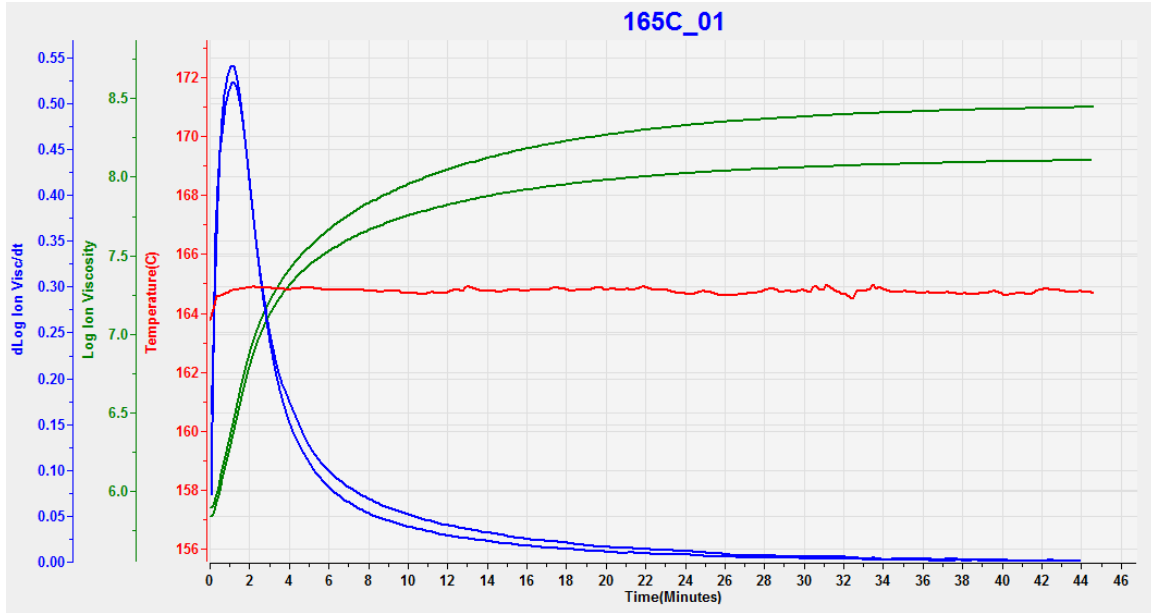
Figure 10-8
CFRP cure at 165 °C, 100 Hz and 1 kHz data

Figure 10-9 overlays log(*IV*) data for the cures at 120 °C, 135 °C, 150 °C and 165 °C. Figure 10-10 overlays slope data for these cures. As expected, higher processing temperatures result in faster cures, but the use of Critical points is necessary to quantify this relationship.
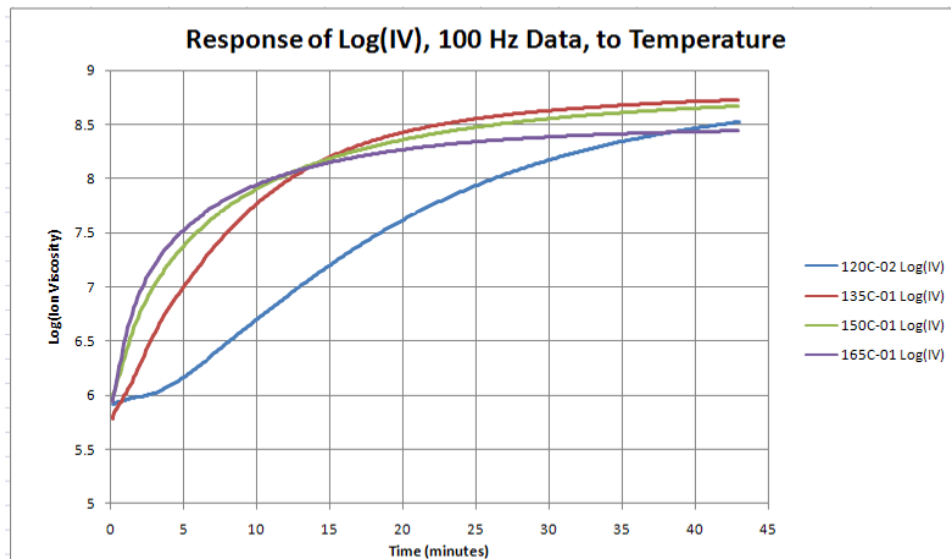
Figure 10-9
Log(*IV*) curves from isothermal cures at different temperatures
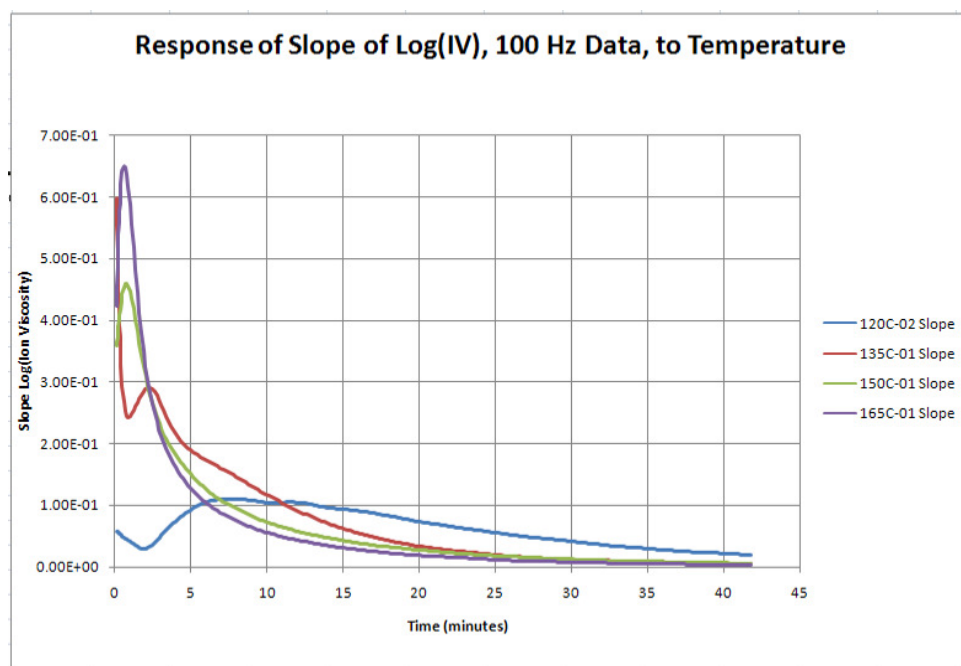
Figure 10-10
Slope curves from isothermal cures at different temperatures

Table 1 shows values for the time to reach maximum slope—CP(3)—and the level of this slope. The time to CP(3) should decrease with higher temperature because the reaction rate is faster. The level of CP(3) indicates the maximum reaction rate and both should increase with higher cure temperature.

Table 1 also shows the time to reach the end of cure—CP(4). For purposes of this analysis, a slope of 5.00 E-2 was arbitrarily chosen, but in practice the user must determine the slope to indicate end of cure based on the needs of the application. As expected, the time to reach CP(4) decreases as cure temperature increases.

Table 10-1
Effect of temperature on Critical Points

Cure Temp. (°C)	CP(1) Crit. Visc.		CP(2) Min. Visc.		CP(3) Max Slope		CP(4) Crit. Slope	
	Value	Time (min)	Value	Time (min)	Value	Time (min)	Value	Time (min)
120	---	---	---	---	8.96E-02	7.282	5.00E-02	26.453
135	---	---	---	---	2.90E-01	2.314	5.00E-02	16.603
150	---	---	---	---	4.58E-01	0.782	5.00E-02	13.612
165	---	---		---	6.50E-01	0.576	5.00E-02	11.970
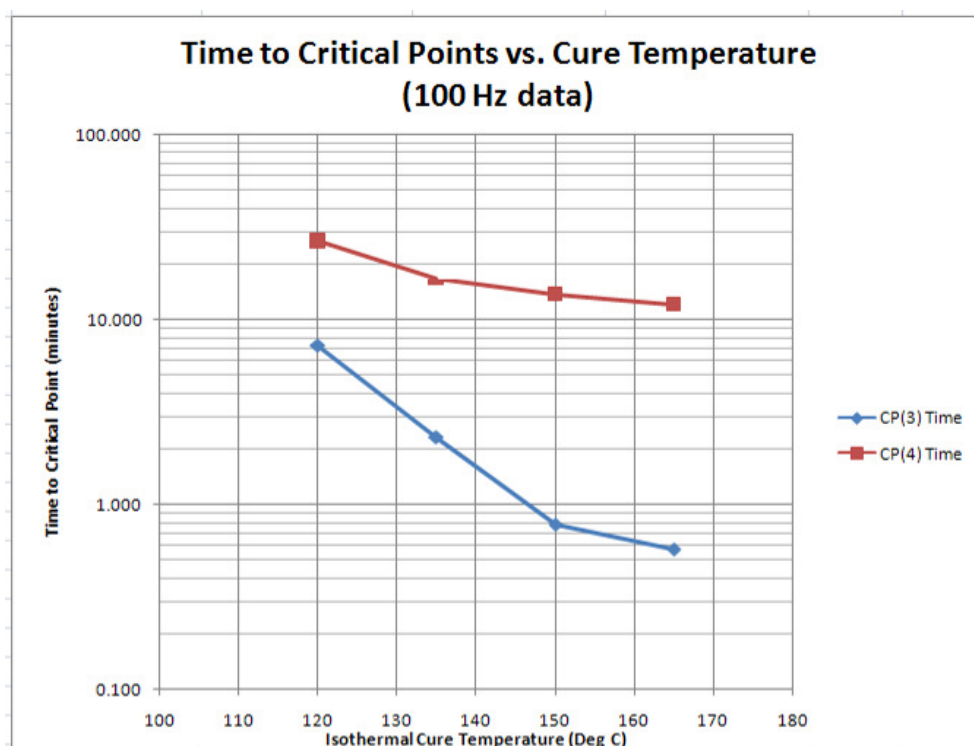
Figure 10-11
Time to Critical Points 3 and 4 vs. cure temperature

Figure 10-11 plots the time to CP(3) and CP(4), and shows how they decease with increasing cure temperature. In particular, note how the time to CP(3), the time to the point of maximum reaction rate, decreases exponentially with an increase in temperature. This indicates an Arrhenius relationship between reaction rate and temperature. The CP(3) data point at 165 °C deviates from a straight trend line of the lower temperatures, possibly because of limited accuracy in identifying CP(3) times that are less than one minute.

Figure 10-12 shows the level of CP(3)—the level of maximum slope—which indicates maximum reaction rate. Like the time to CP(3), the level of CP(3) shows an Arrhenius relationship with temperature. The data at 165 °C may depart from a straight trend line because of limitations in measurement accuracy for the fast reaction.
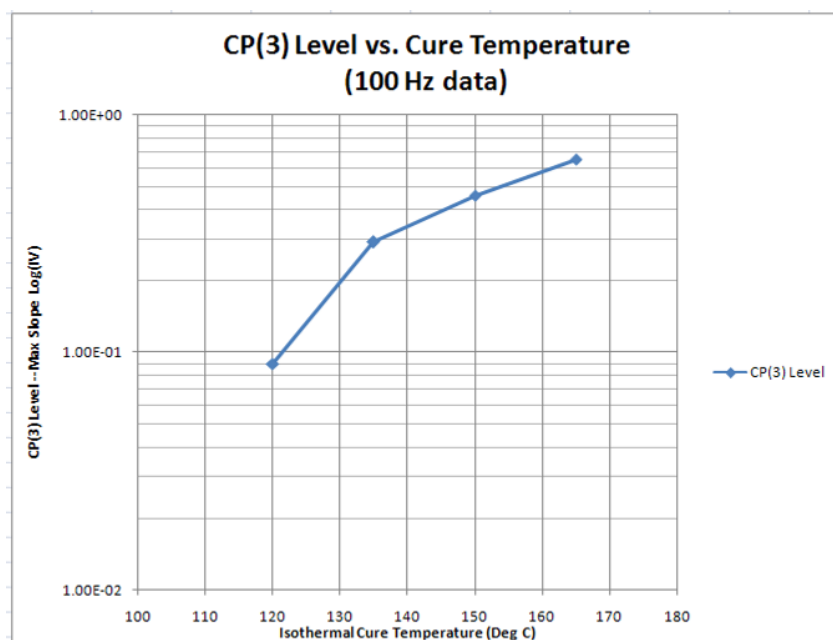
Figure 10-12
CP(3) level vs. cure temperature

Figure 10-13 plots the level of CP(3) vs. the time to reach CP(3). Accounting for measurement accuracy, the level of CP(3) increases exponentially with temperature while the time to CP(3) decreases exponentially with temperature.
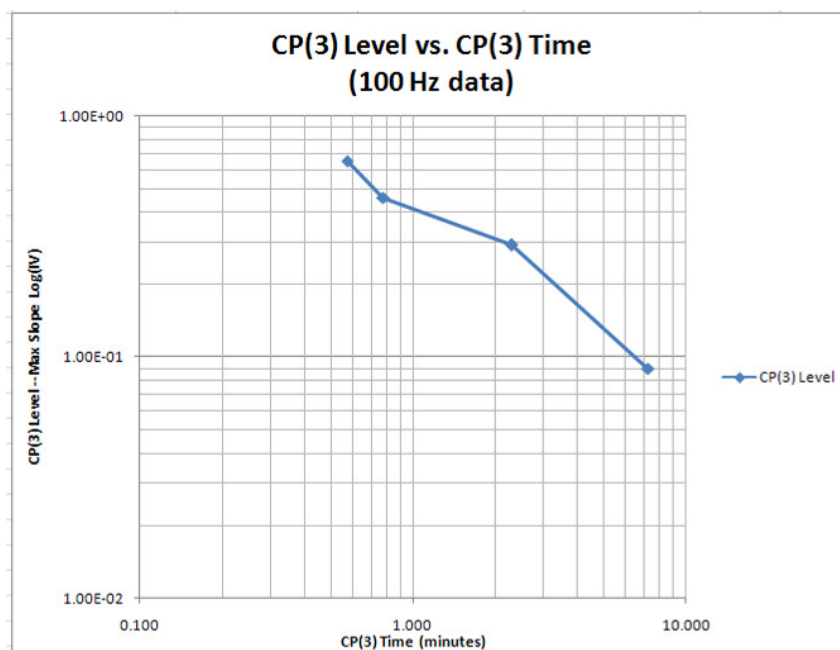
Figure 10-13
CP(3) level vs. CP(3) time

Conclusion

Dielectric measurements allow observation of the cure of thermosets in real time, and the extraction of Critical Points quantify the characteristics of the reaction. The carbon reinforced prepreg data of this report show that results are repeatable and consistent from sensor to sensor. Dielectric cure monitoring over temperatures from 120 °C to 165 °C clearly indicate the direct correlation between temperature and rate of cure.

Chapter 11—Measuring Degree of Cure with DEA

Introduction

   Data from dielectric cure monitoring (DEA) correlate with glass transition temperatures (T_g) obtained from differential scanning calorimetry (DSC). In many cases a linear relationship exists between log(ion viscosity) and T_g. Dielectric measurements can be converted to *Cure Index*, which is a reproducible indicator of the state of cure. For some materials, Cure Index closely follows the degree of cure, *α*, calculated by the DiBenedetto equation, which uses glass transition temperature information.

Ion viscosity and degree of cure

   For thermoset cure, the degree of cure, *α*, is a measure of the amount of reaction. Each bond releases a fixed amount of heat, and the degree of cure is defined as:

(eq. 11-1) $\alpha = \Delta H \, / \, \Delta H_R$

Where:

   ΔH = Total heat released
   ΔH_R = Heat of reaction

The degree of cure measures the total amount of bond formation, which is the *crosslink density*, and *α* therefore is useful for indicating physical state.

   During cure, log(*IV*) increases with crosslink density, which in turn is related to glass transition temperature. Ueberreiter and Kanig[1] reported that crosslink density is directly proportional to the change in T_g. Furthermore, the DiBenedetto[2] equation, below, relates T_g to the extent of conversion, or degree of cure:

(eq. 11-2) $$\frac{(T_g - T_{g0})}{(T_{g\infty} - T_{g0})} = \frac{\lambda \, \alpha}{(1 - (1 - \lambda) \, \alpha)}$$

Where:

   T_g = glass transition temperature
   T_{g0} = glass transition temperature at 0% cure
   $T_{g\infty}$ = glass transition temperature at 100% cure
   λ = experimentally derived parameter
   α = extent of conversion or degree of cure

   This chain of relationships implies a correlation between log(*IV*) and degree of cure. Published data of an isothermal epoxy cure shows the overlap between

log(resistivity) and T_g. In this test, T_g increased in proportion with log(resistivity), which is also log(IV), as shown in Figure 11-1.
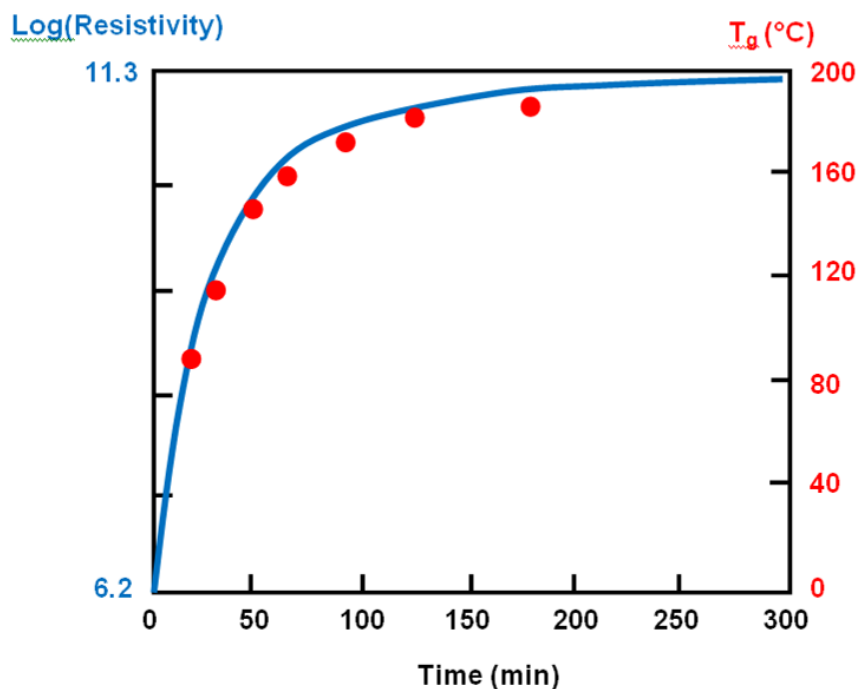

Figure 11-1
T_g and log(resistivity) vs. time during an epoxy cure (200 °C)[3]

For isothermal processing, over limited degrees of reaction, the following expression often applies between degree of cure, α, and ρ_{DC} (or ion viscosity):

(eq. 11-3) $\alpha = k \log(\rho_{DC}) + C$

In equation 11-3 both k and C are constants, and determining the degree of cure at a constant temperature is straightforward. For non-isothermal conditions, however, equation 11-3 cannot apply because resistivity decreases as temperature increases, even at a fixed degree of cure.

Figure 11-2 shows how resistivity varies with temperature for a particular epoxy resin. The dashed lines represent percentage degree of cure as determined by DSC. The solid lines approximate baselines for 0% and 100% degrees of cure.

Figure 11-3 shows the baselines alone, which can be used to determine glass transition temperature by linear interpolation of dielectric data.
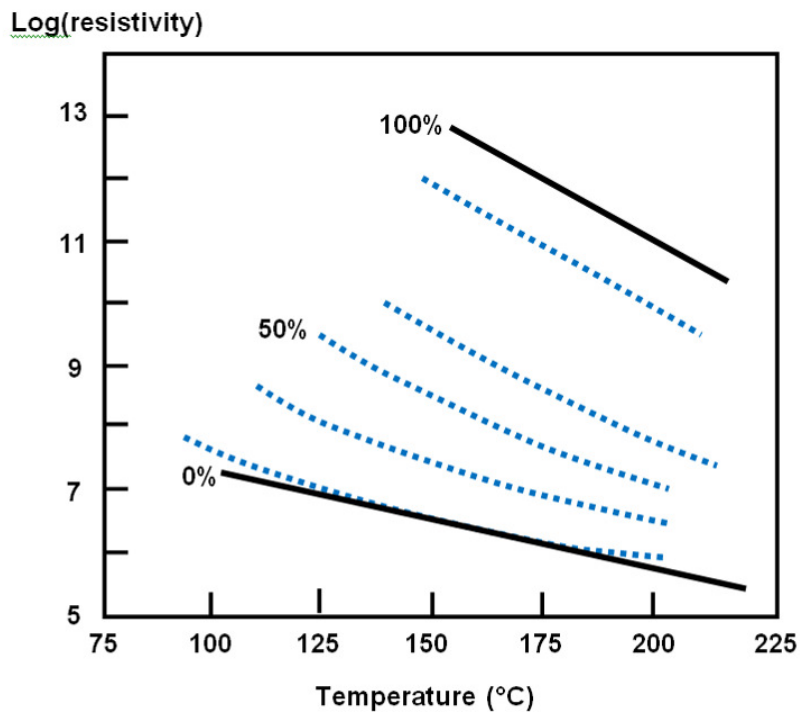
Figure 11-2
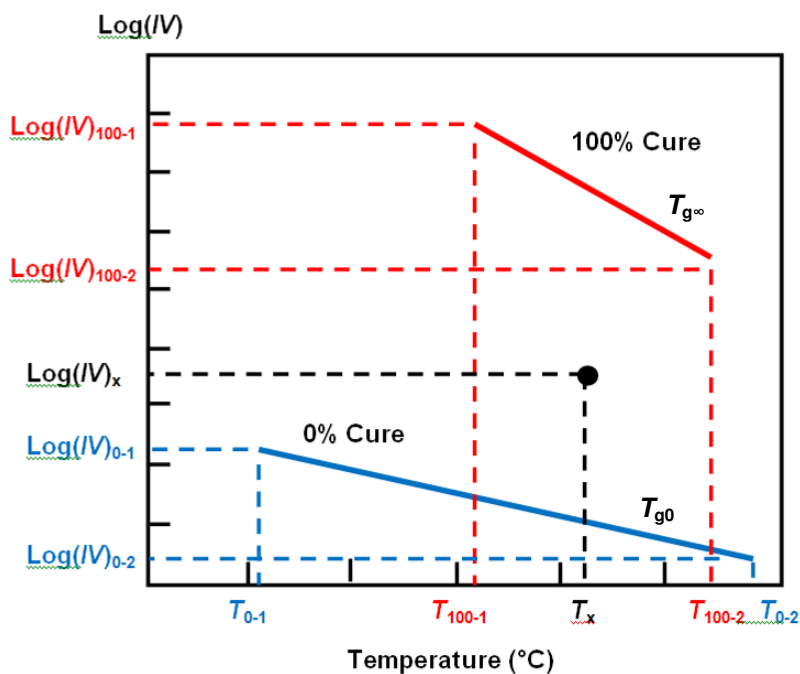**Variation in log(resistivity) with temperature for an epoxy[3]**

Figure 11-3
Baselines for determining T_g during non-isothermal cure

The 0% and 100% cure baselines are determined experimentally. Assuming a linear relationship between T_g and log(IV), the glass transition temperature, as a function of T_x and Log(IV)$_x$, is given by equation 11-4:

$$\text{(eq. 11-4)} \qquad T_g \ = \ T_{g0} + \ \frac{\text{Log}(IV)_x - \text{Log}(IV_0(T_x))}{\text{Log}(IV_{100}(T_x)) - \text{Log}(IV_0(T_x))} \ [T_{g\infty} - T_{g0}]$$

Where:

$\text{Log}(IV_0(T_x))$ $= m_0\,T_x + b_0$	(eq. of 0% baseline)
$\text{Log}(IV_{100}(T_x)) = m_{100}\,T_x + b_{100}$	(eq. of 100% baseline)
$m_0 \ = (\text{Log}(IV)_{0\text{-}1} - \text{Log}(IV)_{0\text{-}2})\,/\,(T_{0\text{-}1} - T_{0\text{-}2})$	(slope, 0% cure)
$m_{100} = (\text{Log}(IV)_{100\text{-}1} - \text{Log}(IV)_{100\text{-}2})\,/\,(T_{100\text{-}1} - T_{100\text{-}2})$	(slope, 100% cure)
$b_0 \ = \text{Log}(IV)_{0\text{-}1} - m_0\,T_{0\text{-}1}$	(y-intercept, 0% cure)
$b_{100} \ = \text{Log}(IV)_{100\text{-}1} - m_{100}\,T_{100\text{-}1}$	(y-intercept, 100% cure)

Using Figure 11-2 as a linear model for T_g, interpolation of dielectric data for non-isothermal cure of the epoxy results in calculated glass transition temperatures as shown in Figure 11-4.
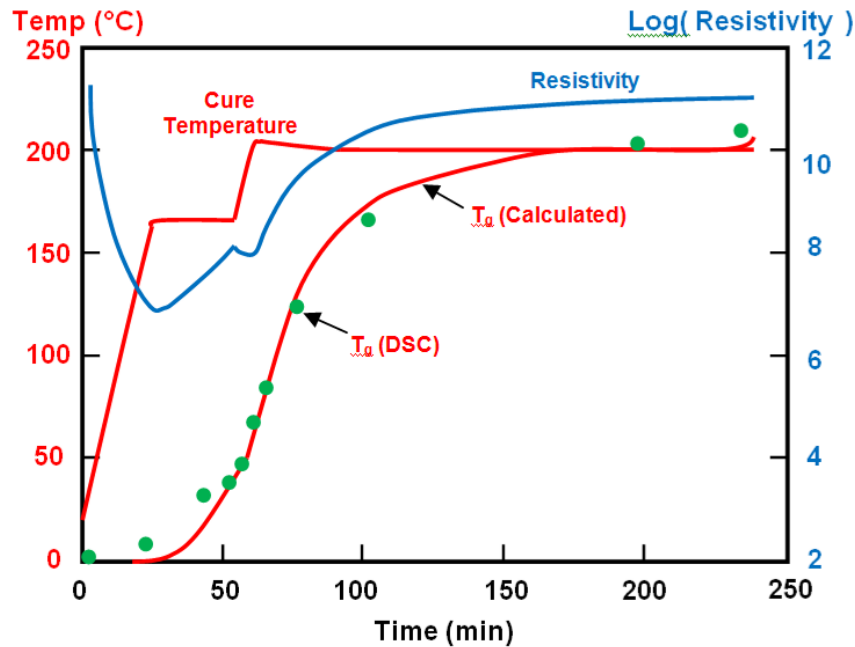

Figure 11-4
Calculated T_g during non-isothermal cure with linear T_g model[3]

For this particular material, glass transition temperatures measured by DSC show good agreement with values calculated from the linear T_g model.

Note that this model may not apply in the presence of multiple reactions, loss of reaction products or loss of solvents. Results also may not be consistent from sample to sample of the same material if variations in background ion level are too great. For most commercial or industrial thermosets, product composition is well controlled and differences in background ion concentration are typically not an issue.

Equation 11-4 may be rearranged to calculate *Cure Index*, which is a reproducible indicator of cure state that does not rely on information about glass transition temperature.

$$\text{(eq. 11-5)} \quad \text{Cure Index} = \frac{[T_{g\infty} - T_{g0}]}{[T_g - T_{g0}]} = \frac{\text{Log}(IV)_x - \text{Log}(IV_0(T_x))}{\text{Log}(IV_{100}(T_x)) - \text{Log}(IV_0(T_x))}$$

Figure 11-5 below shows the percentage Cure Index for the data of Figure 11-4.
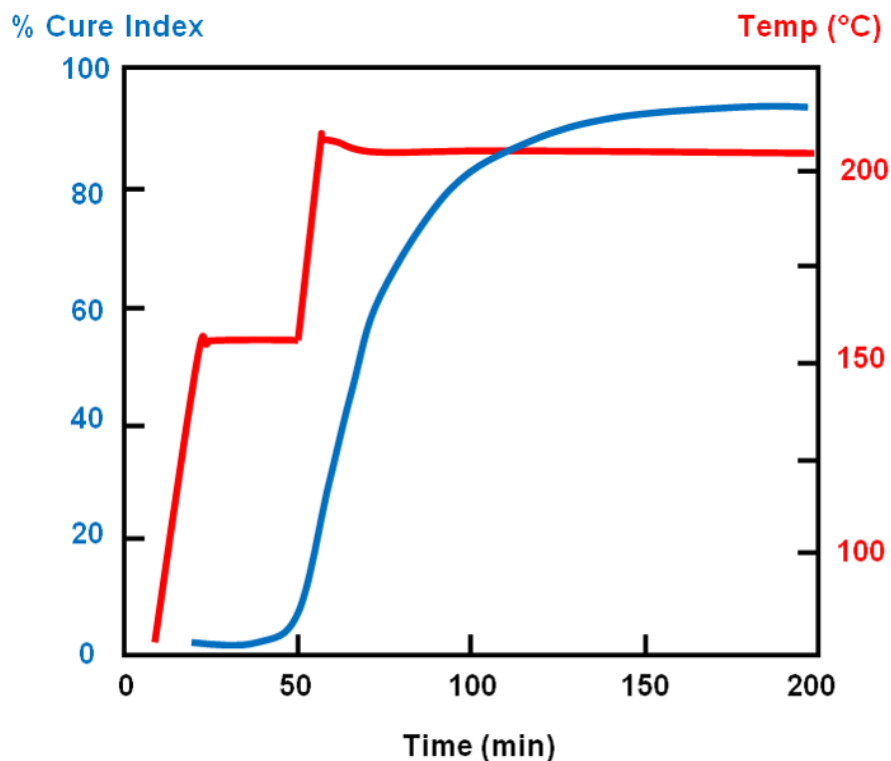
Figure 11-5
Percent Cure Index during non-isothermal cure with linear T_g model[3]

The DiBenedetto equation requires glass transition temperature information to determine degree of cure. If the experimental parameter $\lambda = 1$ for the DiBenedetto equation, then the expression reduces to equation 11-6.

(eq. 11-6)
$$\frac{[T_{g\infty} - T_{g0}]}{[T_g - T_{g0}]} = \alpha$$

In this case the degree of cure, α, expressed by equation 11-6 equals the Cure Index of equation 11-5. The term *Cure Index* was coined by D. R. Day[4] to distinguish it from *degree of cure*. Cure Index is a reproducible measure of cure state, although it may not exactly equal the degree of cure, depending on the value of λ. Nevertheless, Cure Index may still be sufficiently related to α to serve as a substitute to first order.

Example: Cure Index for thermoplastic polyimide imidization

Thermoplastic polyimide (TPI) is a class of materials synthesized from a polyamic acid (PAA) solution. Polyamic acid is a linear, long chain polymer that undergoes a condensation reaction at elevated temperature to become polyimide. This process produces water as a byproduct and is called *imidization*. Typically the precursor solution is B-Staged to remove solvents and begin the reaction.

Unlike thermosets, curing PAA does not crosslink. Polyimide has a much higher resistivity than PAA, however, and as a result dielectric cure monitoring can measure the conversion process. For one test, a thin layer of PAA[5] solution was applied to a dielectric sensor then heated to 150 °C to dry the solution and initiate imidization. Use of a thin coating was necessary for outgassing of evolved water.

This sample was cured isothermally until ion viscosity no longer changed. The process was repeated for temperature steps of 25 °C until the maximum of 300 °C. The plot of Figure 11-6 shows log(IV) and temperature for this test. Note that when temperature changes, ion viscosity decreases suddenly because of the temperature dependence described in Chapter 6 (*Ion Viscosity and Temperature*). Then ion viscosity increases again as more PAA converts to polyimide. The maximum degree of cure at each step increases with temperature, but is not readily apparent from the raw ion viscosity data.

The use of Cure Index provides a simple way to determine how the polyimide cure advances. While Cure Index may not necessarily be proportional to degree of cure, it does yield a reproducible and consistent measure of the conversion process. Figure 11-7 shows measurements of log(IV) for polymide at 0% cure, when it is entirely PAA, and for polyimide cured at 300 °C to guarantee 100% cure. Instead of a linear model, a more accurate thermal model of ion viscosity (see Chapter 6) was used to calculate 0% and 100% baselines.
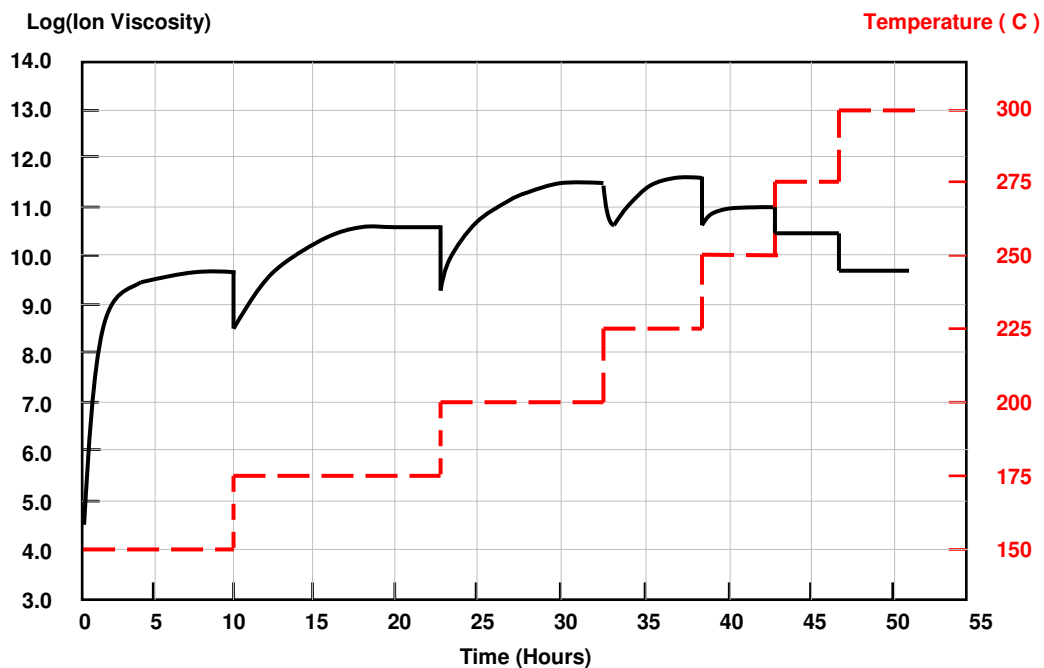
Figure 11-6
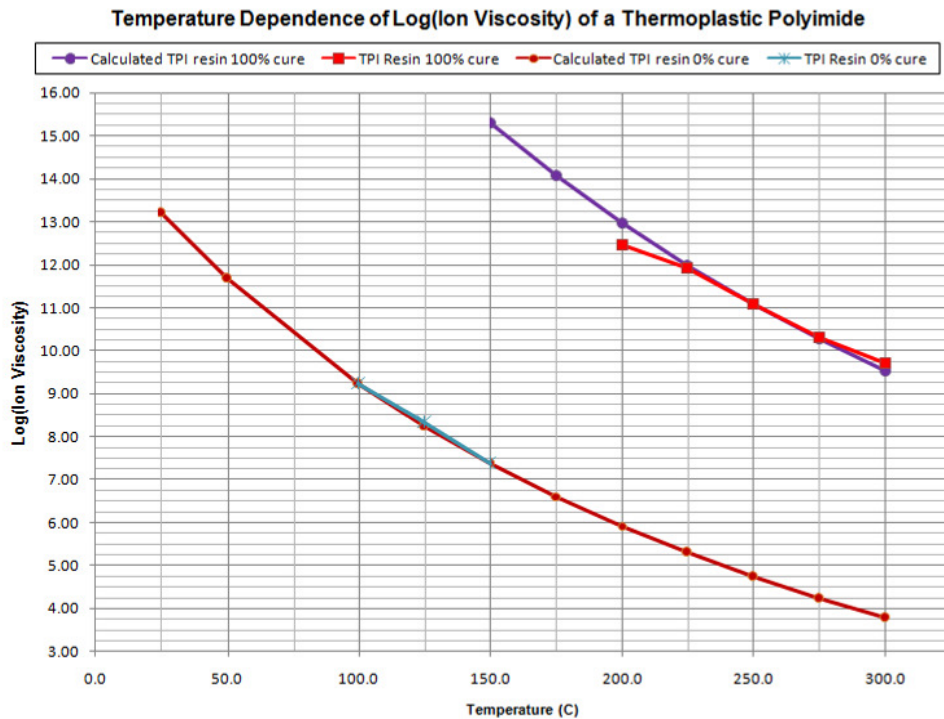**Thermoplastic[5] polyimide cure**

Figure 11-7
Experimental and calculated baselines for 0% and 100% TPI[5] cure

Figure 11-8 shows 0% and 100% Cure Index baselines as well as contours for 25%, 50% and 75% Cure Index, as calculated by interpolation. The end state value of log(IV) at each temperature step is plotted against these contours. The Cure Index for these data show that this polyimide has essentially reached 100% cure when processed at 225 °C.
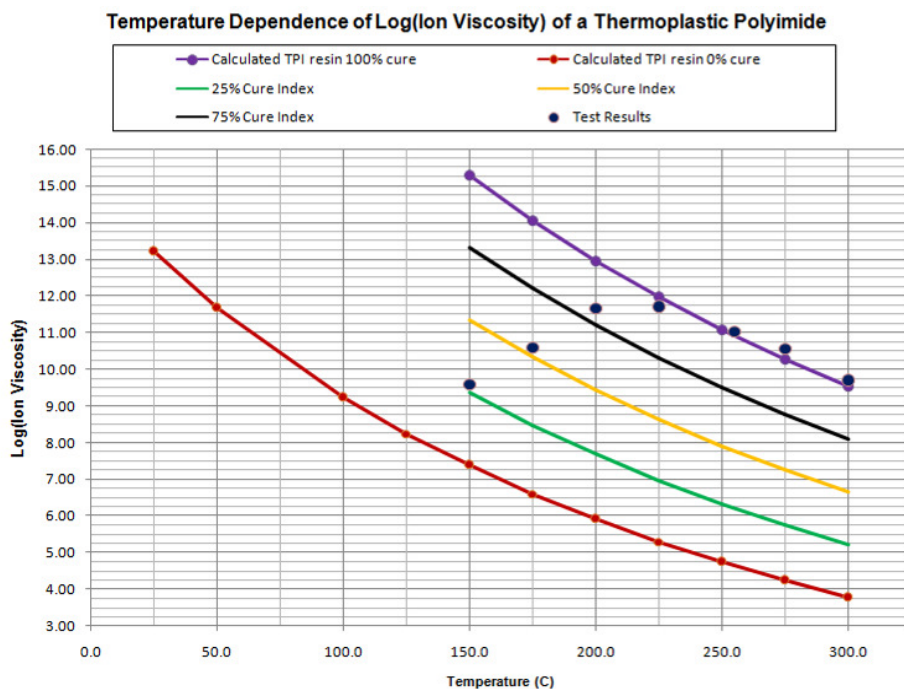

Figure 11-8
Thermoplastic polyimide[5] maximum cure state at isothermal cure temperature

Figure 11-9 shows the maximum Cure Index attainable at various process temperatures, as determined by the data of Figure 11-8. Note that values of Cure Index greater than 1.0 are the result of measurement noise or experimental error. The Cure Index data of Figure 11-9 are useful for determining optimum cure temperature for a particular application. It is not necessary to process this formulation of thermoplastic polyimide at 300 °C to achieve 100 % cure; 225 °C is sufficient. Even lower process temperatures may be suitable, depending on the application.

Before relating Cure Index to degree of cure, it is important to validate this information with other analytical methods, such as differential scanning calorimetry. However, if one assumes Cure Index is proportional to degree of cure, then Cure Index also is a means of estimating the amount of cure remaining before reaching 100% cure, and therefore the amount of water remaining to be released.
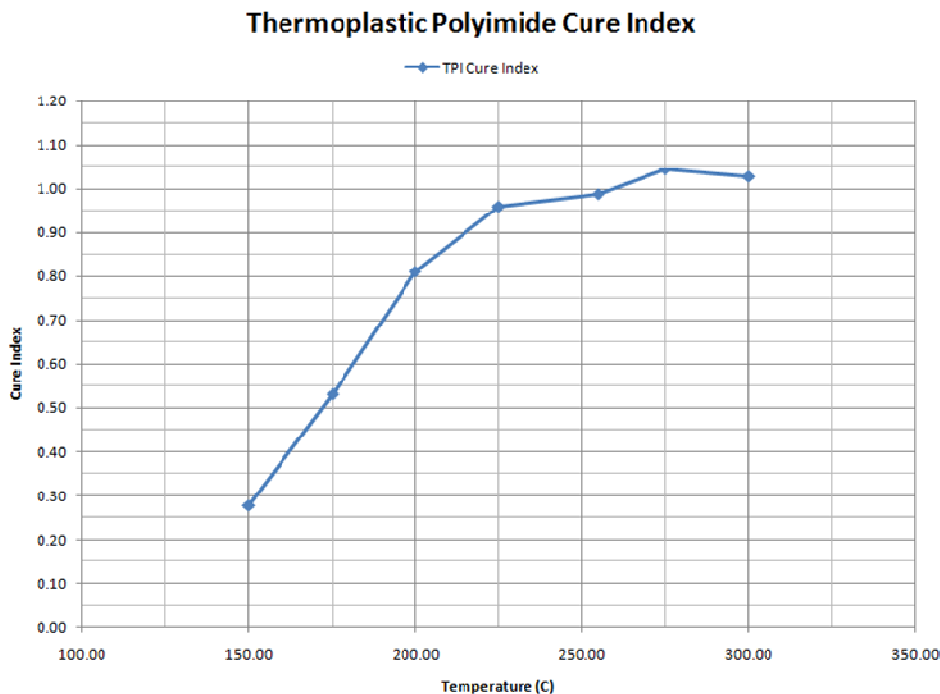
Figure 11-9
Thermoplastic polyimide[5] maximum Cure Index at processing temperature

Conclusion

Dielectric cure monitoring, or DEA, can infer T_g during cure by using temperature and ion viscosity data with baseline information about glass transition temperatures. The resulting T_g can then be used in the DiBendetto equation to determine the degree of cure. *Cure Index* is a simpler method that can yield the same degree of cure as the DeBenedetto equation in the case of $\lambda = 1$. Even though Cure Index may not always equal degree of cure, Cure Index is a convenient alternative measure of cure state that does not require glass transition temperature information.

References

1. Ueberreiter, K.; Kanig, G., *Journal of Chemical Physics*, **18**, 399 (1950).

2. Pascault, J.P. and Williams, R.J.J., "Glass transition Temperature vs. Conversion Relationships for Thermosetting Polymers," *J. of Polymer Science, Part B:Polymer Physics*, **28**, 85-95 (1990).

3. Day, D.R., "Dielectric Properties of Polymeric Materials," Micromet Instruments, (1987).
(Figures have been redrawn for clarity)

4. Day, D.R., "Dielectric Determination of Cure State During Non-Isothermal Cure," *Polymer Engineering and Science*; **29(5)**:334-338, (August 2004).

5. Proprietary thermoplastic polyimide adhesive, derived from FM901 polyamic-acid polymer solution, provided by Fraivillig Technologies Company.

Chapter 12—Dielectric Measurements During Post-Cure

Introduction

Large composite structures such as an airplane wing are processed in autoclaves or molds that apply pressure to form the part until it has cured. The need to maximize use of this equipment may require cycling material through it as quickly as possible, and often a part is removed as soon as it has hardened enough to retain its shape. Afterwards, it may undergo post-cure in an oven for several hours to several days. During this time cure continues at elevated temperature until the composite material has hardened further or achieved other desired properties.

Dielectric measurements can determine the state of the thermoset during post-cure and corroborate when it has reached a specified condition. Because ion viscosity depends on both the degree of cure *and* temperature, conventional dielectric cure monitoring is used under isothermal conditions to eliminate the temperature variable. During post-cure, however, oven temperature may fluctuate significantly, complicating dielectric measurements. Nevertheless, it is possible to take advantage of these fluctuations to get useful information.

Ion viscosity change during post-cure

As a material cures, the increase of ion viscosity with time is easily visible in an isothermal environment, where only the ongoing cure changes dielectric properties. In an environment where temperature also changes, isolating the effect of varying temperature is necessary to determine the effect of continuing cure. Figure 12-1 illustrates the post-cure of a thermoset in an oven. A thermocouple measures the temperature of the sample. Attached to opposite sides of the sample, electrodes form a parallel plate sensor that measures dielectric properties. For other situations, an interdigitated dielectric sensor may be coated with resin or be embedded in the material under test (MUT).
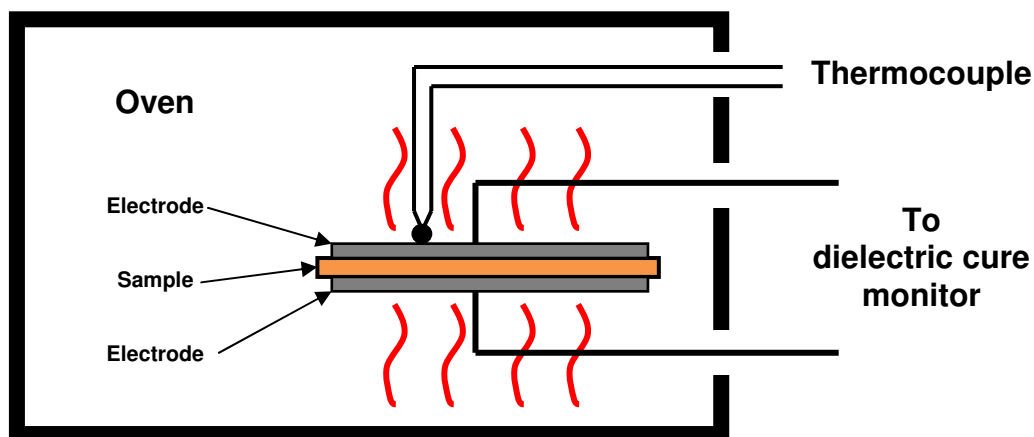

Figure 12-1
Post-cure of a thermoset in an oven

Figure 12-2 shows the ion viscosity of a silicone tube measured with parallel plate electrodes in an oven. For this sample, as for thermoset materials in general, higher temperature decreases ion viscosity and lower temperature increases ion viscosity (See Chapter 6—Ion Viscosity and Temperature).
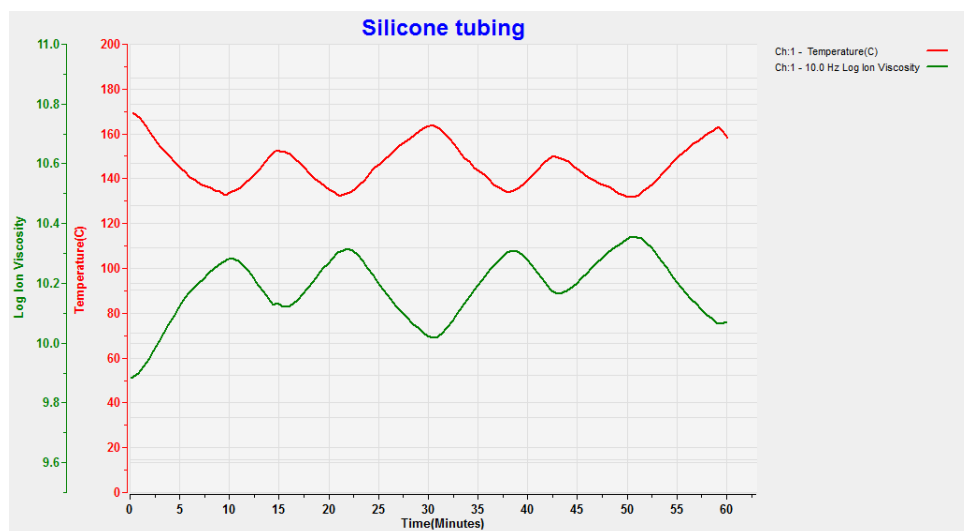
Figure 12-2
Post-cure of a silicone in oven with temperature fluctuation

Plotting ion viscosity against temperature presents the data as a series of "orbits" as shown in Figure 12-3. The shape of the orbit indicates whether cure is present. In the absence of cure, the orbit traces the same trajectory as temperature changes repetitively. Ongoing cure causes the orbit to change with time as ion viscosity increases.
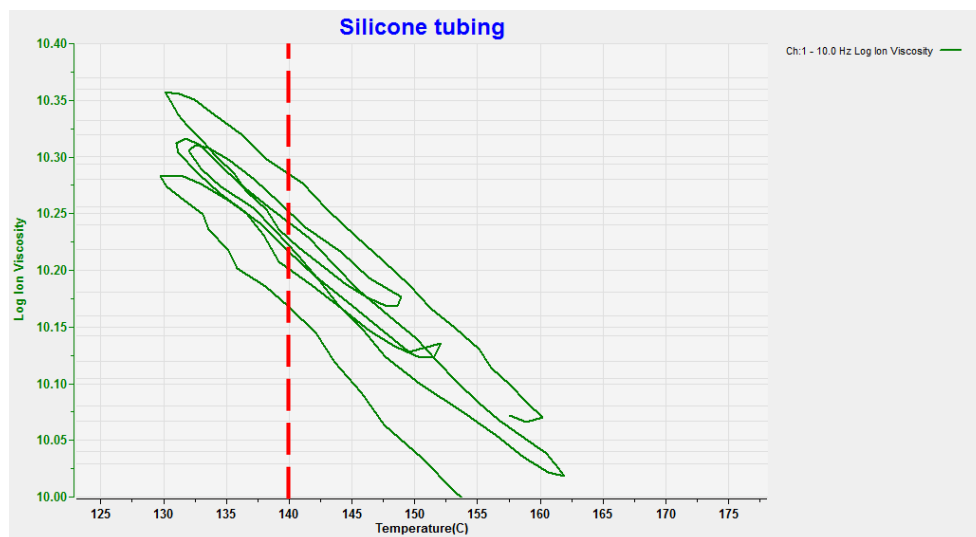
Figure 12-3
Log(*IV*) of silicone tubing sample vs. temperature

When oven temperature increases, thermal lag may cause the bulk of the sample to be slightly cooler than the surface, resulting in ion viscosity measurements that are higher than expected. Conversely, when oven temperature decreases, the bulk of the sample may be slightly warmer than the surface, resulting in ion viscosity measurements that are lower than expected. Other factors such as the exact nature of the thermal contact between the thermocouple and the sample, the sample's thermal conductivity and the location of the heating source may affect this relationship. To account for thermal lag, the average log(IV) from rising and falling temperatures should give a value that better represents the actual ion viscosity.

Figure 12-4 shows log(IV) of the silicone tubing at 140 °C. The log(IV) data has been normalized to a value of 1.0 at time $t = 0$. From the slope of the curves, it is clear that ion viscosity increased during this time, indicating that the silicone continued to cure.
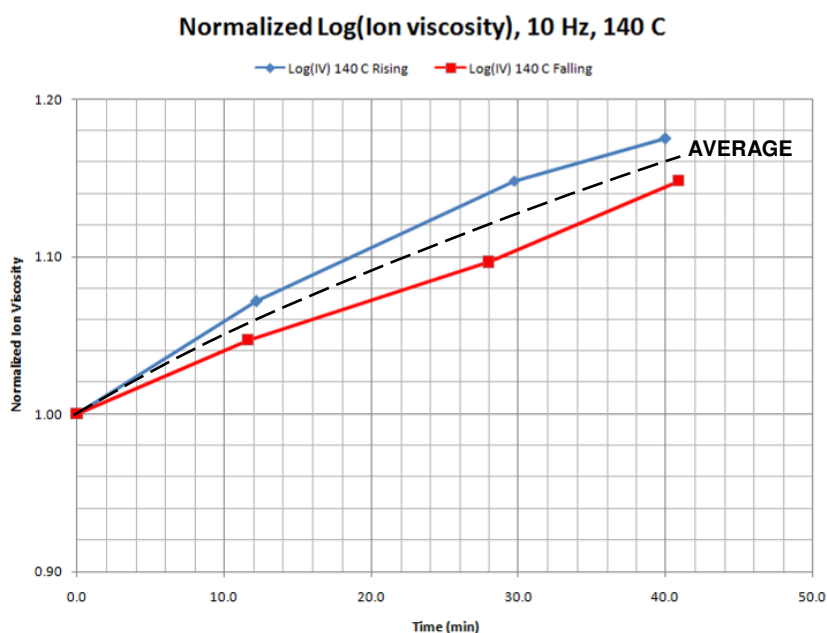

Figure 12-4
Log(IV) at 140 °C, normalized (data from Figure 11-2)

Post-cure of an epoxy resin

For the fabrication of large structures, the manufacturer of an epoxy resin recommends initial cure at temperatures of 40 °C to 50 °C. Processed at these relatively low temperatures, the epoxy has a low degree of cure, and physical properties such as hardness and glass transition temperature (T_g) are inadequate for the finished product. Consequently, the manufacturer also specifies post-cure at elevated temperature to advance the degree of cure and increase T_g and hardness.

Figure 12-5 shows the ion viscosity of this epoxy, measured with a 1 Hz excitation by a dielectric sensor. After 60 minutes at 50 °C, the degree of cure has reached the maximum amount possible for this temperature. The reaction has essentially stopped, indicated by the near zero slope of ion viscosity. The glass transition

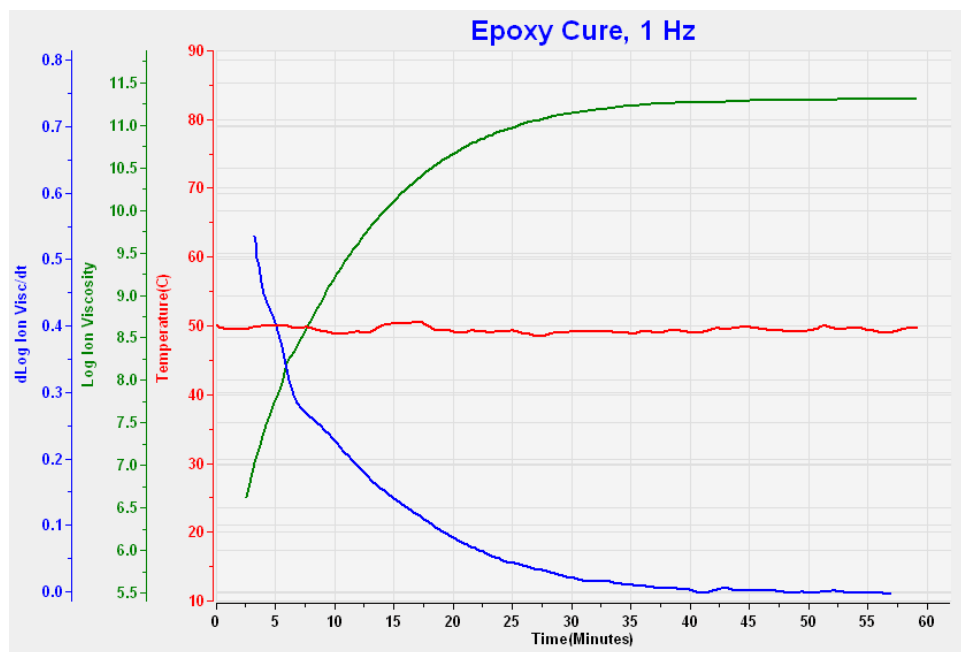temperature is still relatively low and the epoxy is solid but distinctly rubbery at room temperature.

Figure 12-5
Cure of an epoxy at 50 °C

Figure 12-6 shows the temperature and ion viscosity of this epoxy during post-cure. Although the oven was nominally set to 70 °C, the actual temperature of the sample varied greatly and ion viscosity varied in turn. It is possible to identify additional cure by an increase in ion viscosity at points of constant temperature. Figure 12-7 shows the result at 67 °C, which was chosen to provide data over as much time as possible. The ion viscosity increased at first then became constant after about 100 minutes. After this time the epoxy did not cure any further.

Dielectric cure monitoring is effective for determining the cure state of a thermoset. When temperature varies, care must be taken to observe the behavior of ion viscosity at times of fixed temperature. Using this procedure during post-cure, it is possible to monitor the change in degree of cure. By identifying when additional cure has ended, a part can be removed from post-cure as soon as possible, increasing throughput during manufacturing.
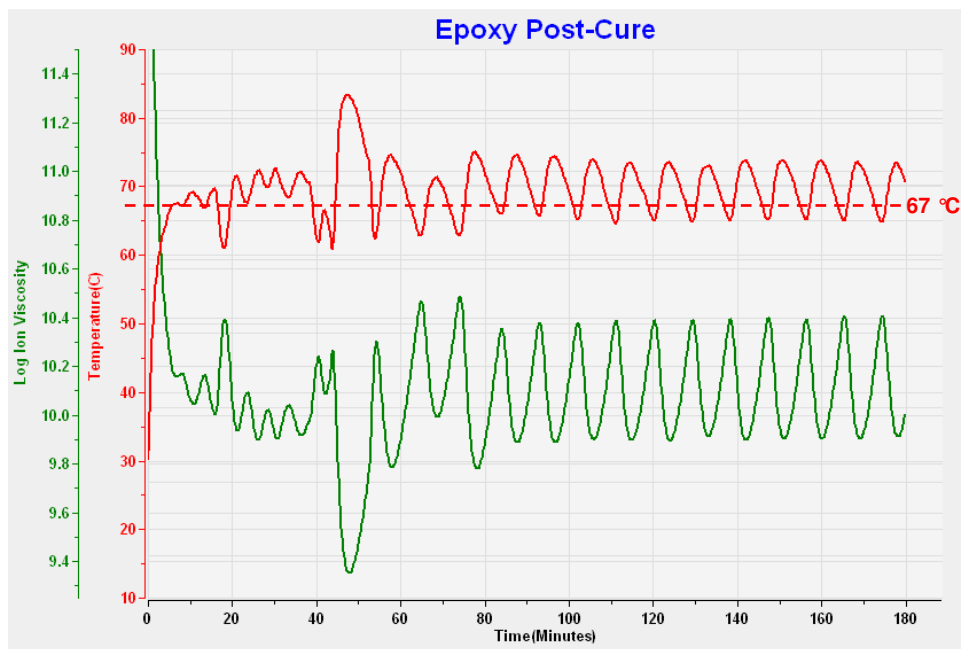
Figure 12-6
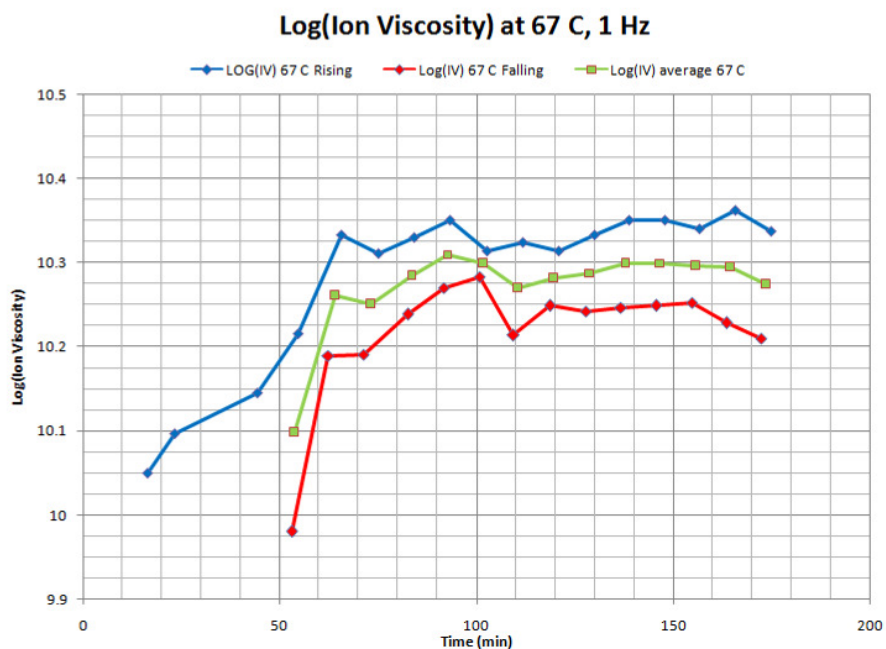**Post-cure of an epoxy in oven with fluctuating temperature**

Figure 12-7
Log(IV) at fixed temperature

Chapter 13—Dielectric Measurement Techniques

Introduction

Dielectric instrumentation measures the conductance G (or resistance R) and capacitance C between a pair of electrodes at a given frequency. The Material Under Test (MUT) between a pair of electrodes can be modeled as a conductance in parallel with a capacitance, as shown in Figure 13-1.
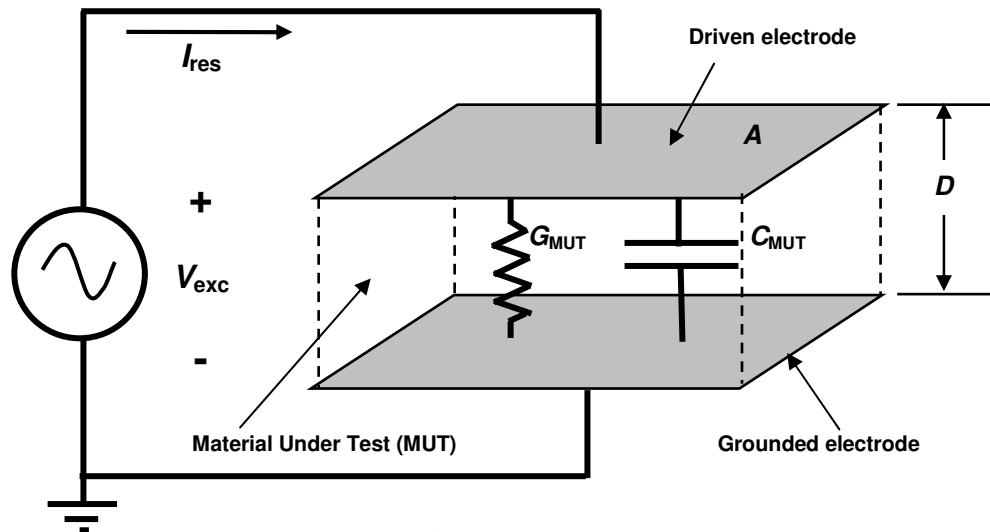

Figure 13-1
Electrical model of dielectric Material Under Test
(Grounded electrode configuration)

Grounded electrode configuration

Figure 13-1 also happens to depict a grounded electrode configuration for measuring the dielectric response. Note that one of the electrodes shares the ground of V_{exc}. An AC excitation voltage V_{exc} is applied between a pair of parallel plate electrodes, and the response current I_{res} is measured. Several methods exist for measuring current, but they all involve passing the current through a component such as a resistor, hall effect device, inductor or capacitor. The voltage induced across the component is measured and current is calculated from the component transfer function.

The amplitude of this current, and its phase shift relative to the excitation signal, are determined by the capacitive and conductive currents. The amplitude of the current and phase relationship between V_{exc} and I_{res} provide the information to calculate admittance Y, as shown in Figure 13-2.
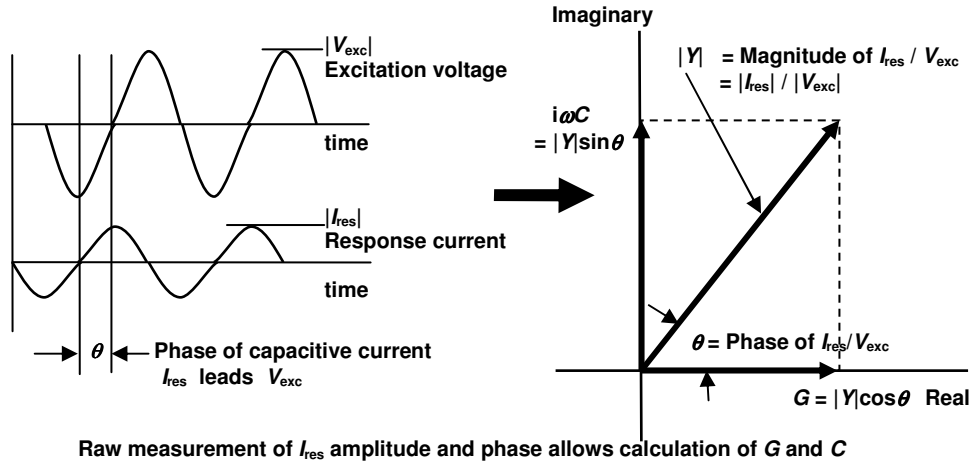
Raw measurement of I_{res} amplitude and phase allows calculation of G and C

Figure 13-2
Signal relationships for grounded electrode configuration

Y, and therefore the conductance G and capacitance C, of the MUT is calculated by equation 13-1:

(eq. 13-1) $Y_{MUT} = G_{MUT} + i\omega C_{MUT} = I_{res} / V_{exc}$

where:

I_{res}	= AC current through MUT	(a complex number, amps)
V_{exc}	= AC voltage across MUT	(a complex number, volts)
C_{MUT}	= Capacitance of MUT	(a real number, Farads)
G_{MUT}	= Conductance of MUT	(a real number, ohms^{-1})
f	= Excitation frequency	(Hz)
ω	= $2\pi f$	(angular frequency, radians/sec)

If the electrode A/D ratio is known, then the dimensionless material properties of σ /ε_o and relative permittivity ε' can be calculated from equations 13-2 and 13-3, as shown in Figure 13-3.

(eq. 13-2) $\sigma /\varepsilon_o = G / (\varepsilon_o A/D)$

(eq. 13-3) $\varepsilon' = C / (\varepsilon_o A/D)$

where:

$\varepsilon_0 = 8.85 \times 10^{-14}$ F/cm   (permittivity of free space)

After dividing by *A/D* ratio and ε_0, *G* and *C* reduce to σ/ε_0 and relative permittivity ε'
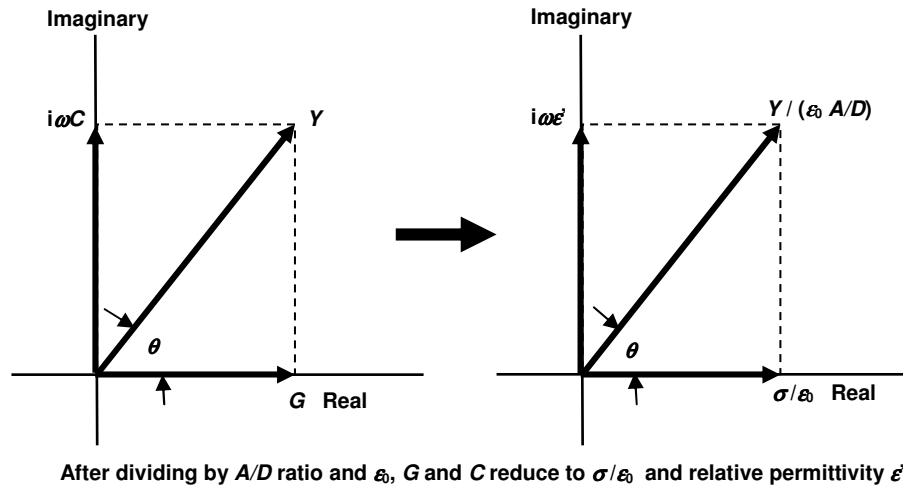
Figure 13-3

In most implementations, the current through the MUT passes into the virtual ground of a current-to-voltage converter, as shown in Figure 13-4. An instrument can measure the voltage output, V_{out}, and current I_{res} can be calculated from the known value of R_{load}. Finally, from the amplitude of I_{res} and the phase of I_{res} relative to V_{exc}, the capacitance and conductance of the material between the electrodes can be calculated from equation 13-1.
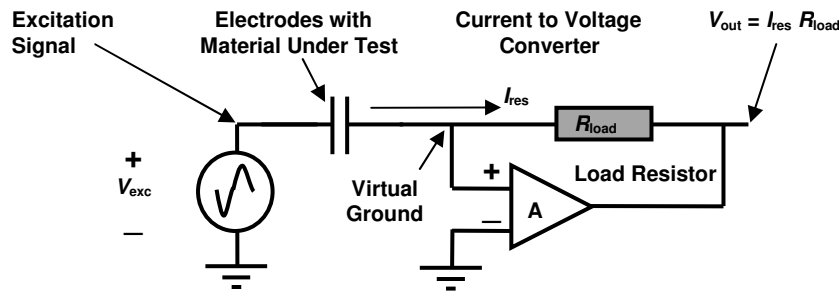
Figure 13-4
Current-to-voltage conversion of I_{res}

While simple, the circuit configuration of 13-4 has the disadvantage of low capacitive signal at low frequencies, and low conductive signal for highly insulating materials. These conditions can and do occur in thermosets at the end of cure, resulting in increased noise and reduced measurement accuracy during that period.

Kelvin (four-wire) connection

The circuit of Figure 13-4 can be modified to exclude the effect of wire resistance by using a Kelvin connection, as shown in Figure 13-5. As in Figure 13-4, a current-to-voltage converter outputs a signal for measurement of the current through the MUT. By Ohm's law, current I_{res} through wire resistances produces voltage drops that reduce the response voltage V_{res} across the electrodes.

In a Kelvin connection, a differential amplifier with high input impedence measures the voltage across these electrodes, using leads that pass no current and therefore produce no voltage drop from the wire resistance. With V_{res} and $I_{res,}$ it is possible to calculate the capacitance and conductance of material between the electrodes using the following relationship:

(eq. 13-4) $$Y_{MUT} = G_{MUT} + i\omega C_{MUT} \;=\; I_{res} \,/\, V_{res}.$$
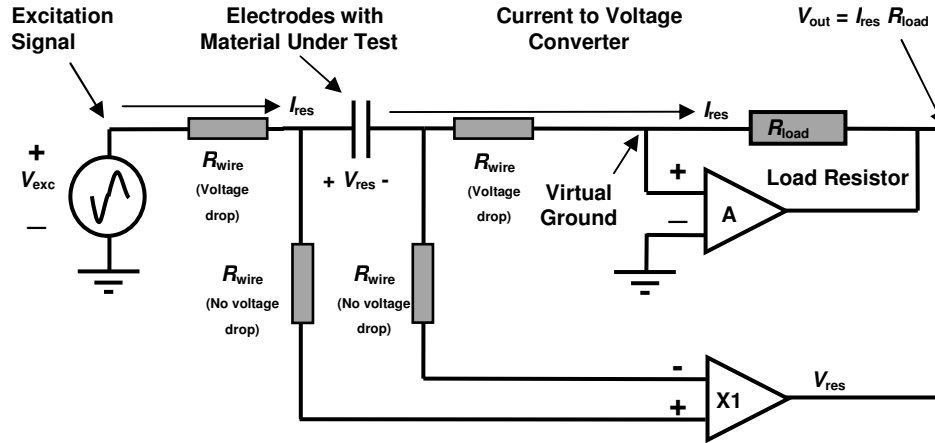

Figure 13-5
Kelvin (4-wire) connection for dielectric measurements

A Kelvin connection requires four wires and an extra amplifier, and is more complex than the configuration of Figure 13-4. It is most useful when the resistance being measured is small and comparable to the wire resistances. For example, 28 AWG wire has a resistance of 64.9 mΩ/ft (212.9 mΩ/m). A 20-foot cable has 40 feet of wire (20 feet to the electrode and 20 feet from the electrode), for a total resistance of 2.6 Ω. For a measurement error of 1%, the MUT must have a resistance of about 260 Ω across the electrodes.

For typical dielectric cure monitoring applications, the resistance of material on a sensor is on the order of 100,000 Ω or greater. Without a Kelvin connection, the error from a 20-foot cable to the sensor is 2.6 Ω / 100,000 Ω = 2.6 x 10^{-5} = 0.0026%. Thus, the extra complexity and cost of the Kelvin connection is difficult to justify for dielectric cure monitoring.

Floating electrode configuration

Dielectric measurements can also be made by driving one electrode with an AC excitation voltage without grounding the second electrode, also known as the floating electrode. This floating electrode configuration is shown in Figure 13-6. Note the load capacitor C_{load} between the floating electrode and ground.
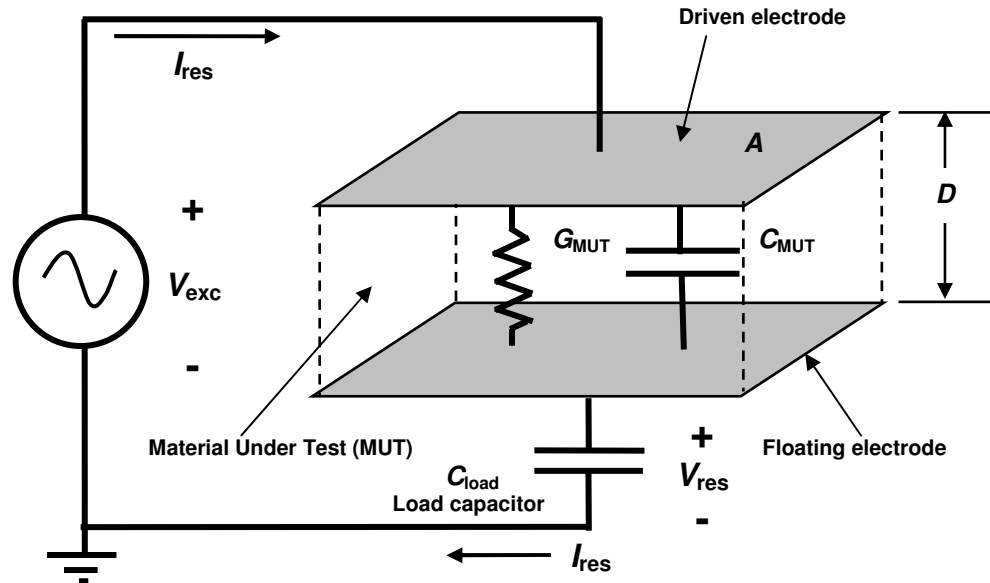

Figure 13-6
Electrical model of Material Under Test
(Floating electrode configuration)

The response voltage, V_{res}, across C_{load} depends on the load capacitance as well as the conductance and capacitance of the MUT. This load capacitance integrates current I_{res} to produce a large signal at low frequencies while also reducing noise. In effect, the current I_{res} is measured by the voltage it creates across the load capacitance, similar to the way the current-to-voltage converter of Figure 13-4 creates a voltage across a load resistance.

In practical implementations, a x1 amplifier buffers the voltage of the floating electrode, as shown in Figure 13-7. This buffer prevents cable capacitances from affecting the floating electrode and the response signal. The buffer also drives a reproduction of the response signal through cabling to the instrumentation.
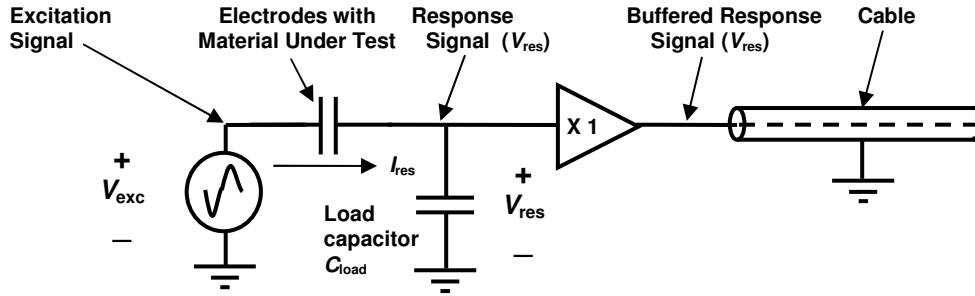
Figure 13-7
Floating electrode configuration

The output of the buffer is V_{res}, which has an amplitude that is attenuated and a phase that is shifted relative to V_{exc}. With a known load capacitance, the response amplitude and phase can be used to calculate the capacitance and conductance of the material between the electrodes. The load capacitance collects and integrates the current I_{res} through the MUT. As a result, the floating electrode configuration produces a larger signal with less noise compared to current to voltage conversion with a resistor. The advantages of the floating electrode configuration become especially apparent when making measurements in highly insulating materials at the end of cure.

Due to the added load capacitor, the equations to obtain conductance and capacitance for the floating electrode configuration are more complex than for the grounded electrode configuration. To span a wide dynamic range, the attenuation of the response signal is often expressed as "gain" on a logarithmic scale, as given by equation 13-5.

(eq. 13-5) $\qquad Gain \text{ (dB)} = 20 \log_{10}(|V_{res}| / |V_{exc}|)$

The gain and phase of the response can be plotted in Gain-Phase space as shown in Figure 13-8. The use of Gain-Phase space is convenient for charting the changing response for curing thermosets, and provides insight into the state of cure.
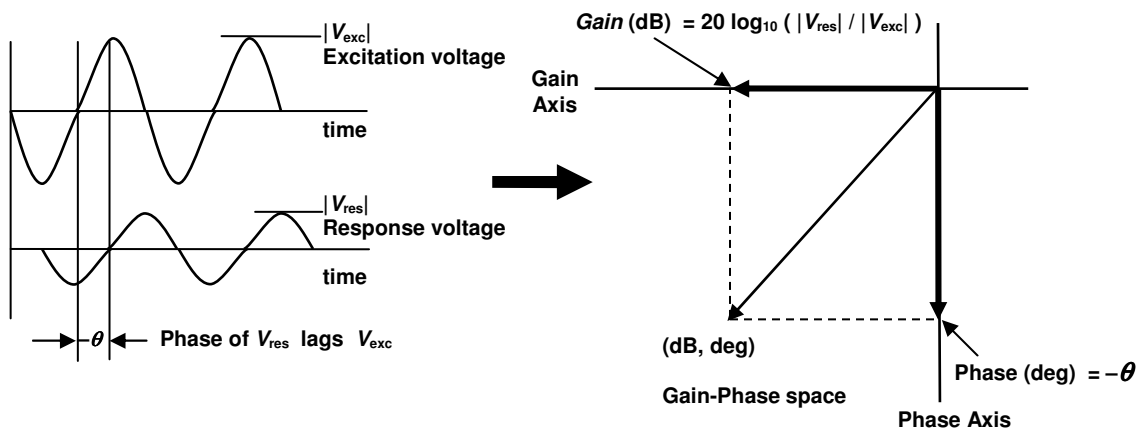

Figure 13-8
Signal relationships for floating electrode configuration

Given *gain* (dB), phase θ (deg), frequency f (Hz) and C_{load} (farad), conductance and capacitance for the floating electrode configuration can be calculated as follows:

(eq. 13-6) $$| V_{\text{res}} / V_{\text{exc}} | = 10^{(Gain/20)}$$

(eq. 13-7) $$A = \cos(-\theta) / | V_{\text{res}} / V_{\text{exc}} |$$

(eq. 13-8) $$B = \sin(-\theta) / | V_{\text{res}} / V_{\text{exc}} |$$

(eq. 13-9) $$G_{\text{tot}} = G_{\text{MUT}} = (2\pi f \; C_{\text{load}} \; B) / ((A - 1)^2 + B^2)$$

(eq. 13-10) $$C_{\text{tot}} = (C_{\text{load}} (A - 1)) / ((A - 1)^2 + B^2)$$

G_{tot} (G_{MUT}) is the total conductance between the electrodes. C_{tot} is the total capacitance between the electrodes, including any stray, or base, capacitance contributed by various sources. *Note that this base capacitance must be subtracted from C_{tot} before further calculation to obtain conductivity and permittivity.*

Subtraction and non-subtraction mode interfaces

Figure 13-9 shows a dielectric sensor in the floating electrode configuration. When the response voltage V_{res} is directly buffered by a x1 amplifier, the interface operates in *non-subtraction* mode. In this arrangement, load capacitance C_{load} is grounded and any cable capacitance on the response signal is in parallel with C_{load}. If the load capacitance is very large compared to sensor capacitance C_{MUT}, then cable capacitance has relatively little effect on the response signal.
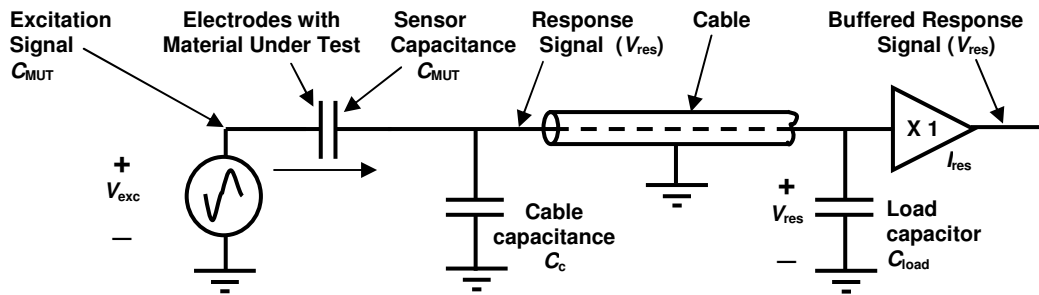

Figure 13-9
Non-subtraction mode interface

From basic circuit theory, the response with capacitances only is:

(eq. 13-11) $$V_{\text{res}} / V_{\text{exc}} = C_{\text{MUT}} / (C_{\text{load}} + C_{\text{MUT}} + C_{\text{c}})$$

For example, if C_{load} is 2000 pF and C_{MUT} is 20 pF, for various cable capacitances the response for the interface of Figure 13-9 is shown in Table 13-1.

Table 13-1
Response of Non-subtraction Mode Interface

C_{load} (pF)	C_{MUT} (pF)	C_c (pF)	V_{res} / V_{exc}	Gain (dB)	$\dfrac{V_{res} / V_{exc}}{V_{res} / V_{exc} \text{ for } C_c = 0 \text{ pF}}$
2000	20	0	0.0099	−40.09	1.00
2000	20	20	0.0098	−40.17	0.99
2000	20	40	0.0097	−40.26	0.98
2000	20	60	0.0096	−40.34	0.97
2000	20	100	0.0094	−40.51	0.95

Even for relatively large cable capacitances, the effect on the response is small.

In contrast, Figure 13-10 shows a dielectric sensor interface operating in *subtraction mode*. Here the sensor capacitance C_{MUT}, not the load capacitance, is grounded. A differential amplifier subtracts the sensor signal from the excitation signal, resulting in a response that ideally is the same as for non-subtraction mode.
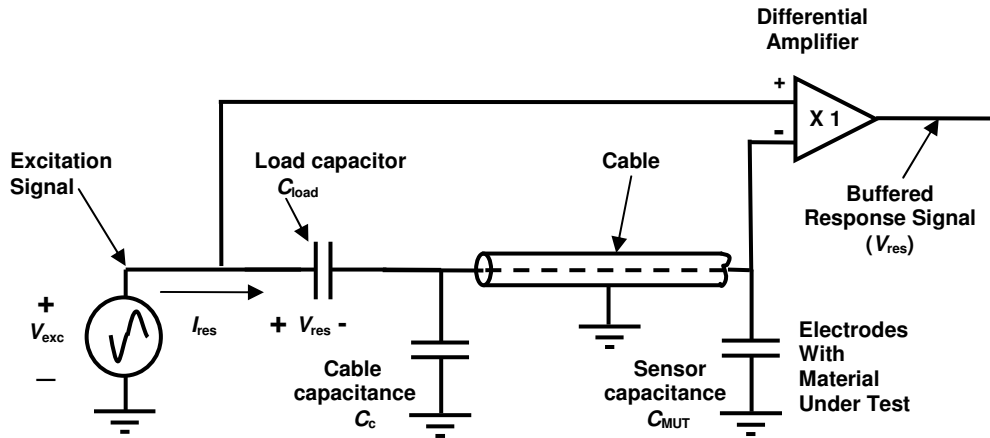

Figure 13-10
"Subtraction" mode interface

Both subtraction mode and non-subtraction mode circuits use equations 13-5 through 13-10 to convert the response signal to conductance and capacitance. Subtraction mode has the advantage of allowing a dielectric sensor to operate with a single electrode, such as the sensor of Figure 13-11.

Figure 13-11
Dielectric sensor with single electrode

A sensor with one electrode uses a nearby grounded surface as an effective second electrode. This surface may be a mold or the platen of a press, either surrounding the sensor or the opposite it as shown in Figure 13-12. Thus a single electrode sensor may be smaller than one that requires two electrodes.
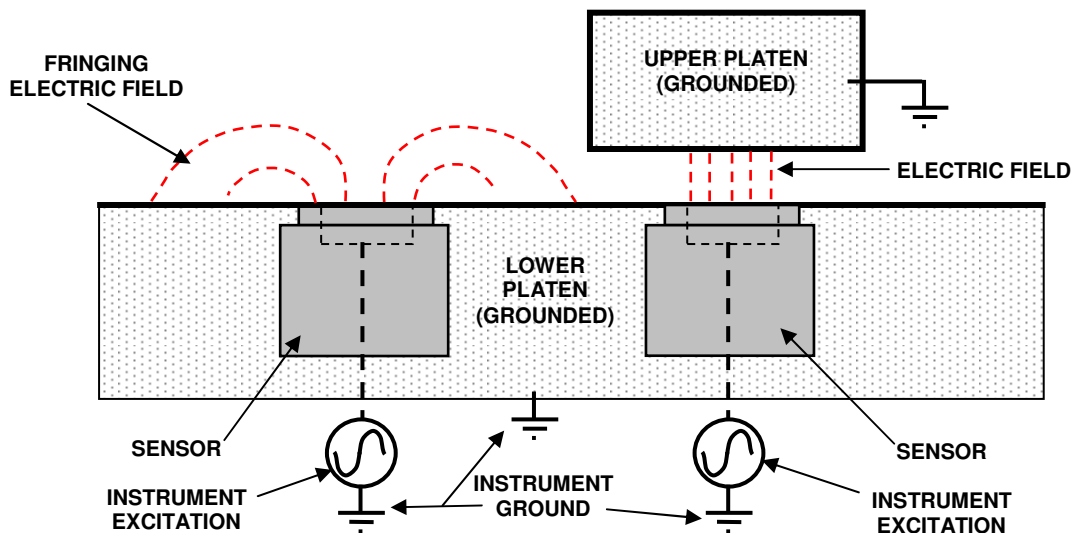

Figure 13-12
Single electrode sensor using nearby grounded surface as second electrode

Non-subtraction mode requires a sensor with two electrodes, while a subtraction mode interface may use sensors with either one or two electrodes. A subtraction mode interface, however, is more influenced by cable capacitance than a non-subtraction mode interface. As apparent in Figure 13-10, for a subtraction mode interface the cable capacitance is in parallel with the sensor capacitance.

From circuit theory, the response with capacitances only is:

(eq. 13-12) $V_{RES} / V_{EXC} = (C_{MUT} + C_C) / (C_{LOAD} + C_{MUT} + C_C)$

Again, for example, if C_{load} is 2000 pF and C_{MUT} is 20 pF, for various cable capacitances the response for the interface of Figure 13-10 is shown in Table 13-2.

Table 13-2
Response of Subtraction Mode Interface

C_{load} (pF)	C_{MUT} (pF)	C_c (pF)	V_{res} / V_{exc}	Gain (dB)	V_{res} / V_{exc} / V_{res} / V_{exc} for C_c = 0 pF
2000	20	0	0.0099	−40.09	1.00
2000	20	20	0.0196	−34.15	1.98
2000	20	40	0.0291	−30.71	2.94
2000	20	60	0.0385	−28.30	3.89
2000	20	100	0.0566	−24.94	5.72

Even for relatively small cable capacitances, the influence on the response is large. The effect of cable capacitance may be subtracted from the response, but uncertainty in the value of cable capacitance will correspondingly affect the accuracy of sensor capacitance measurements.

In subtraction mode, conductance measurement is not affected by cable capacitance. For dielectric cure monitoring, when conductance is the property of interest, subtraction mode offers flexibility in the choice of sensors. For measurements when capacitance is also important, then non-subtraction mode should be used.

DC measurements

Instruments for measuring only the conductance of the material under test have the advantage of simplicity compared to those measuring both conductance and capacitance. These conductance measurement instruments (essentially highly sensitive ohmmeters) use a DC voltage source to drive current through the MUT between the sensor electrodes. This current typically passes into the virtual ground of a current-to-voltage converter, as shown in Figure 13-13. A data acquisition system can measure the DC voltage output, V_{out} , and DC current I_{res} can be calculated from the known value of R_{load}. From the value of I_{res}, the frequency independent (DC) conductance of the material between the electrodes can be calculated from Ohm's law.
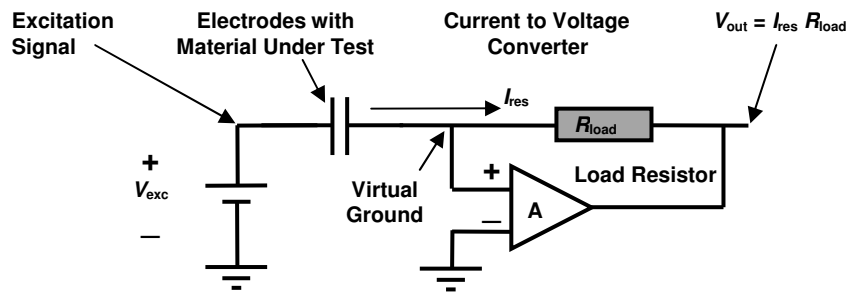
Figure 13-13
DC measurement of dielectric properties (conductance only)

The simplicity of the circuit of 13-13, however, comes at the expense of flexibility and possibly accuracy. DC methods can only measure the DC conductance; measurement of capacitance requires an AC excitation. DC measurements may be confounded by offset voltage drifts, thermal drifts and leakage currents in the interface electronics, which cannot be distinguished from the true DC signal.

Finally, DC measurements are not possible with release layers, which are very thin insulating sheets sometimes used to prevent material from adhering to a mold or platen. Release layers block DC current and therefore prevent measurements of DC conductance.

Digital sampled data system

Some dielectric measurement instruments use sampled data acquisition, as shown in the block diagram of Figure 13-14. A sampled data acquisition system analyzes the sensor response using digital signal processing (DSP), which can extract information from a very noisy signal. This ability results in more accurate, precise and repeatable data than from an instrument using analog computation, but with greater complexity and cost.
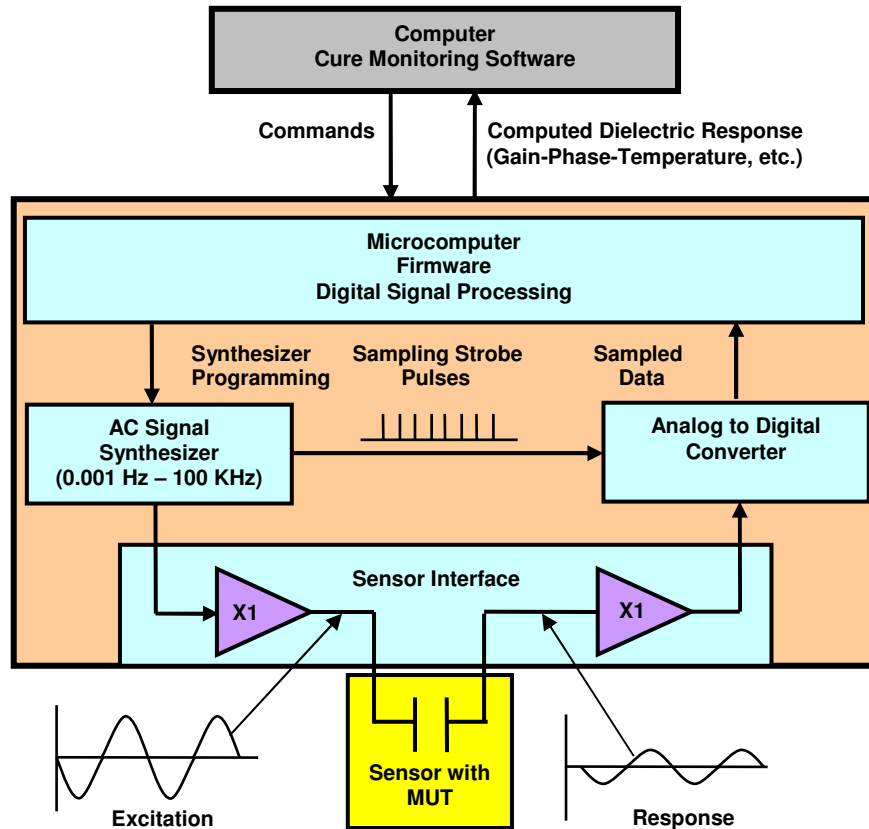

Figure 13-14
Block diagram of a sampled data acquisition system

Analog computation system

Analog measurement techniques are less expensive and much faster, but more noise sensitive and less accurate, than digital sampled data systems. However, analog instruments can perform well in applications where rapid data acquisition is a desired tradeoff for accuracy and precision. The block diagram of Figure 13-15 shows how an instrument can use analog computation to measure dielectric properties.
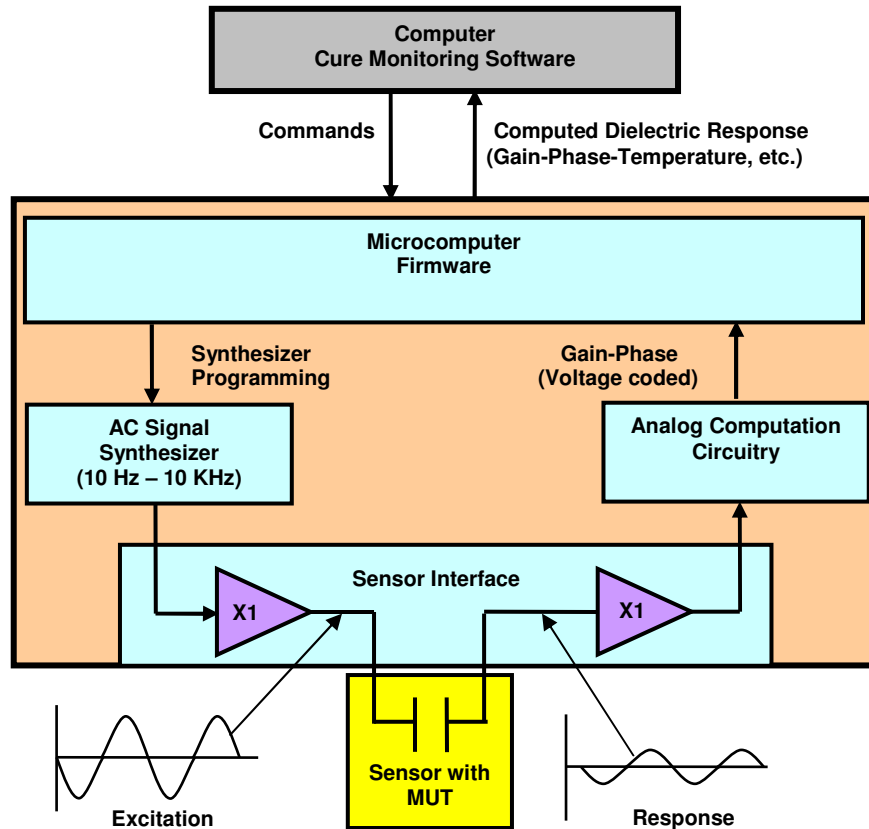
Figure 13-15
Block diagram of analog computation system

Chapter 14–Parallel Plate Measurements

Introduction

Dielectric instrumentation measures the electrical properties of the Material Under Test (MUT) between a pair of electrodes, which can be modeled as a conductance in parallel with a capacitance, as shown in Figure 14-1.
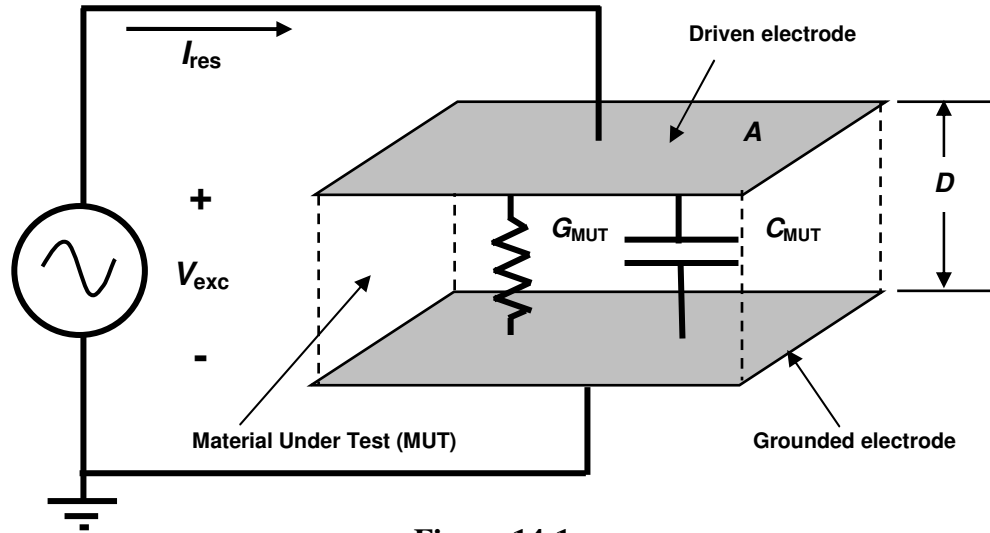

Figure 14-1
Electrical model of dielectric Material Under Test

Raw dielectric measurements at frequency f are conductance G_{MUT} (mohs) and capacitance C_{MUT} (farads). Resistance and other material properties are given by equations 14-1 through 14-5:

(eq. 14-1)	R_{MUT}	$= 1/G_{MUT}$	(resistance)
(eq. 14-2)	ρ	$= R_{MUT}\, A/D$	(resistivity or ion viscosity)
(eq. 14-3)	σ	$= G_{MUT} / (A/D)$	(conductivity)
(eq. 14-4)	ε'	$= C_{MUT} / (\varepsilon_o\, A/D)$	(relative permittivity)
(eq. 14-5)	ε"	$= \sigma / (\varepsilon_o\, \omega)$	(loss factor)

Where:

$\omega = 2\pi f$
$\varepsilon_0 = 8.85 \times 10^{-14}$ F/cm
A/D = ratio of area to distance for electrodes

Dissipation, or tanδ, at measurement frequency f is the ratio of a material's relative loss to its relative permittivity, and is given by the relationship:

(eq. 14-6) $$\tan\delta = \varepsilon''/\varepsilon' = 1 / (\omega C_{MUT} R_{MUT})$$

Dielectric properties can be measured in a test cell, and parallel plate electrodes are usually used for solid material in the form of a laminate or panel. Some test cells have cylindrical geometries for measuring fluids or tubular solids, and many other configurations are possible. In general the *A/D* ratio may also be called the *cell constant*.

ASTM standard for parallel plate dielectric measurements

The ASTM standard D150-98 (Reapproved 2004) **Standard Test Methods for DAC Loss Characteristics and Permittivity (Dielectric Constant) of Solid Electrical Insulation** describes general configurations of electrodes, circuits and instruments. For measurements that do not require best accuracy, unshielded two-electrode systems with corrections may be convenient, but exacting measurements require guarded three-electrode fixtures.

An unshielded two-electrode arrangement produces fringing electric fields between the electrodes and through the sample and surrounding media, as shown in Figure 14-2. These fringe fields create stray capacitance that introduces uncertainty in the *A/D* ratio, or cell constant, and reduces measurement accuracy.
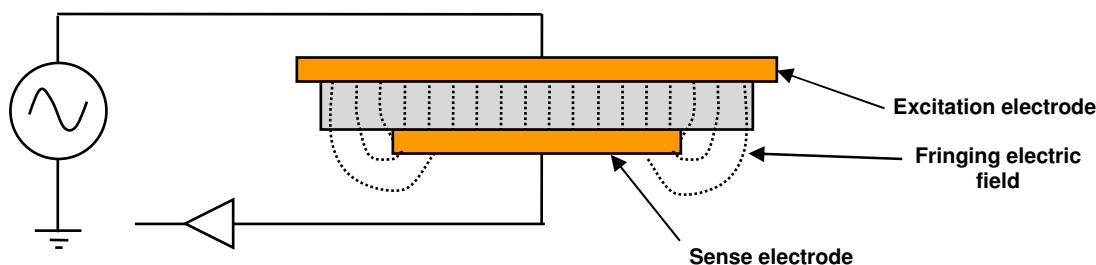

Figure 14-2
Unguarded parallel plate electrodes with fringing electric field

Guarded three-electrode fixtures are the standard for accurate dielectric measurements. In this configuration, a guard electrode surrounds the response electrode. Additional circuitry drives the guard electrode with a reproduction of the response voltage. Most impedence measurement instruments, such as LCR meters, connect the response electrode to a virtual ground; in this case the guard electrode is also grounded.

Figure 14-3 shows how the guard electrode creates a uniform electric field that extends beyond the sample. This configuration eliminates fringing fields and allows exact definition of the *A/D* ratio or cell constant, based on the dimensions of the electrodes alone. Also, because the electric field between excitation and response electrodes is

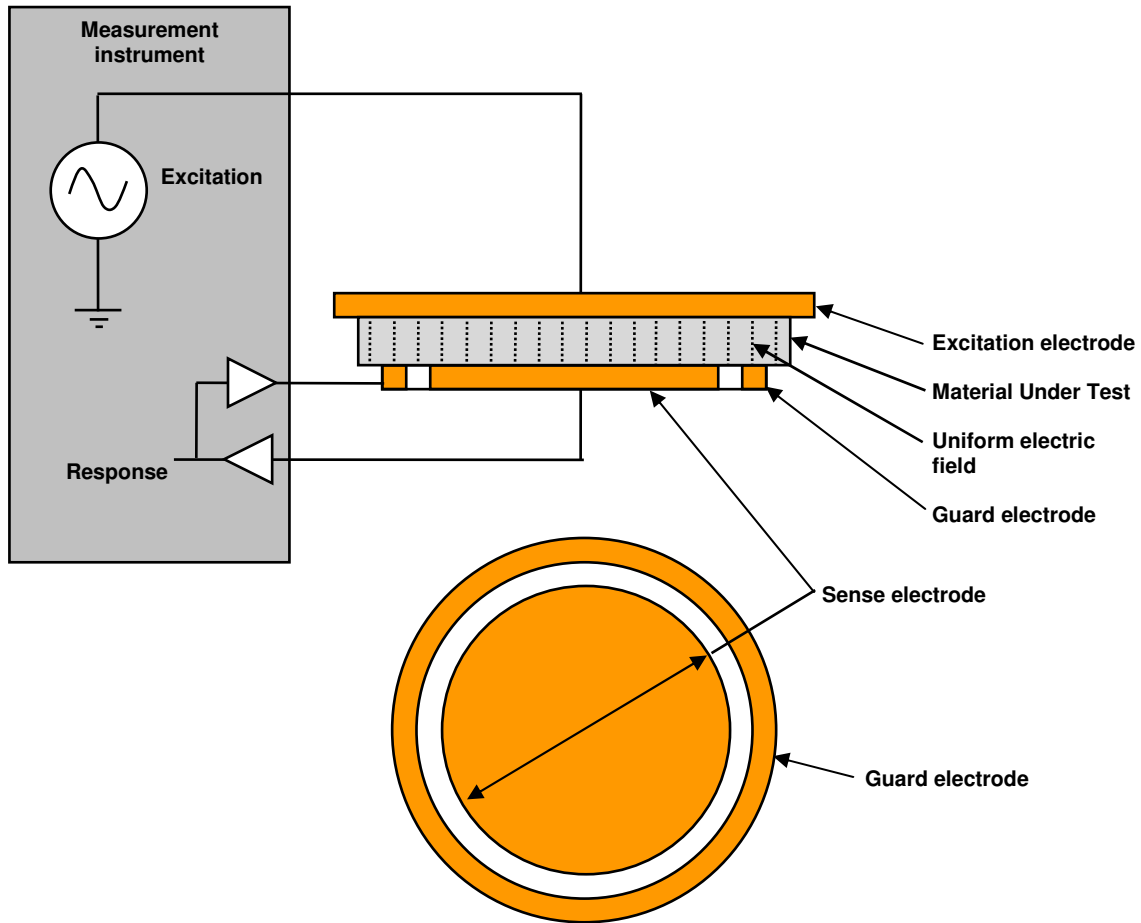confined to the sample, the medium beyond the sample does not influence the measurement.

Figure 14-3
Guarded parallel plate electrodes with uniform electric field

Cabling to instruments

For accurate measurements, good cabling is important. Figure 14-4 shows the typical connection of an instrument to a parallel plate test fixture. The excitation line uses a coaxial cable and the response line uses a triaxial cable. The shield of the coaxial cable is grounded to prevent coupling of the excitation to the response signal. The inner shield of the triaxial cable is driven by a buffered version of the response signal; this method of signal *guarding* reduces the effect of input and cable capacitance for small voltages at high impedence levels. The guard output also drives the guard electrode of the test fixture. The outer shield of the triaxial cable is grounded to prevent transmission of noise to the guard signal. When the response line is a virtual ground, which is the case for most LCR meters, a coaxial cable with grounded shield is sufficient for the response signal.
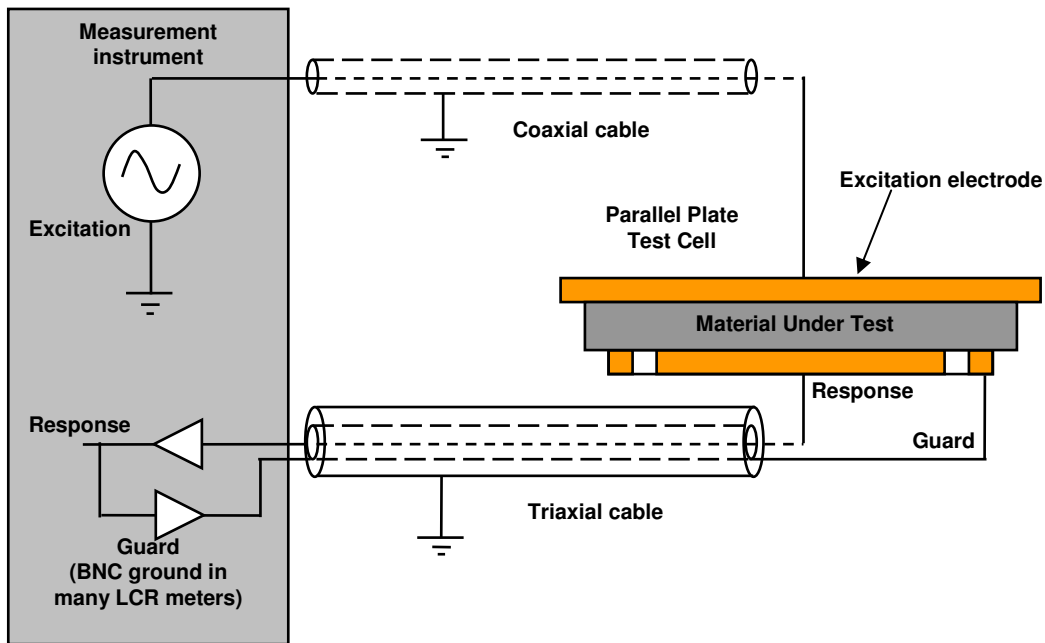

Figure 14-4
Typical excitation and response cabling to a parallel plate test fixture

Contacting electrode measurements

The contacting electrode method requires only one measurement with the electrodes in direct contact with the MUT as shown in Figure 14-5. The surface of the MUT must be flat to prevent an air gap between the sample and electrodes. The MUT should also be incompressible so the separation between the electrodes is the same as the true thickness of the sample.
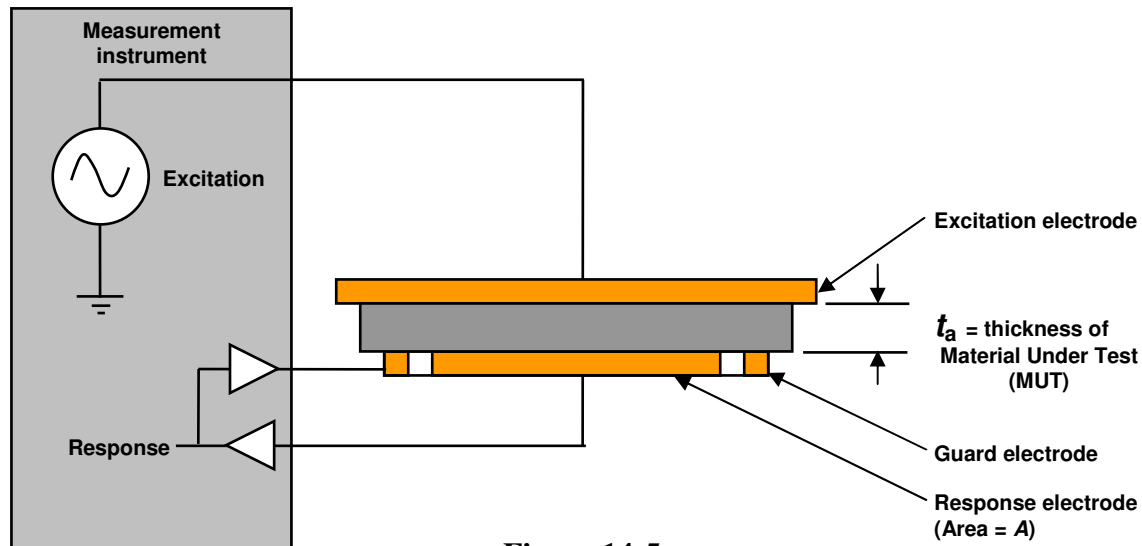
Figure 14-5
Configuration for contacting electrode measurements

Dielectric properties at f, the frequency of measurement, are calculated below:

(eq. 14-7) $\varepsilon' \quad = C_P / (\varepsilon_0 A / t_a)$
(eq. 14-8) $\tan\delta \quad = \varepsilon'' / \varepsilon' = 1 / (\omega C_P R_P)$
(eq. 14-9) $\varepsilon'' \quad = \varepsilon' \tan\delta$

Where: $\omega = 2\pi f$
            $\varepsilon_0 = 8.85 \times 10^{-14}$ F/cm
            C_P = Capacitance of measurement (farad)
            R_P = Resistance of measurement (ohm)

Non-contacting electrode measurements

        The non-contacting electrode method can obtain accurate results for dielectric properties in the presence of an air gap, but requires two measurements. The first measurement determines the capacitance and dissipation of the test fixture at a known separation with only air between the electrodes, as shown in Figure 14-6a. The second measurement determines the capacitance and dissipation at the same separation with the sample inserted between the electrodes, as shown in Figure 14-6b. For this method the air gap and the compressibility of the MUT do not affect the results.
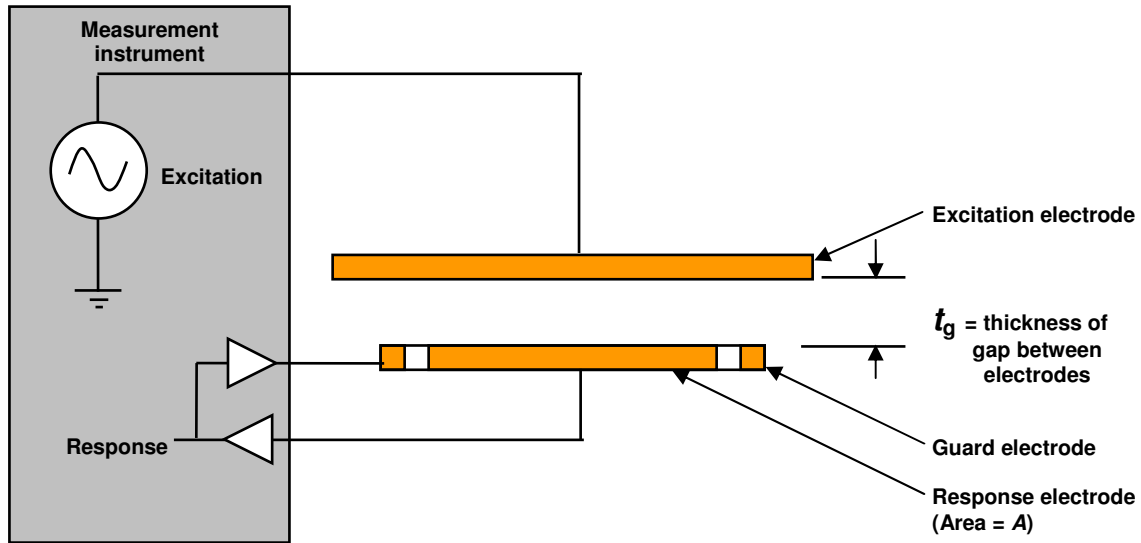
Figure 14-6a
Non-contacting electrode measurement with air only between electrodes
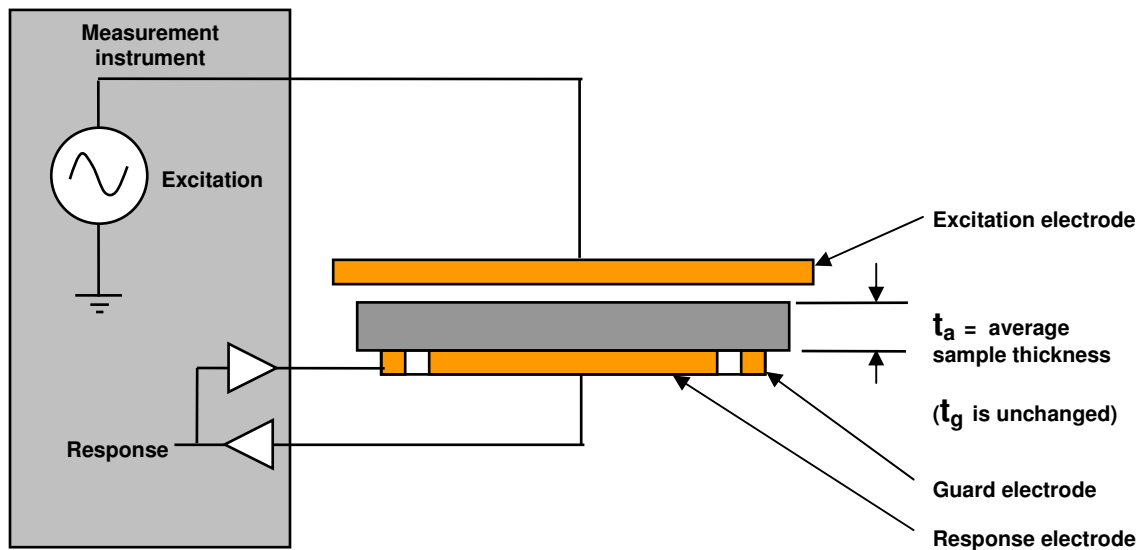**(First measurement)**

Figure 14-6b
Non-contacting electrode measurement with sample between electrodes
(Second measurement)

For low dissipation the dielectric properties at f, the frequency of measurement, are calculated below:

For $(\tan\delta)^2 \ll 1$

(eq. 14-10)	ε'	$=$	$1 / [1 - (a\,b)]$
(eq. 14-11)	$\tan\delta$	$=$	$\tan\delta_{P2} + [\varepsilon'\,c\,d]$
(eq. 14-12)	ε''	$=$	$\varepsilon'\,\tan\delta$

Where:

$\omega = 2\pi f$

C_{P1} = Capacitance (F) without MUT inserted (Fig. 13-6a)

R_{P1} = Resistance (Ω) without MUT inserted (Fig. 13-6a)

$\tan\delta_{P1} = 1 / (\omega\,C_{P1}\,R_{P1})$ = Dissipation without MUT inserted (Fig. 13-6a)

C_{P2} = Capacitance (F) with MUT inserted (Fig. 13-6b)

R_{P2} = Resistance (Ω) with MUT inserted (Fig. 13-6b)

$\tan\delta_{P2} = 1 / (\omega\,C_{P2}\,R_{P2})$ = Dissipation with MUT inserted (Fig. 13-6b)

t_g = Separation (m) between response and excitation electrodes

t_a = Average sample thickness (m)

$a = 1 - (C_{P1} / C_{P2})$

$b = t_g / t_a$

$c = \tan\delta_{P2} - \tan\delta_{P1}$

$d = (t_g / t_a) - 1$

  Results for non-contacting electrode measurements can only be as accurate as the measurements of electrode separation and sample thickness. For situations where the air gap is a large fraction of the sample thickness, calculations for relative permittivity, ε', and dissipation, $\tan\delta$, are very sensitive to uncertainties in t_g and t_a . Consequently, non-contacting electrode measurements are best used for thicker samples where the air gap can be relatively small.

Chapter 15–Calculating A/D Ratio and Base Capacitance

Introduction

The cross section of the planar electrodes shown in Figure 15-1 shows that the total capacitance C_{tot} is the sum of C_{MUT} from the Material Under Test above electrodes and C_{base} from the substrate beneath the electrodes. This second component C_{base} is called the base capacitance.
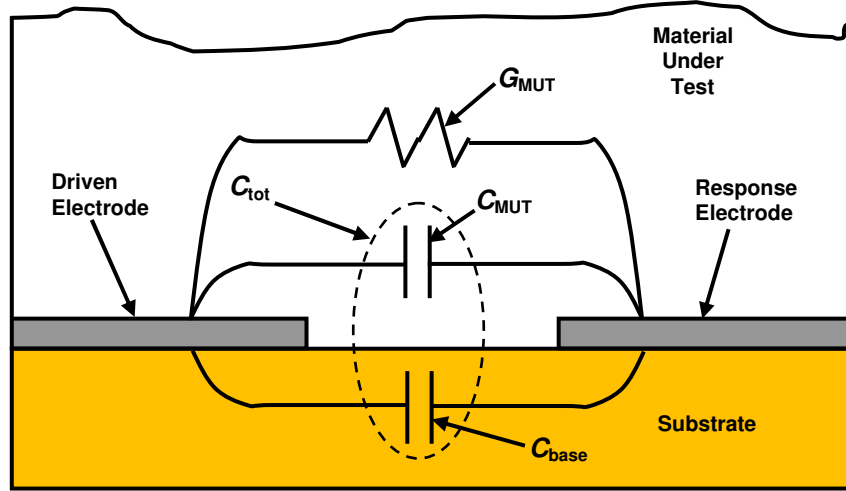

Figure 15-1
Cross section of interdigitated electrode structure

The total capacitance measured by the interdigitated electrodes is:

(eq. 15-1) $$C_{tot} = C_{MUT} + C_{base}$$

The capacitance of the Material Under Test is calculated as shown below:

(eq. 15-2) $$C_{MUT} = \varepsilon_o\, \varepsilon'_{MUT}\, A/D$$

Calculating Base Capacitance with Known *A/D*

It is possible to determine the base capacitance of a sensor by measuring its response in two different, non-conducting materials of known permittivity. To determine base capacitance, measure the sensor capacitance in air.

(eq. 15-3) $$C_{tot\text{-}air} = C_{MUT\text{-}air} + C_{base}$$

Then measure the sensor capacitance in a second, non-conducting fluid. Food grade mineral oil is a good second fluid because it is readily available, has very low

conductivity and uniform characteristics. The relative permittivity of food-grade mineral oil is about 2.2.

(eq. 15-4) $$C_{\text{TOT-oil}} = C_{\text{MUT-oil}} + C_{\text{base}}$$

Sum together equations 15-3 and 15-4.

(eq. 15-5) $$C_{\text{tot-air}} + C_{\text{tot-oil}} = C_{\text{MUT-oil}} + C_{\text{MUT-oil}} + 2\,C_{\text{base}}$$

C_{tot} is measured in each case, and C_{MUT} is calculated in each case from equation 15-2 using the known permittivity of each Material Under Test and the *A/D* ratio of the sensor. Then C_{base} can be calculated using equation 15-6:

(eq. 15-6) $$C_{\text{base}} = 1/2\,[(C_{\text{tot-air}} + C_{\text{tot-oil}}) - (C_{\text{MUT-air}} + C_{\text{MUT-oil}})]$$

Calculating Base Capacitance and *A/D* When Both are Unknown

Both the *A/D* ratio and the base capacitance are required to fully describe a sensor. If they are both unknown then the two measurements described previously can be used to create a system of two equations in two unknowns which can be solved with basic algebra. Equations 15-3 and 15-4 are repeated below:

(eq. 15-3) $$C_{\text{tot-air}} = C_{\text{MUT-air}} + C_{\text{base}}$$
(eq. 15-4) $$C_{\text{TOT-oil}} = C_{\text{MUT-oil}} + C_{\text{base}}$$

The capacitance for the Material Under Test for equations 15-3 and 15-4 can be rewritten using equation 15-2:

(eq. 15-7) $$C_{\text{TOT-air}} = (\varepsilon'_{\text{MUT-air}}\,\varepsilon_{\text{o}})\,A/D + C_{\text{base}}$$
(eq. 15-8) $$C_{\text{TOT-oil}} = (\varepsilon'_{\text{MUT-oil}}\,\varepsilon_{\text{o}})\,A/D + C_{\text{base}}$$

Equations 15-7 and 15-8 make up a system of two equations in two unknowns, where the unknowns are the *A/D* ratio and C_{base}. First, these equations can be solved for the *A/D* ratio:

(eq. 15-9) $$A/D = (C_{\text{TOT-air}} - C_{\text{TOT-oil}}) / (\varepsilon_{\text{o}}\,(\varepsilon'_{\text{MUT-air}} - \varepsilon'_{\text{MUT-oil}}))$$

Knowing the *A/D* ratio, C_{base} can then be calculated from equations 15-6 and 15-2.

Chapter 16–Electrode Polarization and Boundary Layer Effects

Introduction

When the incorrect model is used to determine dielectric properties, low frequency measurements of highly conductive materials may appear to have unusually low conductivity. This phenomenon is caused by electrode polarization, the accumulation of charge against the electrodes, which occurs when the material under test:

- Has high loss factor (high ionic conduction at low frequency)

   AND

- Has a non-conductive film, an oxide layer or an electrochemical potential barrier, resulting in an insulating boundary layer

If the effects of electrode polarization and boundary layers are properly considered, then it is possible to account for their influence and correctly calculate bulk permittivity and conductivity.

Effects of electrode polarization

Electrode polarization distorts dielectric data by artificially increasing *apparent* relative permittivity (ε') and decreasing *apparent* loss factor (ε''). When plotted against time, loss factor curves may display anomalous behavior as shown in Figure 16-1.
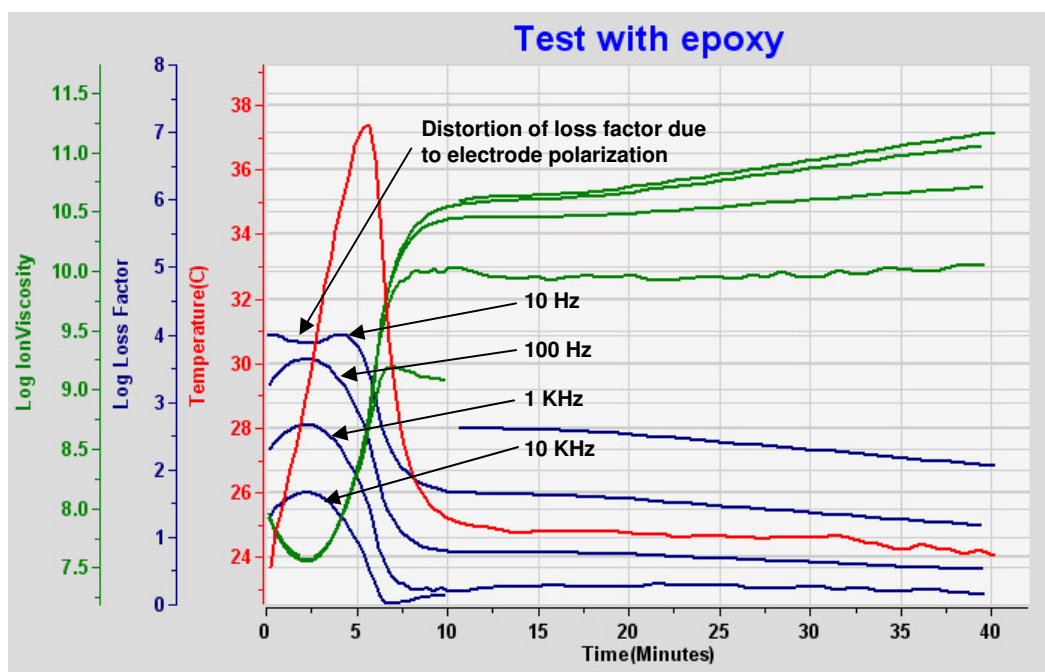

Figure 16-1
Plot showing distortion of loss factor due to electrode polarization

This distortion increases as loss factor increases. In addition, lower frequencies correspond to higher loss factors for a given conductivity, and therefore display even greater distortion. As a result, the 10 Hz loss factor data of Figure 16-1 shows a double hump—a depression with two satellite peaks instead of a single peak. The first satellite peak has been attributed to softening, and the second satellite peak to gelation—but they both are artifacts from use of an incorrect model and do not describe actual dielectric events. In fact, the expected—but unseen—single loss factor peak corresponds to the point of minimum viscosity, an event that would be completely lost if the data were misinterpreted.

The loss factor data of Figure 16-1 can be plotted against permittivity to highlight the nature of these relationships, as shown in Figure 16-2.
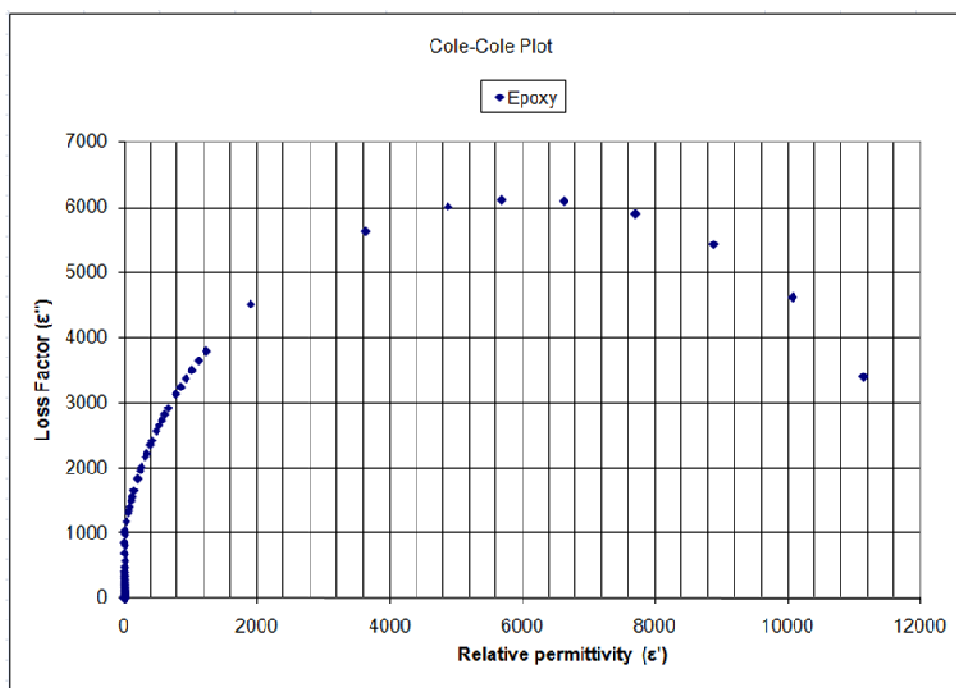

Figure 16-2
Cole-Cole plot of epoxy cure data distorted by electrode polarization

In older literature this Cole-Cole plot behavior has been erroneously explained by a large dipole relaxation response.

Basic Circuit Model of a Dielectric Material

The basic model of a dielectric Material Under Test consists of a conductance G_{MUT} in parallel with a capacitance C_{MUT} as shown below in Figure 16-3.
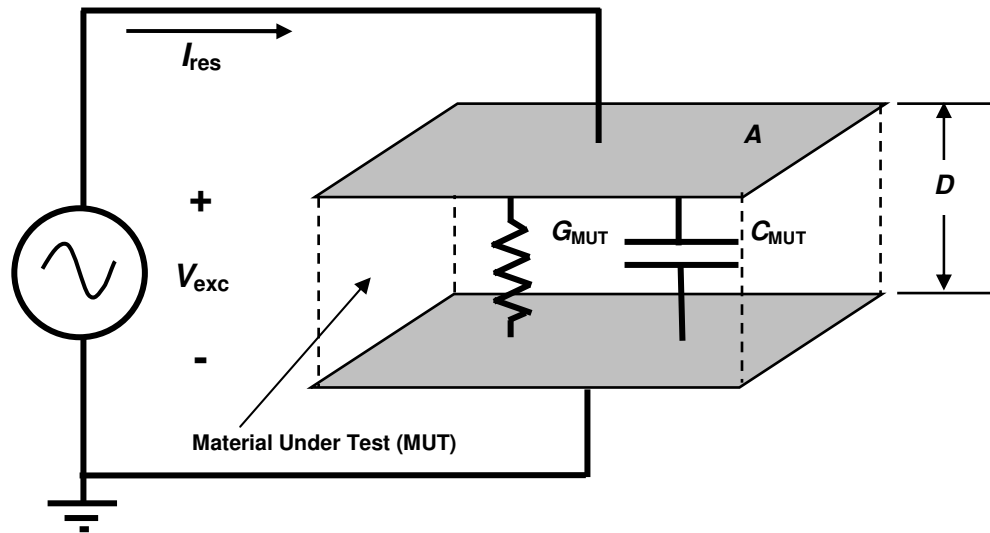
Figure 16-3
Basic model of a dielectric material

This configuration has a simple relationship between the excitation voltage V_{exc} across the material and the response current I_{res} through the material, given by equation 16-1:

(eq. 16-1) $\qquad\qquad I_{res} / V_{exc} = G_{MUT} + i\omega C_{MUT} = Y_{MUT}$

Boundary Layers

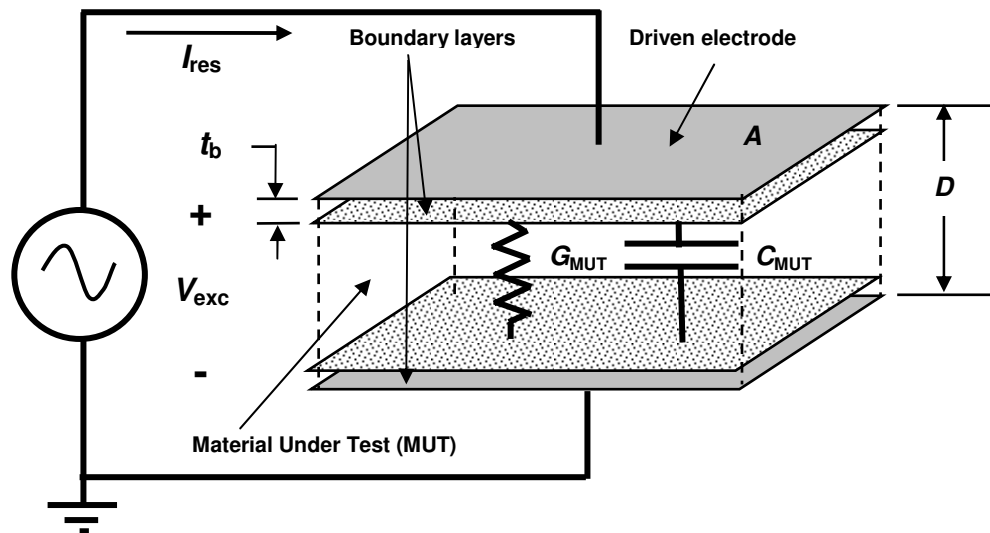   Electrode polarization creates a boundary layer at the interface with the material and changes the model to that shown in Figure 16-4:

Figure 16-4
Model of dielectric material with boundary layer

The boundary layers are very thin (thickness = t_b) and have the surface area of the electrodes. Consequently they have a very large A/D ratio, resulting in a very large capacitance C_B in series with the bulk material. This arrangement is shown in the circuit model of Figure 16-5.
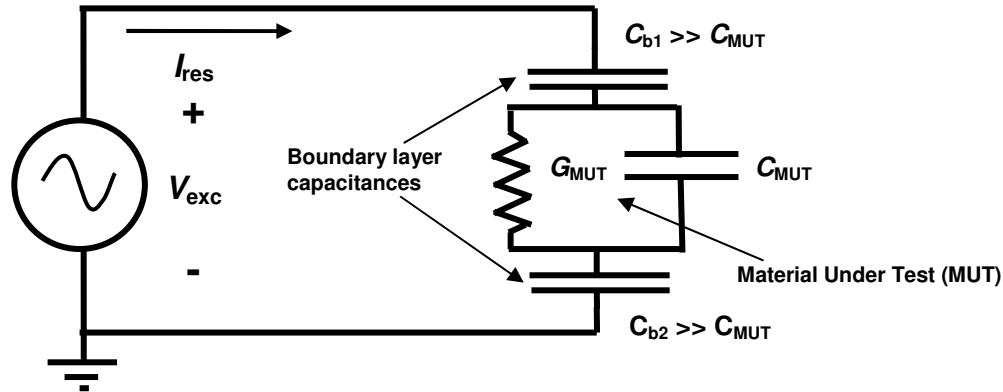
Figure 16-5
Circuit model of dielectric with boundary layer capacitances

Analysis of the boundary layer model is much more complicated than for the basic model, but it is possible to quickly understand the circuit behavior in certain limiting cases.

Low Frequency Response of Boundary Layers

For situations with low excitation frequency or high bulk conductivity, the boundary layer capacitances dominate the circuit response and the model reduces to that of Figure 16-6. Capacitances act as open circuits at low frequencies, so the electrode boundary layer blocks DC current. Measurements of DC conductance are impossible in this case and the material appears primarily capacitive.
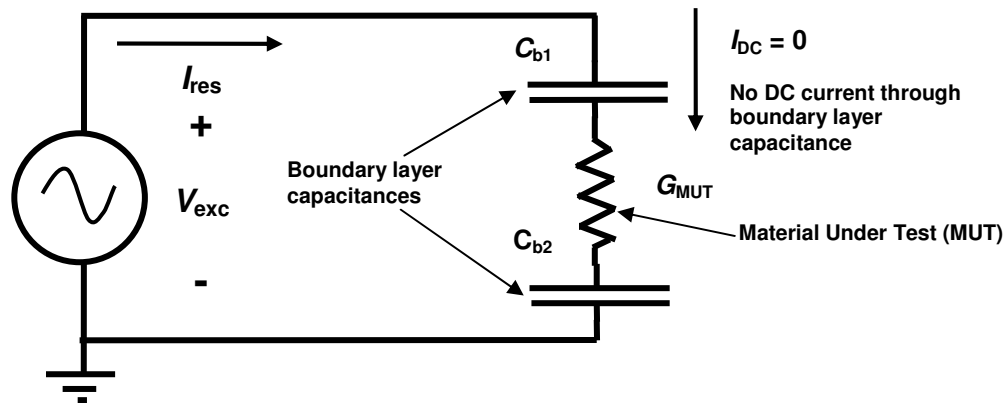
Figure 16-6
Circuit model of dielectric with boundary layer capacitances

In reality these boundary layer capacitances may be "leaky" and some DC current passes through them. The boundary layer conductances G_{b1} and G_{b2}, shown in Figure 16-7, would be uncertain and can range from being very high (and negligible), to being very low (and significant). Furthermore, G_{b1} and G_{b2} may vary with temperature and the state of the material, which itself will vary during cure.

If the basic model of Figure 16-3 is used to interpret measurements, the apparent bulk conductance would be the conductance of the series configuration of G_{b1}, G_{MUT} and G_{b2}, i.e. the inverse of the sum of their resistances, given by equation 16-2:

(eq. 16-2) $\qquad\qquad R_{MUT\ (apparent)} = R_{b1} + R_{MUT} + R_{b2}$ $\qquad$ (where $R = 1/G$)

At best the boundary layer resistances are negligible, but in the worst case for high R_{b1} and R_{b2} the apparent bulk resistance would appear much higher than it should be, because the bulk conductance (and therefore conductivity) would appear much lower than it should be.
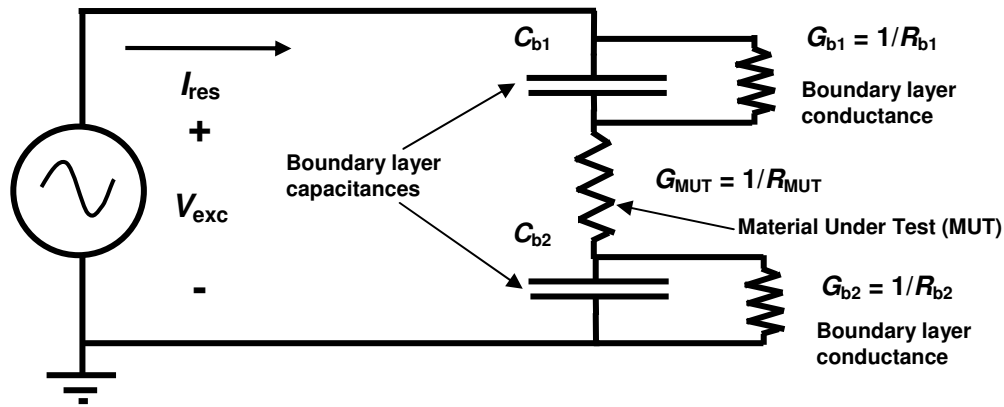

Figure 16-7
Circuit model of dielectric with "leaky" boundary layer capacitances

For qualitative measurements where accuracy is not critical, DC measurements can yield useful information; however, there will always be uncertainty about the magnitude of the boundary layer effect.

High Frequency Response of Boundary Layers

For the limit of high frequency or low bulk conductivity, boundary layer admittance is high compared to the Material Under Test, and boundary layer capacitances act like short circuits. In this case the circuit of Figure 16-7 reduces to the simpler one of Figure 16-8, which is identical to the basic model of a dielectric material. Therefore the high frequency behavior of a dielectric material is the same with or without boundary layers.
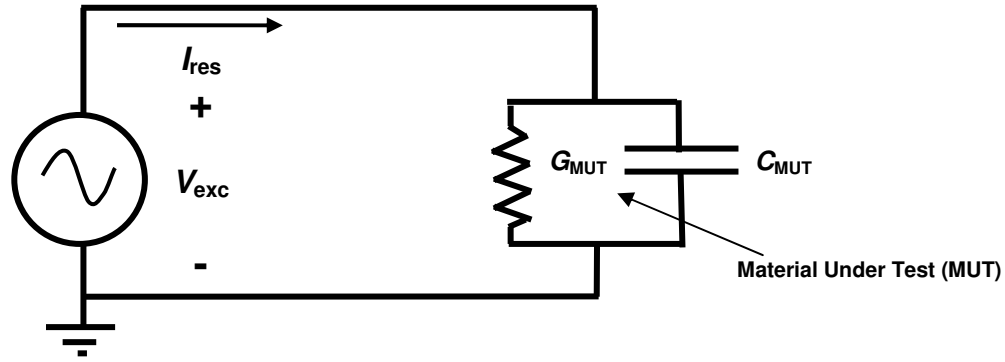
Figure 16-8
Circuit model of dielectric with boundary layer capacitances
(Limiting case of high frequency or low bulk conductivity)

Boundary Layer Effect on Dielectric Cure Monitoring

With the known quantities of:

$$\omega = 2\pi f_{exc}$$
$$\varepsilon_0 = 8.85 \times 10^{-14} \text{ F/cm}$$
$$A/D = \text{ratio of area to distance for electrodes}$$

it is possible to calculate the following dielectric material properties from measurement data:

(eq. 16-3) $\sigma = G_{MUT} / (A/D)$ (conductivity)
(eq. 16-4) $\varepsilon' = C_{MUT} / (\varepsilon_0 A/D)$ (relative permittivity)
(eq. 16-5) $\varepsilon'' = \sigma / (\varepsilon_0 \omega)$ (loss factor)
(eq. 16-6) $\rho = (A/D) / G_{MUT}$ (resistivity)

A common convention describes the cure of a polymeric material in terms of relative permttivity ε' and loss factor ε''. The boundary layer model of Figure 16-6 can be solved using these terms as follows[1]:

(eq. 16-7) $$\varepsilon'_x = \varepsilon' \, (D / 2t_b) \, \frac{(\varepsilon''/\varepsilon')^2 + (D / 2t_b)}{(\varepsilon''/\varepsilon')^2 + (D / 2t_b)^2}$$

(eq. 16-8) $$\varepsilon''_x = \varepsilon'' \, (D / 2t_b) \, \frac{(D / 2t_b) - 1}{(\varepsilon''/\varepsilon')^2 + (D / 2t_b)^2}$$

(eq. 16-9) $\tan \delta_x = \varepsilon''_x / \varepsilon'_x = \tan \delta [((D / 2t_b) - 1) / ((\tan \delta)^2 + (D / 2t_b))]$

Where: t_b = boundary layer thickness
             D = distance between electrodes or plate separation
             ε'_x = uncorrected (apparent) permittivity
             ε''_x = uncorrected (apparent) loss factor
             ε' = actual permittivity
             ε'' = actual loss factor
           $\tan \delta$ = $\varepsilon''/\varepsilon'$

Figure 16-9 shows how boundary layer thickness, temperature, frequency and state of cure influence the Cole-Cole plot of a curing material. With no boundary layer, loss factor decreases with advancing cure, while permittivity remains constant at the value ε_r, called the relaxed permittivity. Thicker boundary layers cause the Cole-Cole plot to develop a curvature which in extreme cases can become a complete semi-circle.
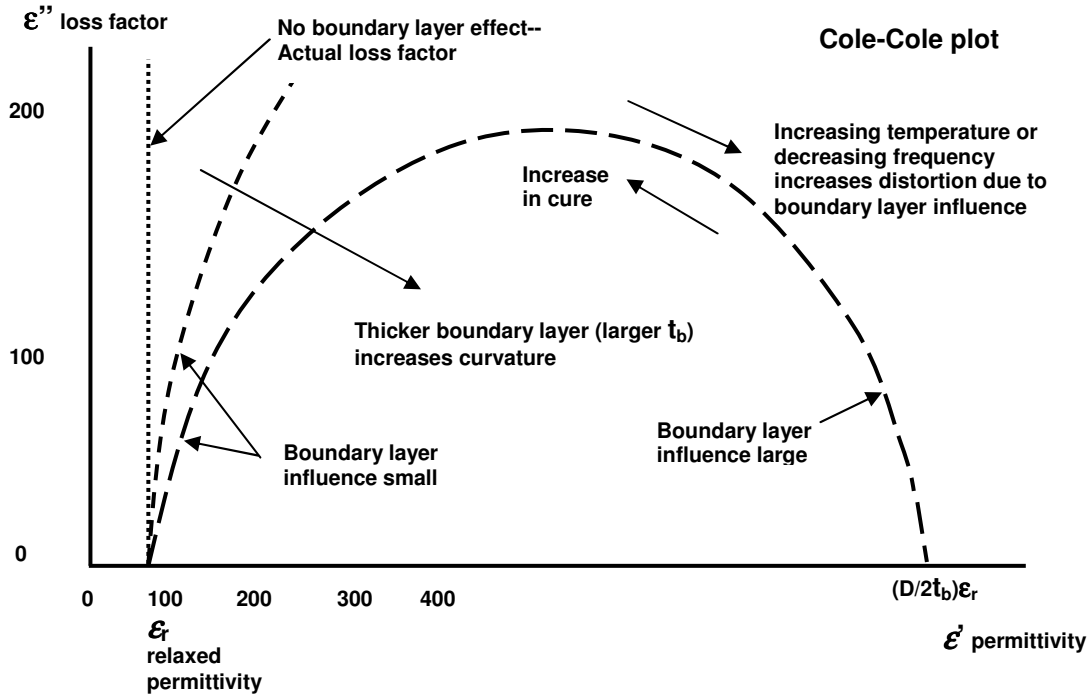

Figure 16-9
Cole-Cole plot of curing material with boundary layer effect

The left intercept of the semi-circle is the relaxed permittivity ε_r, and the right intercept is determined by both ε_r and the ratio $D/2t_b$. This information can be used to calculate the boundary layer thickness t_b. In the absence of an artificial blocking layer such as an applied insulator or an oxide coating, the boundary layer thickness can be used to calculate an approximate mobile ion concentration [C] and ion mobility μ^2:

(eq. 16-10) $[C] = (t_b^2 q^2) / (2kT \varepsilon' \varepsilon_0)$

(eq. 16-11) $\mu = \sigma / ([C] q)$

Where : k = Boltzmann's constant (eV/K)
                 T = temperature in degrees Kelvin (K)
                 q = magnitude of electronic charge (coulombs)
                 μ = free ion mobility (cm^2 / (V-s))

Electrode Polarization Correction

It is possible to manipulate equations 16-7, 16-8 and 16-9 to correct the effect of electrode polarization in certain cases. Figure 16-10 shows data that has been adjusted in this manner.
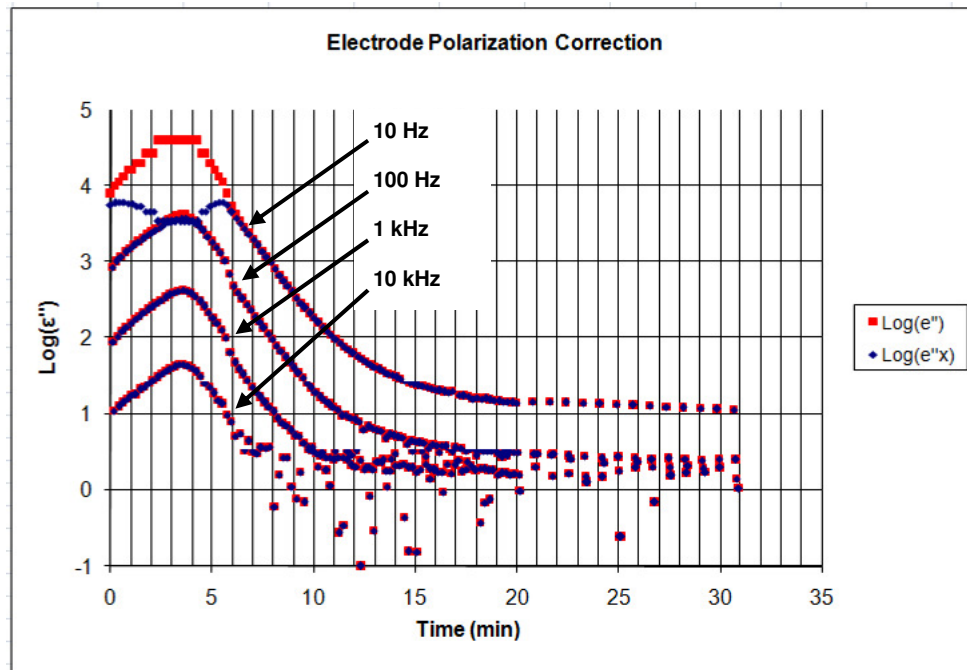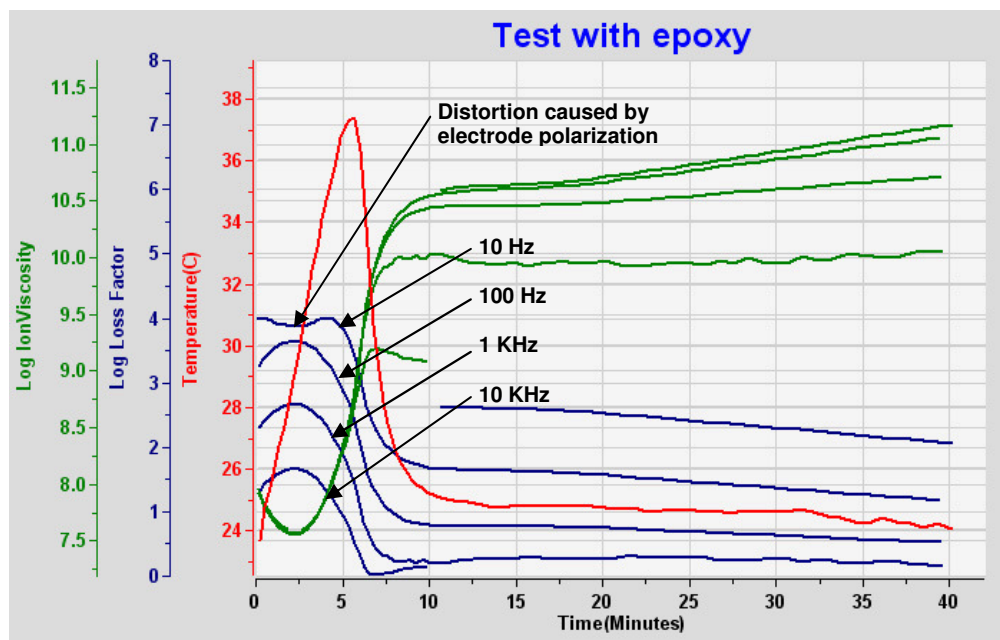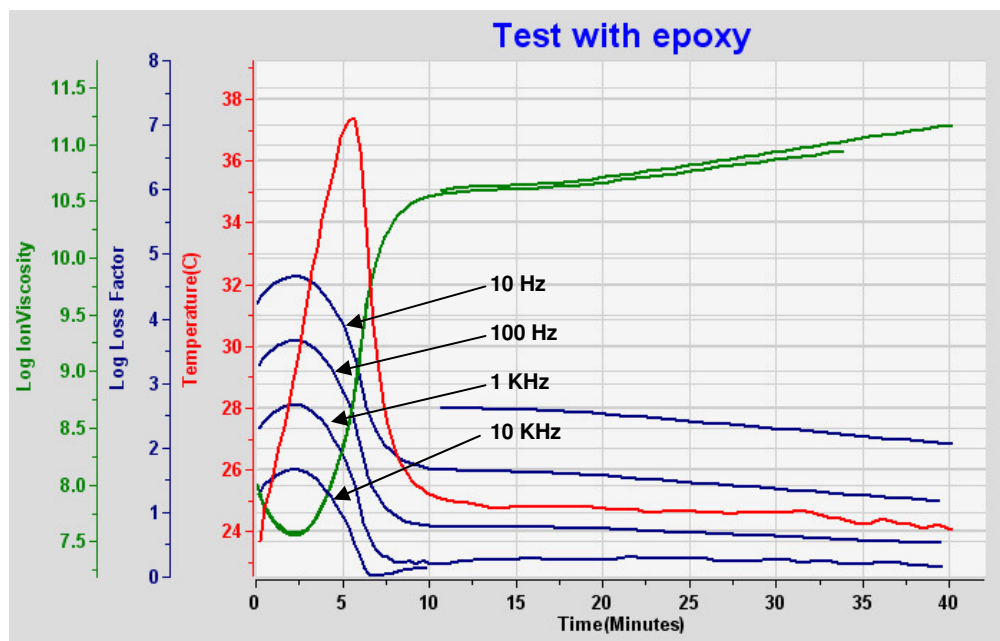

Figure 16-10
Correction of the boundary layer effect

Log($e''x$) is the logarithm of the original loss factor $e''x$, which was acquired during cure of an epoxy resin. Log($e''x$) data at 10 Hz shows distortions and the characteristic double hump from the boundary layer effect. This anomaly occurs at the time of maximum loss factor—maximum conductivity—as indicated by peaks from data at the higher frequencies of 100 Hz, 1.0 kHz and 10 kHz. Log(e'') is the logarithm of the corrected loss factor e'', and the corrected 10 Hz curve shows a loss factor peak consistent with peaks for higher frequencies.

Figure 16-11 compares data from the cure of this epoxy both before and after boundary layer correction.

Epoxy cure data showing distortion due to boundary layers

Epoxy cure data after electrode polarization correction

Figure 16-11
Comparison of data before and after electrode polarization correction

Note that loss factor is inversely proportional to frequency, as given by equation 16-5, repeated below:

(eq. 16-5) $$\varepsilon'' = \sigma' / (\varepsilon_o \, \omega)$$

During the early portion of cure, frequency independent DC conductivity (σ_{DC}) typically dominates loss factor and the corrected curves for 10 Hz, 100 Hz, 1 kHz and 10 kHz are all parallel and separated by factors of 10, as expected.

References

1. Day, D.R.; Lewis, T.J.; Lee, H.L. and Senturia, S.D., *Journal of Adhesion*, V18, p.73 (1985)

2. MacDonald, J.R., *Phys. Rev.*, v92, p.4 (1953)

Chapter 17—Electrical Modeling of Polymers

Introduction

The dielectric—literally "two-electric"—properties of conductivity σ, and permittivity ε, arise from ionic current and dipole rotation in bulk material. For polymers, mobile ions are often due to impurities and additives, while dipoles result from the separation of charge on nonpolar bonds or across a molecule. When analyzing dielectric properties, it is possible and convenient to separate the influence of ions from dipoles, as shown in Figure 17-1.a., to consider their individual effects.

Ions and Dipoles

The flow of ions in an electric field is called current, and is determined by conductivity σ, or its inverse resistivity ρ. The bulk effect of mobile ions can be modeled as a conductance G, as shown in Figure 17-1.b. This conductance changes as ion mobility changes. In turn, mobility depends on the state of a material—its viscosity when liquid or its modulus when solid. As a result, electrical measurements can be a means of probing material state.

The mechanical property of fluid viscosity impedes ionic motion, leading to the term *ion viscosity* to describe the electrical property of resistivity ρ. More specifically, *ion viscosity* should be reserved to describe the frequency independent resistivity ρ_{DC}. During the cure of thermosetting resin systems, comparisons of mechanical viscosity and ion viscosity have demonstrated that often the two differ by only an offset and a scaling factor. Thus ion viscosity can provide valuable insight into the condition of a polymer during processing. Furthermore, measurable changes in ion viscosity occur up to the end of cure— past the time when mechanical viscosity can no longer be measured.

The current through a conductance is in phase with the voltage across it, as shown in Figure 17-1.c. Admittance Y is given by equations 17-1 and 17-2:

(eq. 17-1) $\qquad\qquad\qquad Y = I/V$

(eq. 17-2) $\qquad\qquad\qquad Y = G + i\omega C$

Where:
$\quad I \ = $ current (A)
$\quad V = $ voltage (V)
$\quad G = $ conductance (moh)
$\quad C = $ capacitance (F)
$\quad \omega = 2\pi f \ (\text{s}^{-1})$
$\quad f \ = $ frequency (Hz)

Current I and voltage V in general are complex quantities. An admittance consisting only of conductance G can be represented as a vector along the Real axis in the complex plane, as shown in Figure 17-1.d.
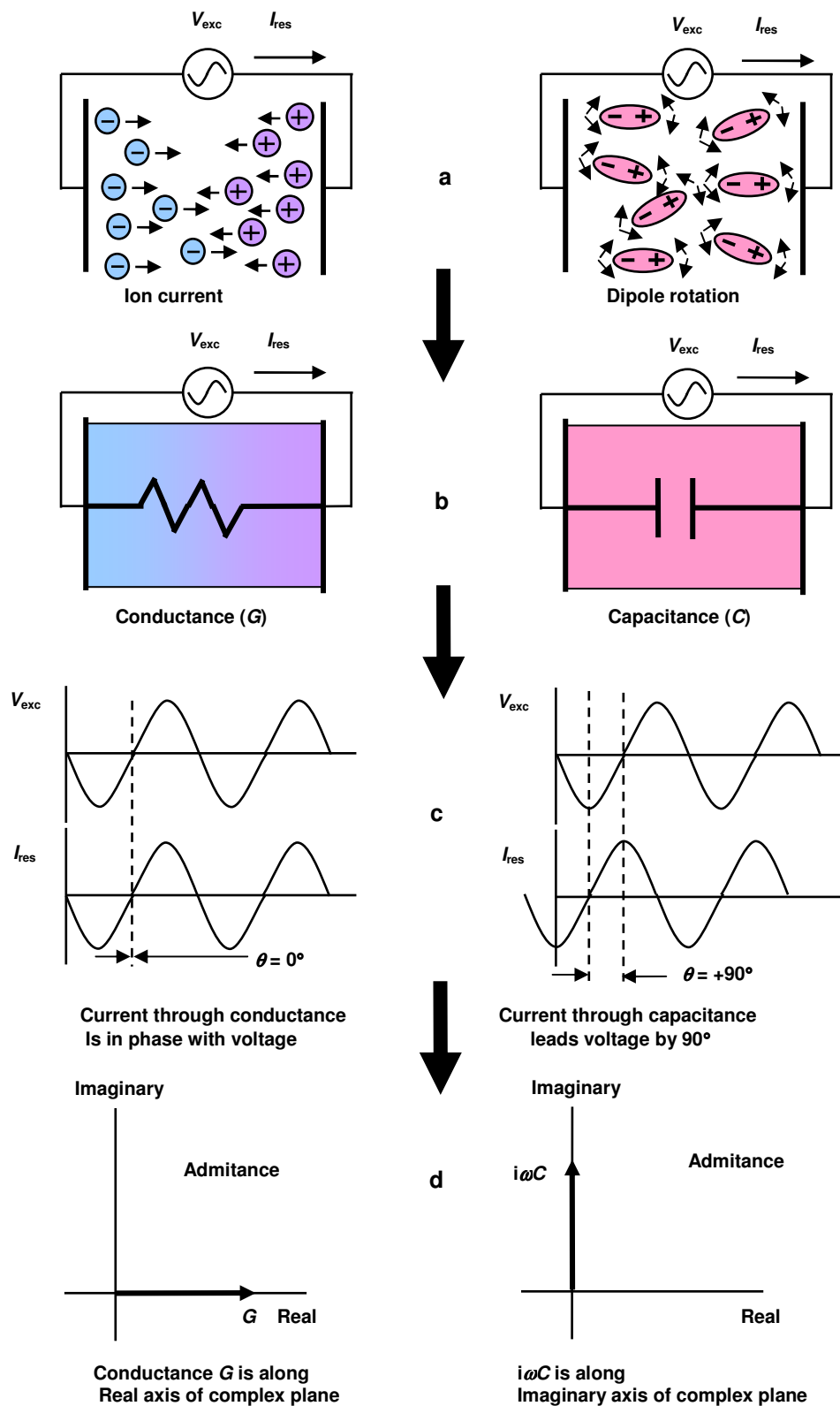
Figure 17-1
Relationships between physical and electrical behavior

The rotation of dipoles is a second material phenomenon, as shown in Figure 17-1.a, and gives rise to permittivity ε. As dipoles change their orientation in response to an electric field, they store energy which is released when their orientation returns to the relaxed state. This energy storage can be modeled as a capacitor, as shown in Figure 17-1.b.

The sinusoidal current through a capacitance leads the voltage across it by 90° as shown in Figure 17-1.c. An admittance consisting only of ωC can be portrayed on the complex plane as a vector along the Imaginary axis, as shown in Figure 17-1.d.

Raw dielectric measurements are conductance G (mohs) and capacitance C (farads). Resistance and other material properties are given by equations 17-3 through 17-7:

(eq. 17-3)	$R = 1/G$	(resistance)
(eq. 17-4)	$\rho = R\,A/D$	(resistivity or ion viscosity)
(eq. 17-5)	$\sigma = G / (A/D)$	(conductivity)
(eq. 17-6)	$\varepsilon' = C / (\varepsilon_o\,A/D)$	(relative permittivity)
(eq. 17-7)	$\varepsilon'' = \sigma / (\varepsilon_o\,\omega)$	(loss factor)

Where: $\varepsilon_0 = 8.85 \times 10^{-14}$ F/cm   (permittivity of free space)
A/D = ratio of area to distance for electrodes

Although A/D is classically applied to parallel plate geometries, it may be generalized to other configurations as a scaling factor, or cell constant, which makes equations 17-4, 17-5 and 17-6 true. In this case, A is not necessarily the area of the electrodes and D is not necessarily the distance between them. Two dimensional numerical simulations of electrodes in lossy media have validated this generalization across a wide range of conductivity.

The combined quantities G and C may be visualized on the complex plane as shown in Figure 17-2, where G is the real component of the admittance and ωC is the imaginary component. After bulk quantities G and C are divided by A/D and ε_0, the material properties of σ/ε_0 and relative permittivity ε' remain, resulting in rescaled values on the complex plane.
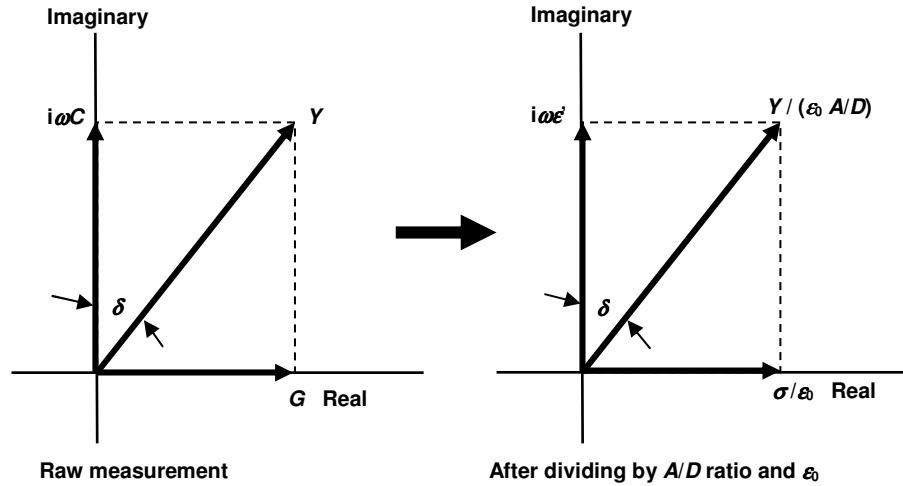
Figure 17-2
Relationship between bulk and material properties

The angle δ between Y and the imaginary axis may be incorporated into a quantity called dissipation factor, or loss tangent, tan δ, given by equation 17-8:

(eq. 17-8) $\tan \delta = \sigma/(\omega \varepsilon_0 \varepsilon')$

Use of loss factor in equation 17-8 yields the more common expression for loss tangent:

(eq. 17-9) $\tan \delta = \varepsilon''/\varepsilon'$

If a material has low conductivity or the frequency is very high, then ε'' and the ratio $\varepsilon''/\varepsilon'$ are small. In this case tan $\delta \sim \delta$ and δ may be approximated by equation 17-10:

(eq. 17-10) $\delta \sim \varepsilon''/\varepsilon'$

Electrical model of Material Under Test (MUT)

Dielectric measurements of a Material Under Test (MUT) yield a bulk conductance G_{MUT} in parallel with a bulk capacitance C_{MUT}, which can be used in the electrical model of Figure 17-3. In general, both components have frequency dependent and frequency independent terms. Similarly, the material properties of conductivity σ and permittivity ε have frequency dependent and independent behavior.
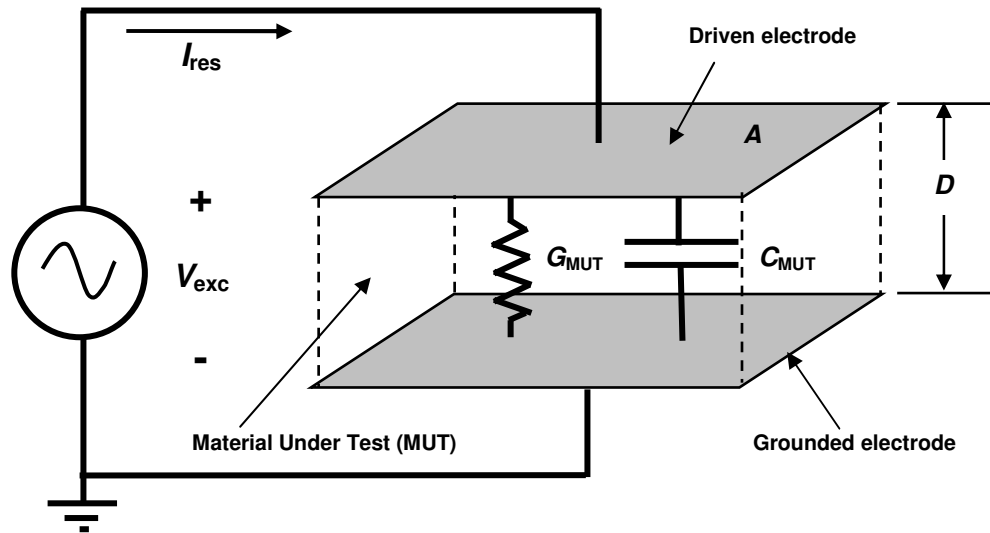
Figure 17-3
Electrical model of a polymer

It is easier to understand the electrical behavior of a polymer by considering Figure 17-4, which uses circuit components corresponding to the following physical phenomena:

- Flow of ions
    - Ion current in an electric field is determined by mobility in the polymer network
    - Current is frequency independent to first order in common polymers
    - Modeled by conductance G_{ion}
- Rotation of induced dipoles
    - Induced dipoles result from charge separation on nonpolar bonds
    - Induced dipoles rotate in an electric field without energy loss
    - Rotation has a frequency independent response
    - Modeled by capacitance $C_{induced}$
- Rotation of static dipoles
    - Static dipoles result from charge separation on molecules
    - Static dipoles rotate in an electric field with energy loss from friction
    - Rotation has a frequency dependent response with relaxation time τ
    - Modeled by conductance G_{static} in series with capacitance C_{static}
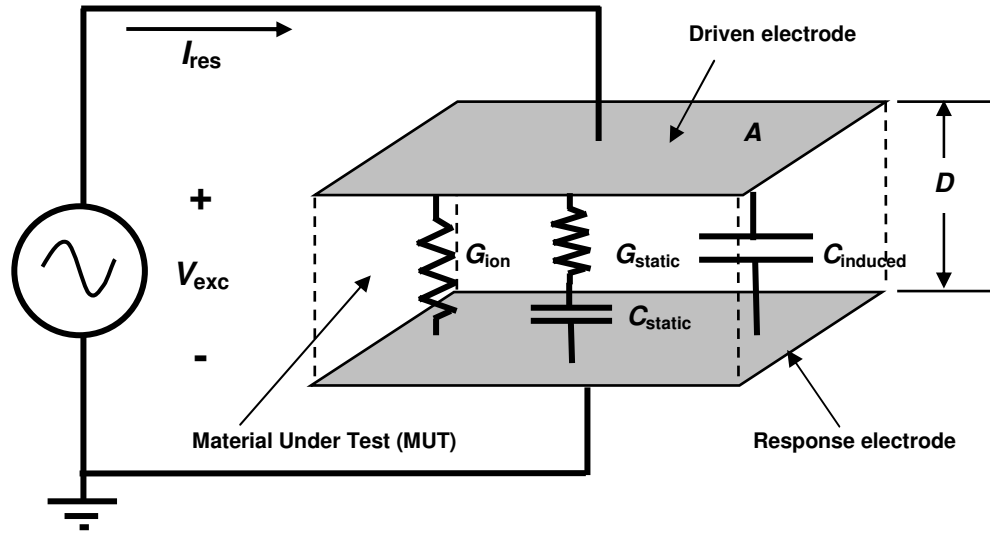
Figure 17-4
Electrical model of polymer physical behavior

It is possible to interpret the model of Figure 17-4 in terms of the measured quantities of conductance G_{MUT} and C_{MUT}. From circuit theory, the admittance of Figure 17-4 is given by equation 17-11:

(eq. 17-11) $\qquad Y_{MUT} = G_{ion} + i\omega C_{induced} + i\omega C_{static}/(1 + i\omega\tau)$

Where: $\qquad \tau \qquad = R_{static}\, C_{static} \qquad\qquad$ (dipole relaxation time)
$\qquad\qquad\qquad R_{static} \quad = 1/G_{static}$

Admittance can be expressed by keeping real and imaginary terms together:

(eq. 17-12) $\quad Y_{MUT} = [G_{ion} + \omega^2\tau C_{static}/(1 + (\omega\tau)^2)] + i\omega[C_{induced} + C_{static}/(1 + (\omega\tau)^2)]$

Combining equations 17-2 and 17-12 yields the following expressions for the measured bulk quantities:

(eq. 17-13) $\qquad\qquad G_{MUT} = G_{ion} + C_{static}\,[\omega^2\tau/(1 + (\omega\tau)^2)]$

(eq. 17-14) $\qquad\qquad C_{MUT} = C_{induced} + C_{static}/(1 + (\omega\tau)^2)$

Combining equations 17-5, 17-6, 17-7 and 17-13 results in the expressions for conductivity, loss factor and relative dielectric constant:

(eq. 17-15) $\sigma_{MUT} = \sigma_{ion} + \varepsilon_{static} \, [\omega^2 \tau / (1 + (\omega\tau)^2)]$

(eq. 17-16) $\varepsilon''_{MUT} = \sigma_{ion}/(\omega\varepsilon_0) + [\varepsilon_{static}/\varepsilon_0][\omega\tau/(1 + (\omega\tau)^2)]$

(eq. 17-17) $\varepsilon'_{MUT} = (\varepsilon_{induced}/\varepsilon_0) + (\varepsilon_{static}/\varepsilon_0)/(1 + (\omega\tau)^2)$

At low frequencies the *relaxed relative permittivity* is the sum of dielectric constants due to both static and induced dipoles. At high frequencies the *unrelaxed relative permittivity* is due only to induced dipoles. They are defined as follows:

(eq. 17-18) $\varepsilon'_r = (\varepsilon_{static} + \varepsilon_{induced})/\varepsilon_0$ (relaxed relative permittivity)

(eq. 17-19) $\varepsilon'_u = \varepsilon_{induced}/\varepsilon_0$ (unrelaxed relative permittivity)

The relative dielectric constant resulting from static dipoles may be expressed in terms of the relaxed and unrelaxed relative dielectric constants by using equations 17-18 and 17-19:

(eq. 17-20) $\varepsilon_{static}/\varepsilon_0 = \varepsilon'_r - \varepsilon'_u$

Combining equations 17-16, 17-17, 17-19 and 17-20 yields equations for the dielectric response:

(eq. 17-21) $$\varepsilon''_{MUT} = \sigma_{ion}/\omega\varepsilon_0 + (\varepsilon'_r - \varepsilon'_u)\, \frac{\omega\tau}{1 + (\omega\tau)^2}$$

(eq. 17-22) $$\varepsilon'_{MUT} = \varepsilon'_u + \frac{\varepsilon'_r - \varepsilon'_u}{1 + (\omega\tau)^2}$$

Where: ε'_u = Unrelaxed (high frequency) relative permittivity
ε'_r = Relaxed (low frequency) relative permittivity
ω = $2\pi f$ (radians/s)
τ = $R_{static} \, C_{static}$ (s)

Debye equations for dipolar rotation

　　　　Neglecting the ionic conductivity term, equations 17-21 and 17-22 also happen to be the loss factor and permittivity as expressed by the Debye equations, which describe the behavior of rotating dipoles. General admittance Y is given by equation 17-2, presented earlier:

(eq. 17-2) $$Y = G + i\omega C$$

Equation 17-2 may be rearranged to define admittance as a complex admittance $i\omega C^*$:

(eq. 17-23) $$i\omega C^* = i\omega(C - iG/\omega)$$

Dividing both sides of equation 17-23 by $i\omega\varepsilon_0$ and the A/D ratio yields a complex permittivity ε^*:

(eq. 17-24) $$\varepsilon^* = \varepsilon' - i(\sigma/\varepsilon_0\omega)$$

Finally, from the definition of loss factor (eq. 17-7), the complex permittivity may be expressed as follows:

(eq. 17-25) $$\varepsilon^* = \varepsilon' - i\varepsilon''$$

The classic Debye equation for dielectric relaxation, as a complex number and function of frequency, is:

(eq. 17-26) $$\varepsilon^*(\omega) = \varepsilon'_u + \frac{\varepsilon'_r - \varepsilon'_u}{1 + i\omega\tau}$$

Where:　　　ε'_u = Unrelaxed (high frequency) relative permittivity
　　　　　　ε'_r = Relaxed (low frequency) relative permittivity
　　　　　　ω = $2\pi f$ (radians/s)
　　　　　　τ = Dipole relaxation time (s)

Separating real and imaginary components of equation 17-26 yields the Debye equations for loss factor and relative permittivity:

(eq. 17-27)
$$\varepsilon'' = \text{Im}(\varepsilon^*(\omega)) = \frac{(\varepsilon'_r - \varepsilon'_u)\,\omega\tau}{1 + (\omega\tau)^2}$$

(eq. 17-28)
$$\varepsilon' = \text{Re}(\varepsilon^*(\omega)) = \varepsilon'_u + \frac{\varepsilon'_r - \varepsilon'_u}{1 + (\omega\tau)^2}$$

Loss factor ε'' and relative permittivity ε' are plotted as a function of $\omega\tau$ in Figure 17-5. The loss peak and the inflection point of relative permittivity both occur at $\omega\tau = 1$.
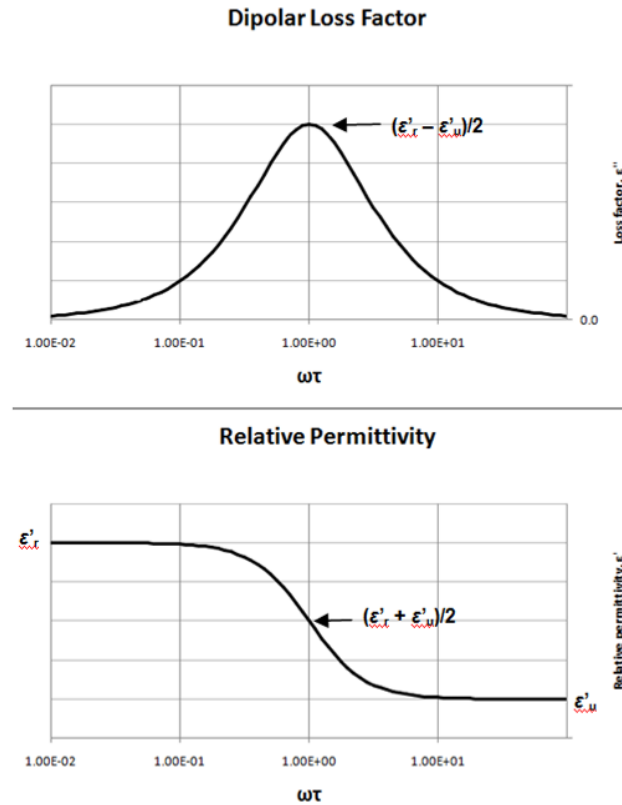
Figure 17-5
Debye relaxation behavior for loss factor and relative permittivity

A common diagram is the Cole-Cole plot shown in Figure 17-6. When loss factor is plotted vs. permittivity, the Debye equations form a semi-circle. This ideal behavior results from the assumption of a single dipolar time constant τ. In reality, a single relaxation time does not account for the effect of molecular weight distributions, varying locations along a polymer chain or the environment .
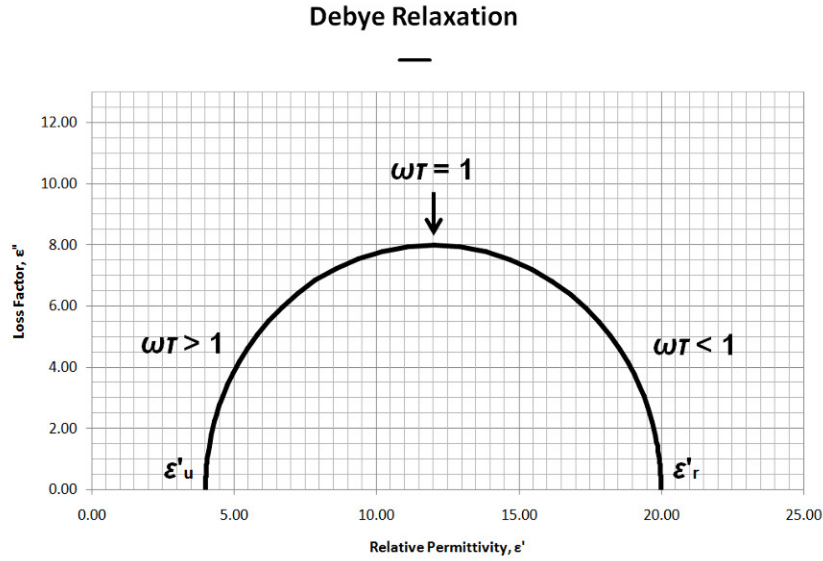
Figure 17-6
Cole-Cole plot of Debye relaxation

Variants of the Debye equations

In polymers and thermosets, it is common to find non-ideal dipole relaxation behavior, resulting in Cole-Cole plots that are squashed compared to the semi-circle of the Debye equations. This response has been attributed to the superposition of a range of relaxation times. The Cole-Cole plot may also be asymmetric, supposedly corresponding to asymmetric distributions of relaxation times.

Three common variants of the Debye equations attempt to empirically model non-ideal dipole behavior:

- Cole-Cole relaxation[1,2] (squashed plots)

$$\text{(eq. 17-29)} \qquad \varepsilon^*(\omega) = \varepsilon'_u + \frac{\varepsilon'_r - \varepsilon'_u}{1 + (i\omega\tau)^{1-\alpha}} \qquad (0 \leq \alpha \leq 1)$$

Cole-Cole Relaxation

— 1-alpha = 0.5
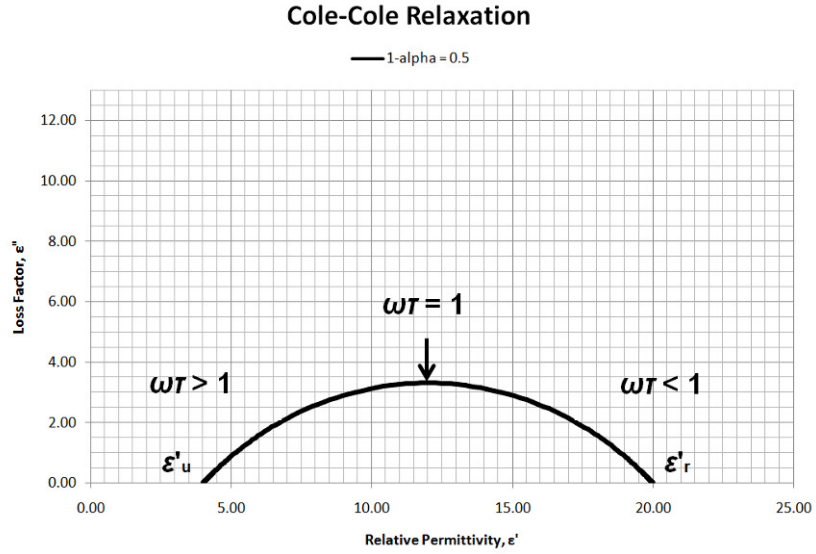
Figure 17-7
Cole-Cole plot of Cole-Cole relaxation

- Cole-Davidson[3] relaxation (asymmetric plots)

(eq. 17-30)
$$\varepsilon^*(\omega) = \varepsilon'_u + \frac{\varepsilon'_r - \varepsilon'_u}{(1 + i\omega\tau)^{\beta}}$$
$(0 \leq \beta \leq 1)$

Cole-Davidson Relaxation

— Beta = 0.5
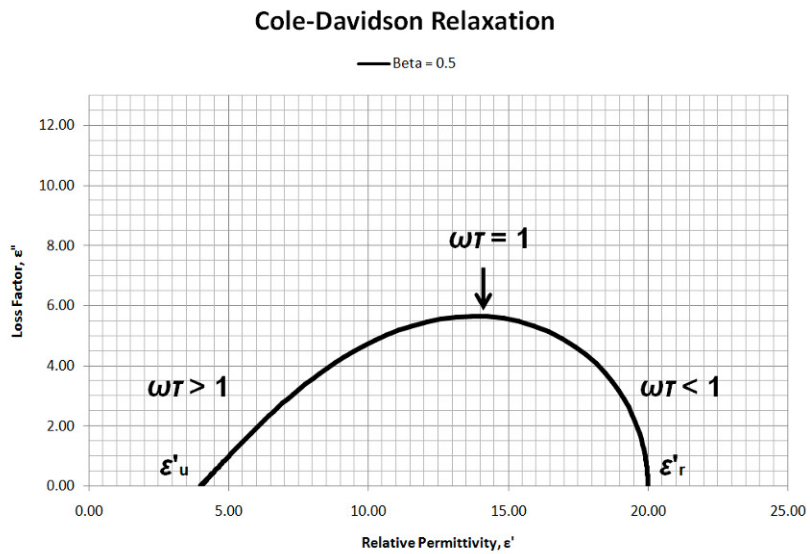
Figure 17-8
Cole-Cole plot of Cole-Davidson relaxation

- Havriliak-Negami relaxation[4] (squashed and asymmetric plots)

(eq. 17-31)
$$\mathcal{E}^*(\omega) = \mathcal{E}'_u + \frac{\mathcal{E}'_r - \mathcal{E}'_u}{(1 + (i\omega\tau)^\alpha)^\beta}$$
$$(0 \leq \alpha \leq 1)$$
$$\text{and}$$
$$(0 \leq \beta \leq 1)$$

Havriliak-Negami Relaxation
Alpha = 0.5, Beta = 0.5
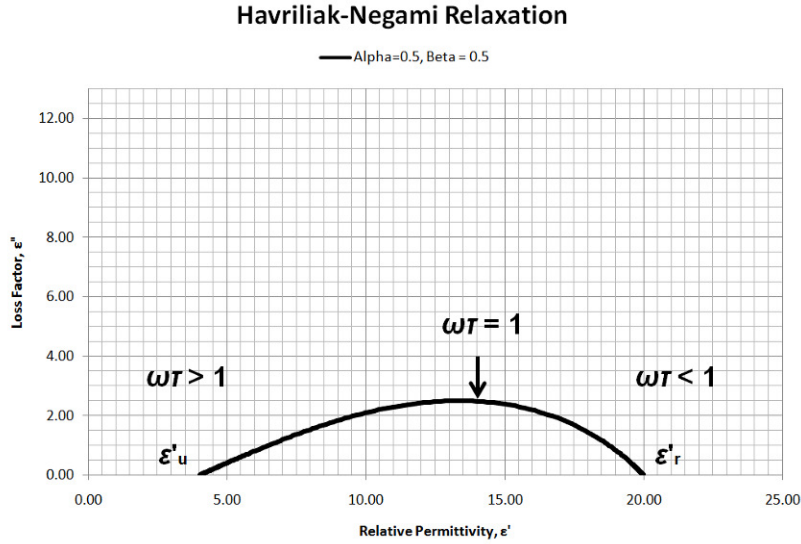
Figure 17-9
Cole-Cole plot of Havriliak-Negami relaxation

The Havriliak-Negami equation is simply a combination of the Cole-Cole and Cole-Davidson equations. If $\beta = 1$, then the result is Cole-Cole behavior. If $\alpha = 1$, then the result is Cole-Davidson behavior. If both $\alpha = 1$ and $\beta = 1$, then the Havriliak-Negami relaxation reduces to Debye relaxation.

The Havriliak-Negami relaxation of equation 17-31 may be factored into imaginary and real terms to yield expressions for loss factor and relative permittivity:

(eq. 17-32) $\mathcal{E}'' = (\mathcal{E}'_r - \mathcal{E}'_u)\,(1 + 2(\omega\tau)^\alpha \cos(\pi\alpha/2) + (\omega\tau)^{2\alpha})^{-\beta/2}\sin(\beta\theta)$

(eq. 17-33) $\mathcal{E}' = \mathcal{E}'_u + (\mathcal{E}'_r - \mathcal{E}'_u)\,(1 + 2(\omega\tau)^\alpha \cos(\pi\alpha/2) + (\omega\tau)^{2\alpha})^{-\beta/2}\cos(\beta\theta)$

Where:

(eq. 17-34) $\theta = \tan^{-1}[(\omega\tau)^\alpha \sin(\pi\alpha/2) / (1 + (\omega\tau)^\alpha \cos(\pi\alpha/2))]$
      α = Empirical "broadness" parameter
      β = Empirical "asymmetry" parameter
      $\mathcal{E}'_u$ = Unrelaxed (high frequency) relative permittivity
      $\mathcal{E}'_r$ = Relaxed (low frequency) relative permittivity
      $\omega = 2\pi f$ (radians/s)
      τ = Dipole relaxation time (s)

Contribution of ionic conduction to loss factor

      Pure dielectric materials show only the Debye-type dipolar relaxation behavior; however, in reality almost all materials have some ionic content or impurity. The presence of mobile ions adds an ionic conduction term to loss factor, as seen in equation 17-21, repeated below:

(eq. 17-21)
$$\varepsilon"_{MUT} = \sigma_{ion}/\omega\varepsilon_0 + (\varepsilon'_r - \varepsilon'_u)\frac{\omega\tau}{1 + (\omega\tau)^2}$$

In the case of equation 17-21, dipole relaxation is expressed with the Debye equation. More generally, loss factor may be expressed as the sum of ionic and dipolar loss factors, which is plotted in Figure 17-10:

(eq. 17-35)
$$\varepsilon"_{MUT} = \varepsilon"_{ion} + \varepsilon"_{dipole}$$
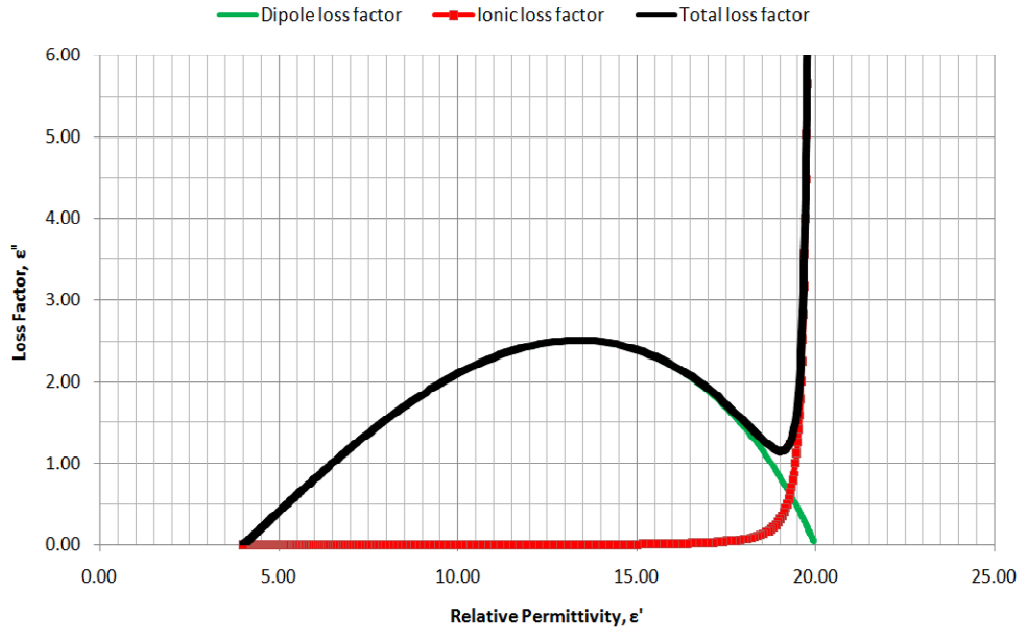
Figure 17-10
Addition of ionic and dipolar loss factors

Alternatively, the total loss factor is the sum of terms with frequency independent conductivity (σ_{DC}) and frequency dependent conductivity (σ_{AC}):

(eq. 17-36) $$\varepsilon"_{MUT} = (\sigma_{DC} + \sigma_{AC})/\omega\varepsilon_0$$

Where: $$\sigma_{DC} = \sigma_{ion}$$

$$\sigma_{AC} = \varepsilon_0\,(\varepsilon'_r - \varepsilon'_u)\,\frac{\omega^2\tau}{1 + (\omega\tau)^2}$$

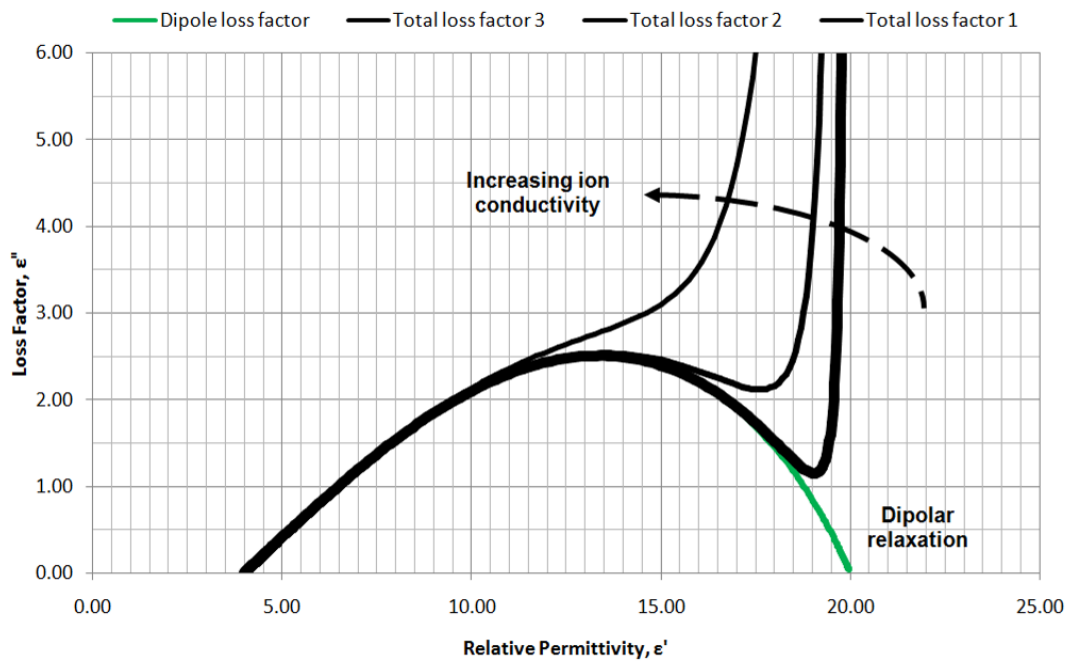As ionic conductivity increases, the effect on a Cole-Cole plot is shown in Figure 17-11:

Figure 17-11
**Total loss factor as a function of increasing ionic conductivity**

When loss factor is plotted as a function of frequency, it is easier to see the relative contributions from ionic conductivity and dipolar relaxation. Dielectric measurements measure total loss factor, and information from a single frequency cannot separate the effects of ions and dipoles. If conductivity is sufficiently low, however, a frequency sweep can reveal the dipole loss peak, as shown in Figure 17-12 for low and intermediate conductivities. Note that high conductivity in Figure 17-12 has hidden the dipole peak.
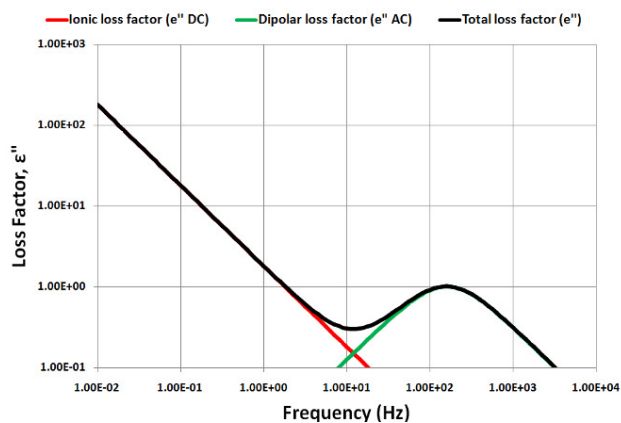
Low conductivity
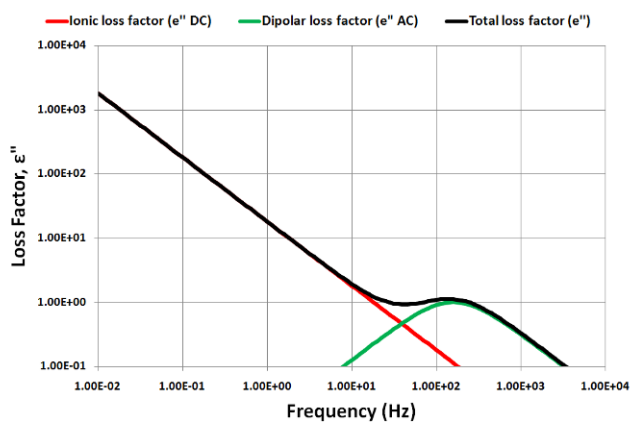
Intermediate conductivity
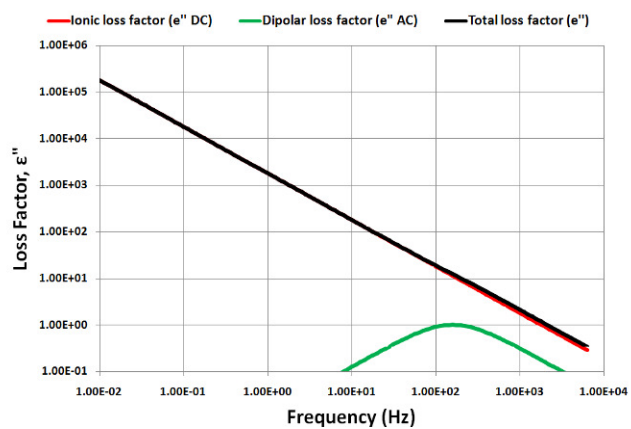
High conductivity

Figure 17-12
Effect of low, intermediate and high conductivity on loss factor (modeled)

As these plots illustrate, loss factor due to ions always dominates the response at sufficiently low frequencies. Dielectric cure monitoring takes advantage of this behavior to measure ionic conductivity without the influence of dipoles. The amount of crosslinking in a polymer or thermoset determines free ion mobility and therefore electrical conductivity. The amount of crosslinking also determines viscosity up to the gel point and modulus after the gel point. As a result, measurements of frequency independent conductivity σ_{DC} can probe the cure state of a material. Uniquely, dielectric measurements can observe the state of cure in-situ and in real time.

Electrode polarization and the low frequency response of boundary layers

The presence of mobile ions in a polymer does not affect how its dipoles rotate. Therefore the frequency response of relative permittivity should not depend on the amount of ionic conductivity. Figure 17-13 shows this ideal behavior for relative permittivity—which is the same at low, intermediate and high conductivities—for the example modeled in Figure 17-12.
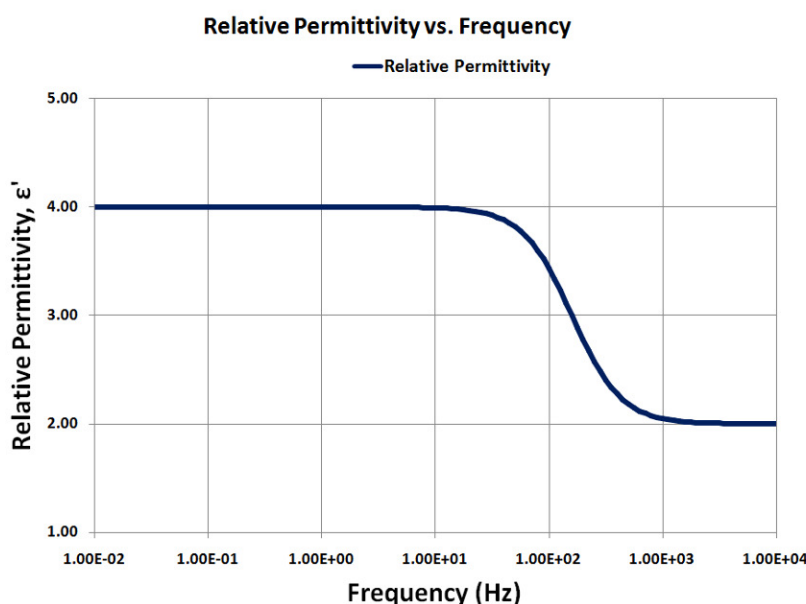

Figure 17-13
Ideal frequency response of relative permittivity
(Corresponding to example modeled in Figure 17-12)

Actual dielectric measurements of polymers usually reveal very large increases in permittivity at low frequencies or high conductivities. This behavior differs significantly from the Debye response and is *not* caused by a true change in permittivity. Instead, it is the result of an interaction between the material and the electrodes used to make measurements.

When a polymer has very high loss factor, ions accumulate at the electrode, where they are not exchanged because of an electrically insulating layer, such as a film or oxide

or electrochemical potential barrier. This phenomenon is called *electrode polarization.* A boundary layer forms, depleted of ions, and only the dipolar response remains. As a result, the boundary layer acts as a capacitor in series with the bulk material.

In the presence of electrode polarization, very high permittivities result from use of the model of Figure 17-4, which is incorrect for the situation. The correct model of Figure 17-14 and the corresponding circuit of Figure 17-15 must be used instead.
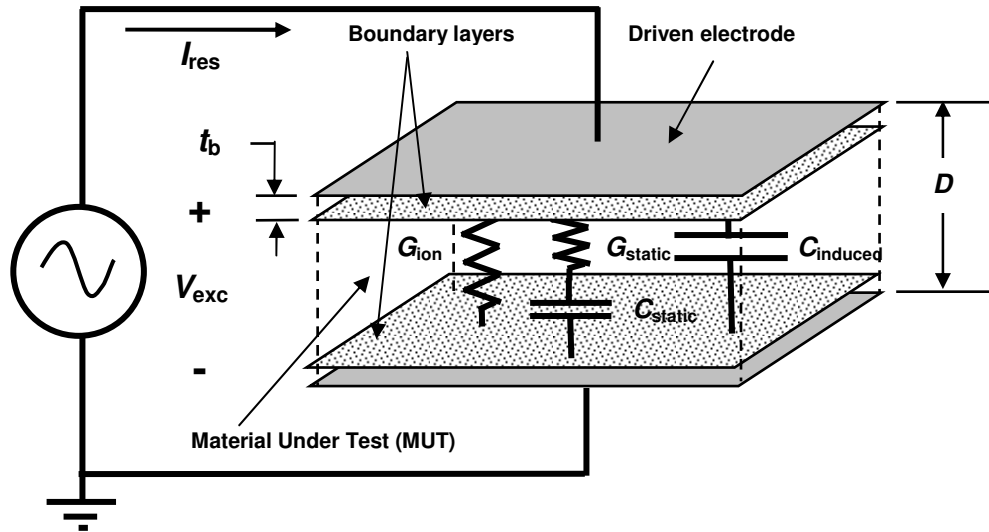

Figure 17-14
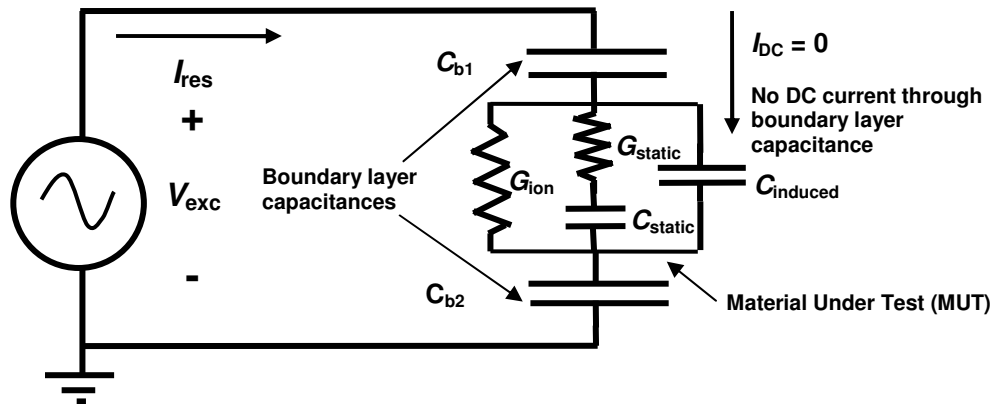**Boundary layer capacitances resulting from electrode polarization**

Figure 17-15
Circuit model of polymer with boundary layer capacitances

The boundary layer is very thin compared to the separation between electrodes. Consequently, boundary layer capacitance is much larger than bulk capacitance; it dominates the circuit response and acts as an open circuit to block DC current. Measurements of DC conductance are impossible in this case and the material appears primarily capacitive.

The low frequency electrical circuit of Figure 17-16 may be used to understand the resulting dielectric response. Here the two boundary layer capacitances, which are in series, have been combined into a single component with half the capacitance $C_b/2$. At low frequencies the admittances of capacitances due to static and induced dipoles are very low and only the conductive component G_{ion} contributes significantly to the response. This configuration is the same as the circuit representing the behavior of dipoles (G_{static} in series with C_{static} of Figure 17-4), and would have behavior similar to Debye relaxation.
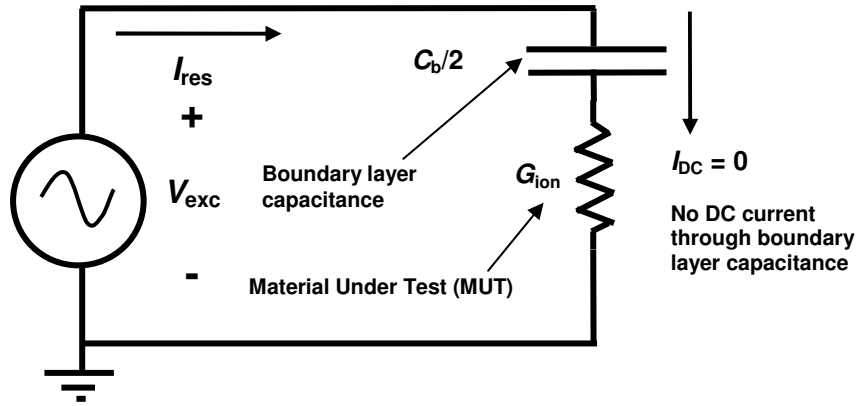

Figure 17-16
Low frequency circuit model with boundary layer capacitance

The uncorrected relative permittivity and loss factor resulting from electrode polarization are given by the following equations[5]:

$$(\text{eq. 17-37}) \quad \varepsilon'_x = \varepsilon' \, (D / 2t_b) \, \frac{(\varepsilon''/\varepsilon')^2 + (D / 2t_b)}{(\varepsilon''/\varepsilon')^2 + (D / 2t_b)^2} \qquad \text{Apparent relative permittivity}$$

$$(\text{eq. 17-38}) \quad \varepsilon''_x = \varepsilon'' \, (D / 2t_b) \, \frac{(D / 2t_b) - 1}{(\varepsilon''/\varepsilon')^2 + (D / 2t_b)^2} \qquad \text{Apparent loss factor}$$

Where: t_b = boundary layer thickness
           D = distance between electrodes or plate separation
           ε' = actual permittivity
           ε'' = actual loss factor

At low loss factors (high frequencies or low conductivities), electrode polarization has little effect on either the measured permittivity or loss factor. At sufficiently high loss factors, however, the apparent permittivity begins to increase, causing loss factor on the Cole-Cole plot of Figure 17-17 to deviate from its ideal, vertical trajectory.
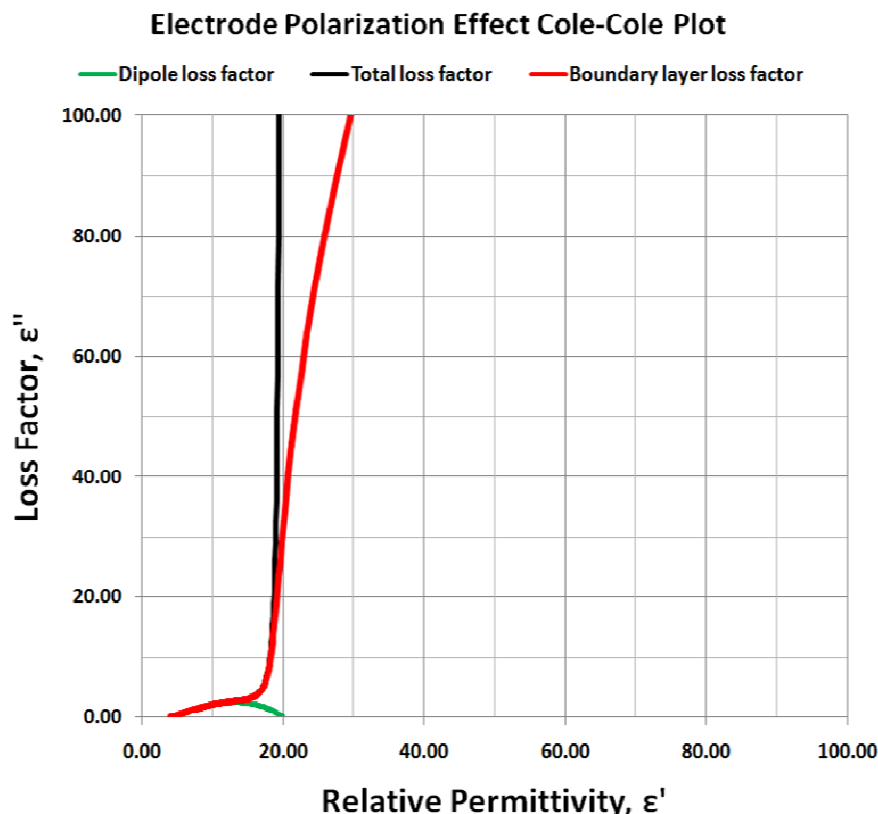

Figure 17-17
Deviation of Cole-Cole plot trajectory caused by electrode polarization

As the *true* material loss factor increases even further, the *apparent* permittivity continues to increase and at some point the *apparent* loss factor actually begins to decrease. The Cole-Cole plot becomes the arc of Figure 17-18. Eventually, when the true loss factor is high enough (i.e. frequency is sufficiently low or conductivity is sufficiently high), the apparent permittivity reaches a very high limit and the apparent loss factor approaches zero. The result is a semi-circle on the Cole-Cole plot like that produced by the Debye relaxation, but with a much larger radius. This radius depends on the thickness of the boundary layer relative to the separation between electrodes.

Because of electrochemical potential barriers, electrode polarization almost always occurs. If the resulting boundary layer is very thin, the effect on loss factor is reduced, and the radius of the Cole-Cole plot is very large. While the change in apparent loss factor may be small, the change in apparent relative permittivity usually remains significant.

Figure 17-18
Cole-Cole plot trajectories caused by electrode polarization
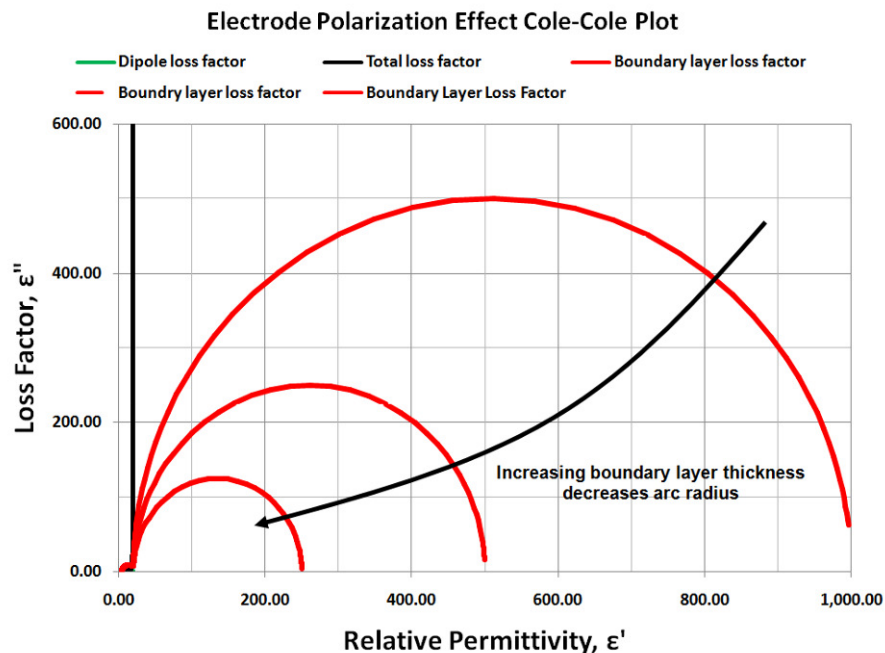
Figure 17-19 compares the frequency response of true permittivity, which has a Debye-type relaxation, with the apparent permittivity resulting from a boundary layer. In this case the modeled behavior demonstrates how the relative relationship between the dipolar and the boundary layer time constants determines visibility of the dipole relaxation.

Under the same conditions modeled in Figure 17-19, Figure 17-20 compares the frequency response of true loss factor with the apparent loss factor resulting from a boundary layer. Note that the apparent loss factor has a peak of very high value at very low frequency, while true loss factor does not. In the past this artificial loss peak has been attributed to a large dipole relaxation. The differences between dipole and boundary layer loss peaks are:[6]
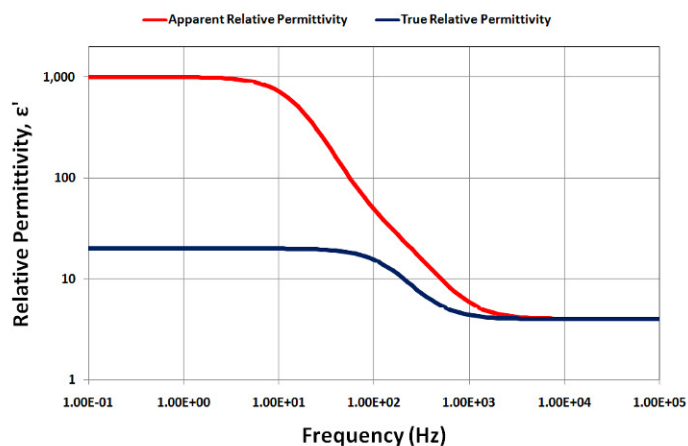
- Dipole loss peaks for most polymers are rarely greater than 3 and almost never greater than ~10

- Boundary layer loss peaks are usually greater than ~100

- Boundary layer loss peaks vary with electrode separation, while dipole loss peaks do not
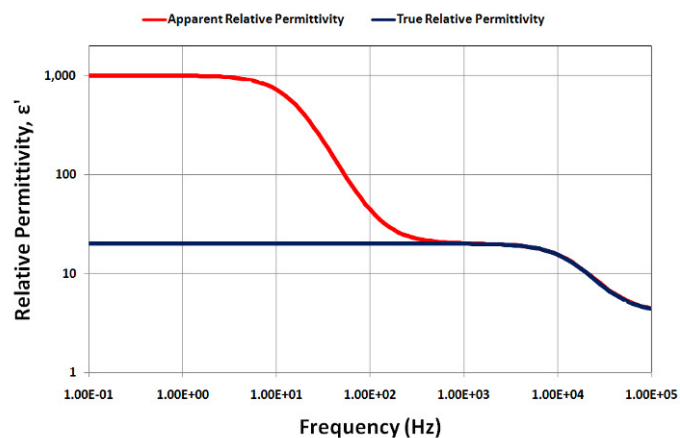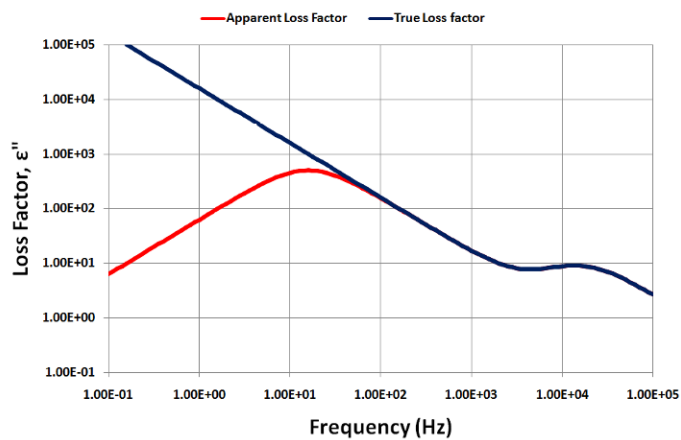
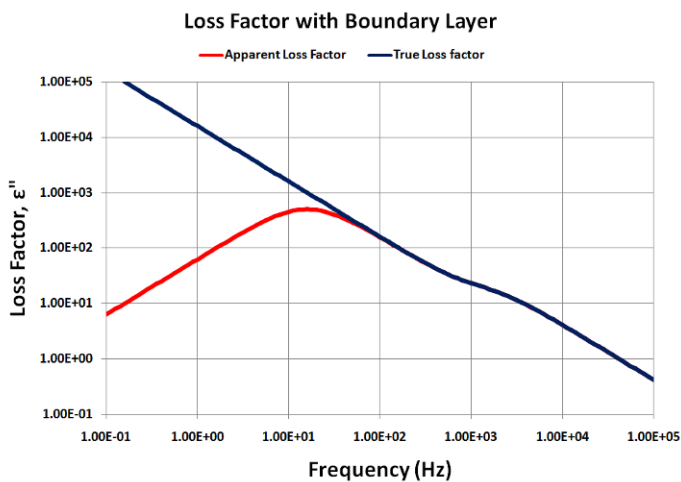**Small dipole time constant**
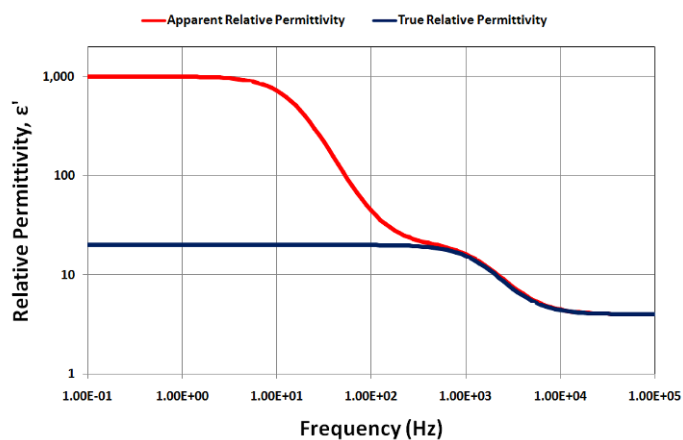
Intermediate dipole time constant
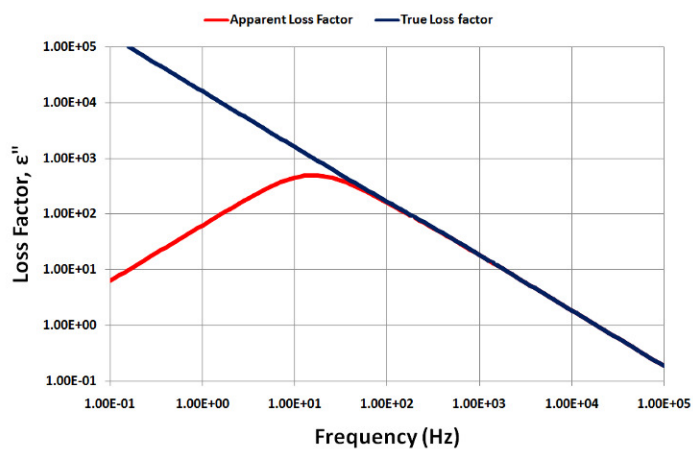

Large dipole time constant

Figure 17-19
Relative permittivity and the influence of electrode polarization

Small dipole time constant

Intermediate dipole time constant

Large dipole time constant

Figure 17-20
Loss factor and the influence of electrode polarization

Figures 17-21 and 17-22 show the effect of boundary layers on apparent dielectric properties during cure of "five-minute" epoxy. In this case, unlike for Figures 17-19 and 17-20, permittivity and loss factor are changing with time and temperature.
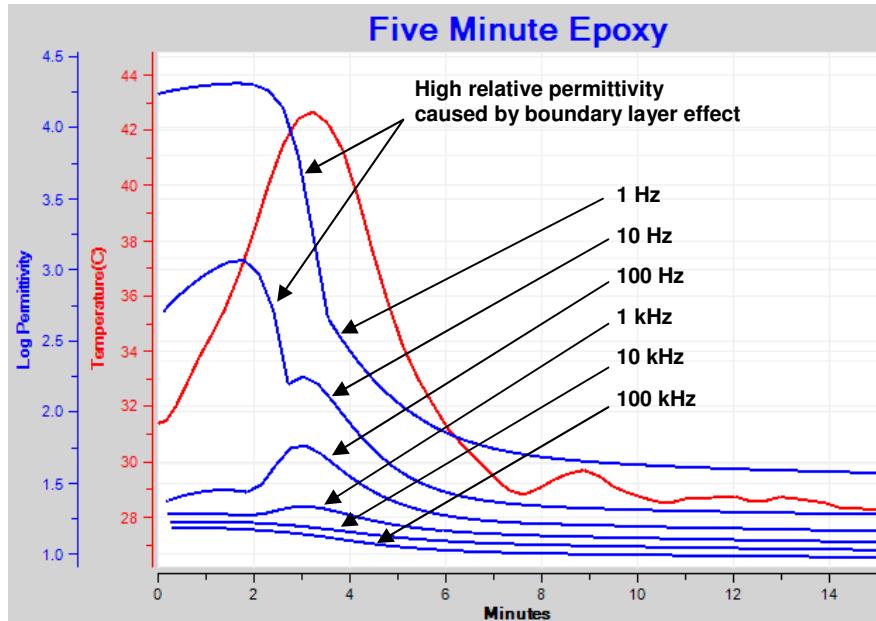

Figure 17-21
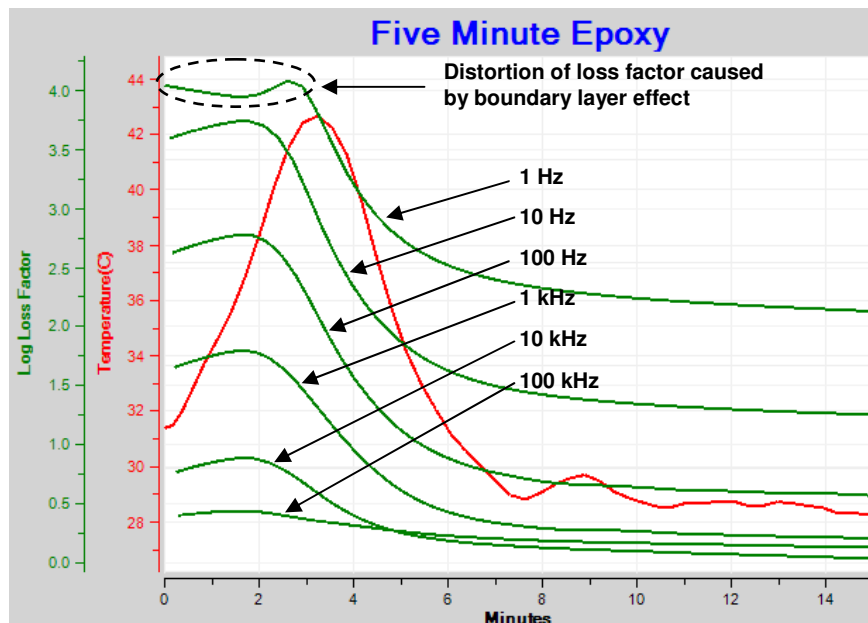**Relative permittivity of curing epoxy, showing effect of boundary layer**

Figure 17-22
Loss factor of curing epoxy, showing effect of boundary layer

The curing reaction is exothermic and temperature increases at first, which causes viscosity to decrease. Consequently, both conductivity and loss factor increase during this initial period. After a certain time, temperature is high enough for the accelerating reaction rate to dominate—viscosity begins to increase because the amount of polymerization overcomes the decrease in viscosity due to temperature. At this point conductivity and loss factor also decrease.

After loss factor reaches its peak, it declines to approach a constant value at the end of cure. For frequencies of 10 Hz or greater, this peak in loss factor is well behaved. For 1 Hz, however, the boundary layer effect distorts loss factor by depressing the peak and creating two satellite peaks in its place. Before researchers understood electrode polarization in polymers, the second satellite peak was thought to coincide with gelation. In fact, these peaks are artifacts of an incorrect electrical model. Fortunately, in many cases it is possible to mathematically correct the distortion caused by boundary layers (See Chapter 16, *Electrode Polarization and Boundary Layer Effects*).

For this epoxy, relative permittivity has a clear Debye-type relaxation visible at 100 kHz and 10 kHz. At 1 kHz and 100 Hz, relative permittivity displays a peak, which is caused by the temperature response of permittivity. Note that maximum permittivity coincides with the maximum temperature of this test. At 10 Hz the boundary layer effect artificially increases apparent permittivity and partially hides this peak in permittivity. Finally, at 1 Hz the boundary layer dominates completely and relative permittivity exceeds 10,000 at its maximum—a completely unrealistic value.

Inhomogeneities and Maxwell-Wagner-Sillars polarization

Until now this chapter has discussed only homogeneous polymers. The electrical response, however, is not as straightforward with multi-layer films, fiberglass composites or materials with several phases. The Maxwell-Wagner-Sillars[7,8] effect (sometimes simply called the Maxwell-Wagner effect) describes dielectric behavior resulting from charge accumulation at the boundaries of inhomogeneities. The Maxwell-Wagner-Sillars model uses small spheres embedded in an infinite dielectric as shown in Figure 17-23. In essence, Maxwell-Wagner-Sillars polarization is the same as electrode polarization, resulting in a large parasitic capacitance in series with bulk material.

This model has a dielectric response like that of a boundary layer, with very high *apparent* permittivities and distortions in *apparent* loss factor. Depending on the nature of the inhomogeniety, the Maxwell-Wagner-Sillars effect can become very complicated. In the case of multi-layer films, the dielectric behavior can be identical to that of a boundary layer because the geometries are the same.

Some analysis of insulating fibers in a conductive material has attempted to simulate the cure of fiberglass or Kevlar epoxy composites. For reasonable fiber geometries, permittivity is affected but loss factor is not, which agrees with experimental evidence.[6] In some cases loss factor increases, possibility because of an increase in ion concentration from the fibers.
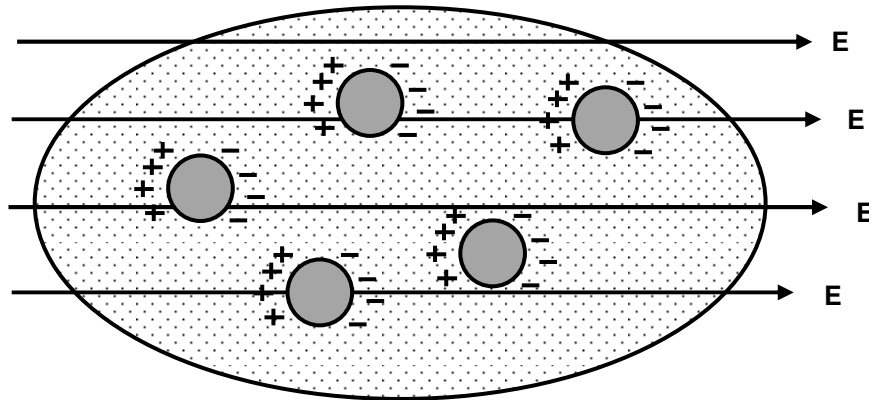
Figure 17-23
Maxwell-Wagner-Sillars polarization

Summary of the electrical model of polymers

- Induced dipole rotation
    - Modeled by $C_{induced}$, bulk capacitance from induced dipoles on nonpolar bonds
    - Frequency independent response

- Static dipole rotation
    - Modeled by C_{static} in series with G_{static}, capacitance and conductance from molecular dipoles
    - Frequency dependent response
    - Cole-Cole plot is an arc between relaxed and unrelaxed permittivity limits
    - Dipole loss factor peaks rarely greater than 3 and almost never greater than ~10

- Ionic conduction
    - Modeled by G_{ion}, bulk conductance from mobile ions
    - Frequency independent response
    - Cole-Cole plot is a vertical line

- Electrode polarization
    - Modeled by C_b, boundary layer capacitance on electrodes
    - Frequency dependent response in combination with G_{ion}
    - Cole-Cole plot is an arc over unrealistically large permittivities
    - Boundary layer loss factor peaks usually greater than ~100

- Maxwell-Wagner-Sillars polarization
    - Modeled by spheres in a dielectric material
    - Frequency dependent response in combination with G_{ion}
    - Cole-Cole plot similar to result from electrode polarization

References

1. Cole, K.S.; Cole, R.H., "Dispersion and Absorption in Dielectrics - I Alternating Current Characteristics". *Journal of Chemical Physics,* **9**: 341–352 (1941).

2. Cole, K.S.; Cole, R.H., "Dispersion and Absorption in Dielectrics - II Direct Current Characteristics". *Journal of Chemical Physics,* **10**: 98–105 (1942).

3. Davidson, D.W. and Cole, R.H., "Dielectric relaxation in glycerol, propylene glycol, and normal-propanol". *Journal of Chemical Physics*, 19(12):1484–1490 (1951).

4. Havriliak, S.; Negami, S., "A complex plane representation of dielectric and mechanical relaxation processes in some polymers". *Polymer*, **8**:161-210 (1967).

5. Day, D.R.; Lewis, T.J.; Lee, H.L. and Senturia, S.D., *Journal of Adhesion*, V18, p.73 (1985).

6. Day, D.R., *Dielectric Properties of Polymeric Materials*, Micromet Instruments, (1988).

7. Wagner, K.W., *Arch. Elektrotech*. 2:378 (1914).

8. Sillars, R.W., *J. Inst. Elm. Engrs* (London) 80:378 (1937).

Chapter 18—Using Ion Viscosity for Cure Monitoring

Introduction

Electrical measurements of material between a pair of electrodes can be converted to the dielectric properties of permittivity and conductivity. For a polymer or thermoset, conductivity has a frequency independent component (σ_{DC}) caused by mobile ions and a frequency dependent component (σ_{AC}) arising from dipole rotation. The inverse of conductivity is resistivity ρ, which also has frequency independent (ρ_{DC}) and frequency dependent terms (ρ_{AC}).

Frequency independent resistivity is also called ion viscosity (*IV*), which correlates with the cure state of thermoset materials. For dielectric cure monitoring it is important to recognize when to use ion viscosity and understand how to isolate it from other factors.

Loss factor during cure

It is easiest to begin with the loss factor of a Material Under Test, $\varepsilon"_{MUT}$, as given by equation 18-1:

(eq. 18-1) $$\varepsilon"_{MUT} = (\sigma_{DC} + \sigma_{AC})/\omega\varepsilon_0$$

Figure 18-1 shows loss factor for the room temperature cure of a "Five-minute" epoxy.
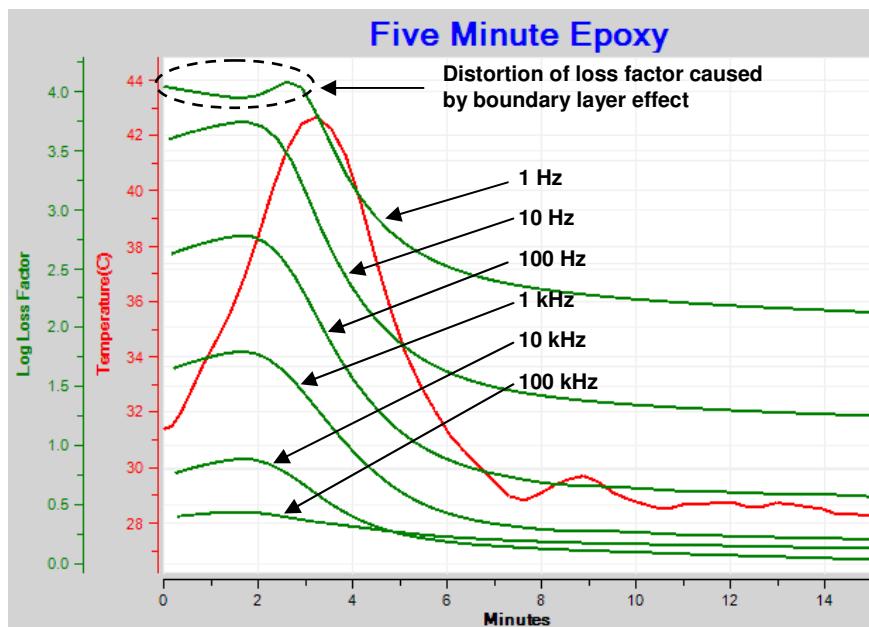

Figure 18-1
Loss factor of curing epoxy, showing effect of boundary layer

When σ_{DC} dominates dielectric measurements, loss factor is inversely proportional to frequency. For example, if $\sigma_{DC} \gg \sigma_{AC}$ then loss factor at 10 Hz would be ten times greater than loss factor at 100 Hz.

In the early part of this cure, loss factor is inversely proportional to frequency for 10 kHz and less, and σ_{DC} dominates at these frequencies. Loss factor for 1 Hz shows distortions characteristic of a boundary layer caused by electrode polarization. As cure progresses, the relative influence of dipoles grows, σ_{AC} increases and after a time loss factor is no longer inversely proportional to frequency for 1 kHz, 10 kHz and 100 kHz. At the end of cure, loss factor for these frequencies almost overlap, indicating the strong influence of dipole relaxation.

At the end of cure, loss factors for 1 Hz and 10 Hz still show the inversely proportional relationship associated with frequency independent conductivity, and these two frequencies are suitable to redefine as ion viscosity.

Figure 18-2 shows resistivity ρ derived from the loss factor data of Figure 18-1, using equation 18-2.

(eq. 18-2) $$\rho = 1/(\omega \varepsilon_0 \, \varepsilon''_{MUT})$$

Where: $\varepsilon_0 = 8.85 \times 10^{-14}$ F/cm   (permittivity of free space)
$\omega = 2\pi f \ (s^{-1})$
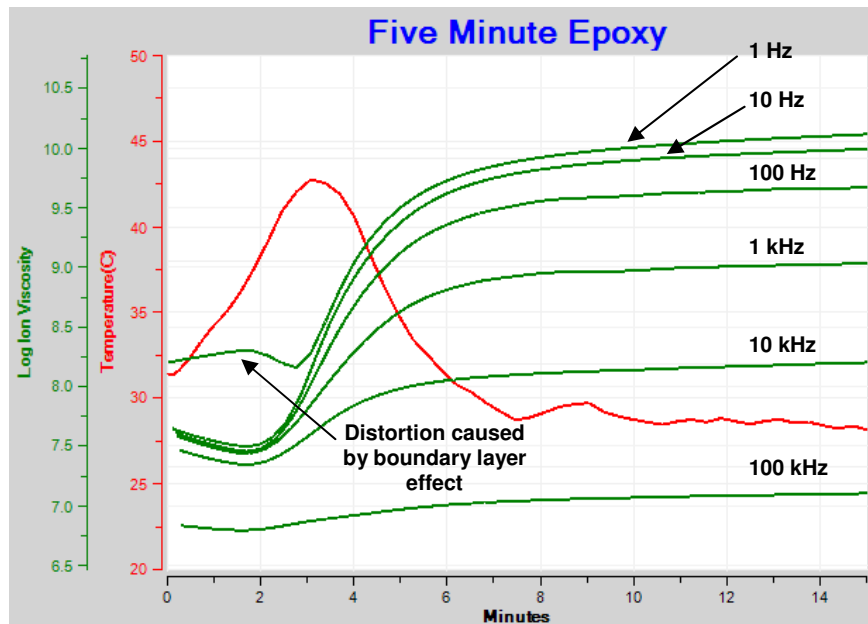f = frequency (Hz)

Figure 18-2
Resistivity of curing epoxy (plotted against log(ion viscosity) axis)

Here, resistivity has both frequency independent and frequency dependent terms, given by equations 18-3, 18-4 and 18-5. In this case, ionic conductivity σ_{DC} is dominant where curves overlap, and dipolar response is dominant where they do not.

(eq. 18-3) $$\rho = 1/(\sigma_{DC} + \sigma_{AC})$$

(eq. 18-4) $$\sigma_{DC} = \sigma_{ion}$$

(eq. 18-5) $$\sigma_{AC} = \varepsilon_0\, \omega\, \frac{(\varepsilon'_r - \varepsilon'_u)}{1 + (\omega\tau)^2}$$

Where: ε'_u = Unrelaxed (high frequency) relative permittivity
ε'_r = Relaxed (low frequency) relative permittivity
$\omega = 2\pi f$ (radians/s)
τ = Dipole relaxation time (s)

Finally, ion viscosity (IV) is defined as the frequency independent resistivity, given by equation 18-6:

(eq. 18-6) $$IV = \rho_{DC} = 1/\sigma_{DC}$$

Distinguishing ion viscosity from resistivity

It is possible to use two adjustable, empirical parameters to define whether loss factor—and consequently conductivity and resistivity—are dominated by ionic conduction. These parameters are called *Loss Factor Cut*off and *Permittivity Cutoff*, and are useful for algorithms to automatically distinguish ion viscosity from general resistivity.

- **Loss Factor Cutoff (see Figures 18-3 and 18-4)**
    - Sometimes called *Dipole Cutoff*
    - Maximum loss factor showing the influence of dipole relaxation
    - Below Loss Factor Cutoff, frequency dependent conductivity (σ_{AC}) dominates the dielectric response
    - Above Loss Factor Cutoff, frequency independent conductivity (σ_{DC}) dominates the dielectric response
    - ε" is converted to ion viscosity only for ε" > Loss Factor Cutoff

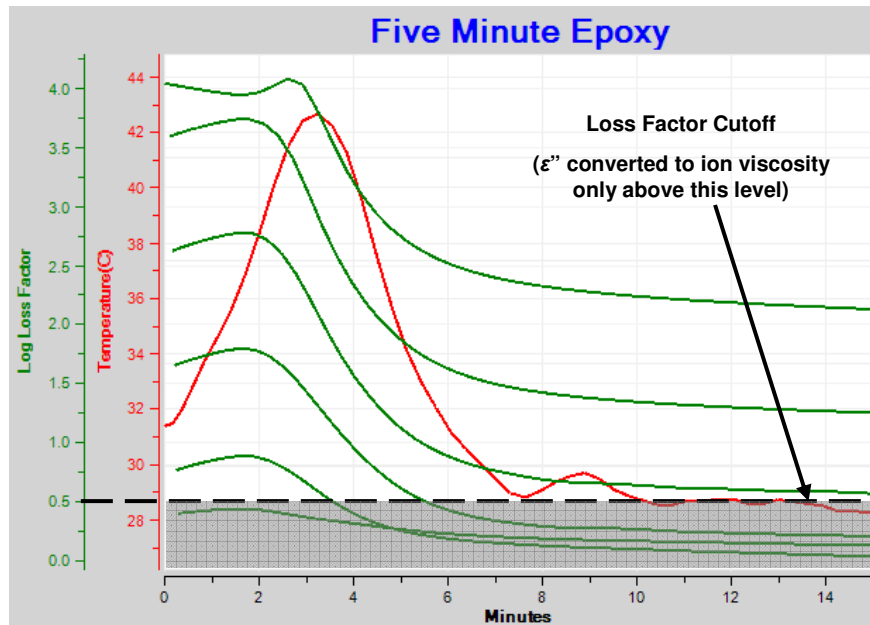Figures 18-3 and 18-4 show the relationship between dielectric data and a Loss Factor Cutoff with the value of 3.0.

Figure 18-3
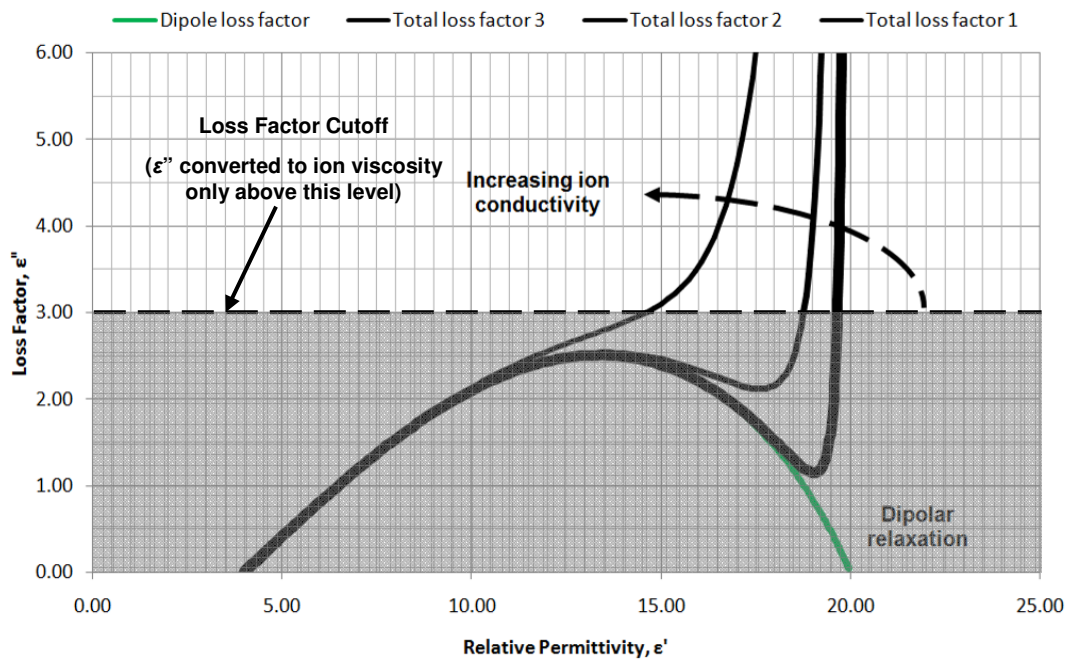**Loss factor cutoff applied to Five Minute Epoxy cure data**

Figure 18-4
Loss factor cutoff on Cole-Cole plot (example)

Figure 18-5 shows multiple ion viscosity curves when the Loss Factor Cutoff is too low. As a result, some of the ion viscosity curves do not overlap and do not indicate clearly which data correspond to mechanical viscosity and the state of cure. Note the distortion in the 1 Hz curve from the boundary layer effect.
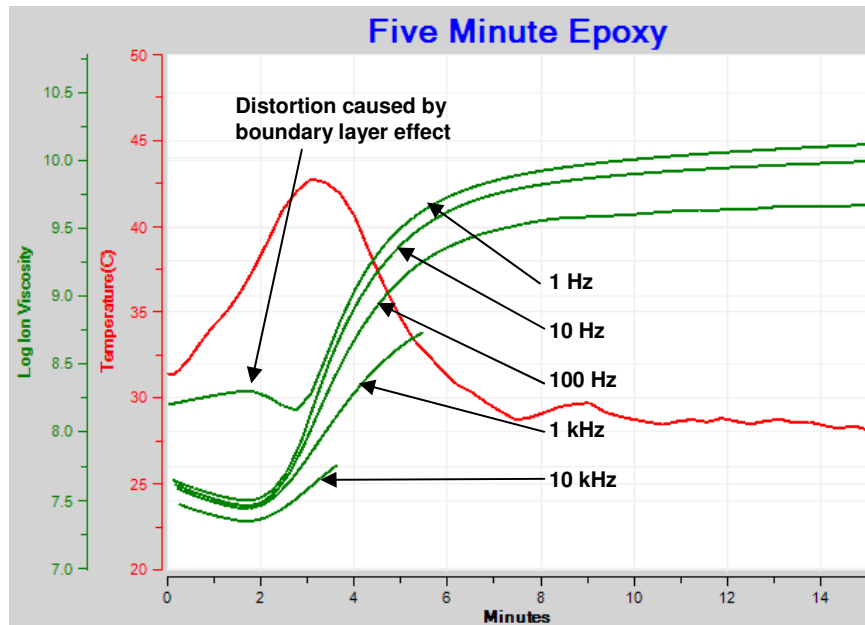

Figure 18-5
Ion viscosity data when Loss Factor Cutoff is too low

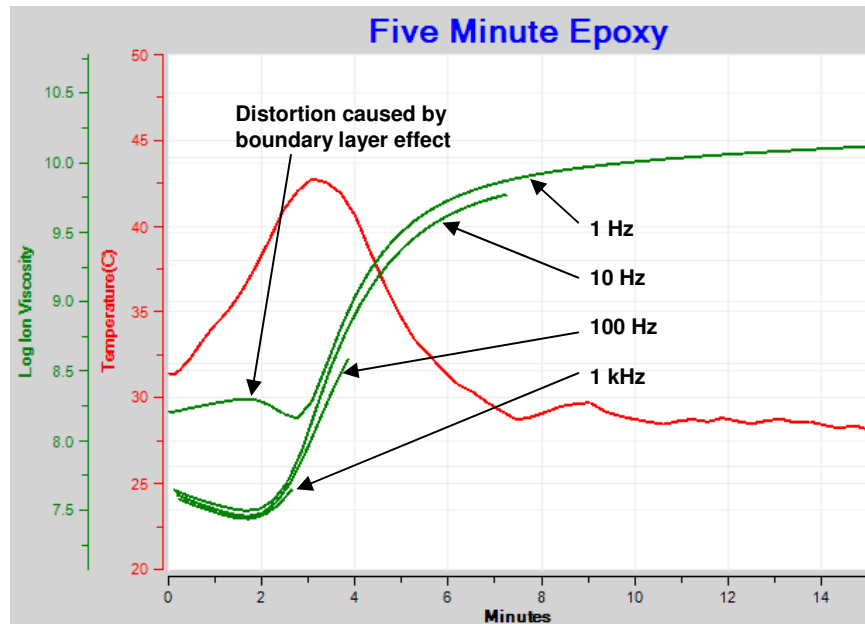Results with a appropriate value of Loss Factor Cutoff are shown in Figure18-6.

Figure 18-6
Ion viscosity data with appropriate Loss Factor Cutoff

Now the plotted ion viscosity curves largely overlap, indicating data dominated by frequency independent conductivity, which correlates well with cure state. The overlap is seldom perfect because ionic conductivity is frequency independent to first order but may have other influences that make the response non-ideal.

In Figure 18-6 the distortion caused by boundary layers is still present in the 1 Hz data. Using the second parameter, *Permittivity Cutoff*, can eliminate measurements affected by this phenomenon.

- **Permittivity Cutoff**
    - Maximum permittivity for acceptable loss factor data
    - Below Permittivity Cutoff, loss factor is relatively undistorted by boundary layer effect
    - Above Permittivity Cutoff, loss factor begins to artificially decrease because of boundary layer effect
    - ε" is converted to ion viscosity only for ε" < Permittivity Cutoff

The Cole-Cole plot of Figure 18-7 shows the distortion in loss factor caused by boundary layers, and range of loss factor that can be converted to ion viscosity with a Permittivity Cutoff of 100,000.

Figure 18-7
Cole-Cole plot of Five Minute Epoxy cure data

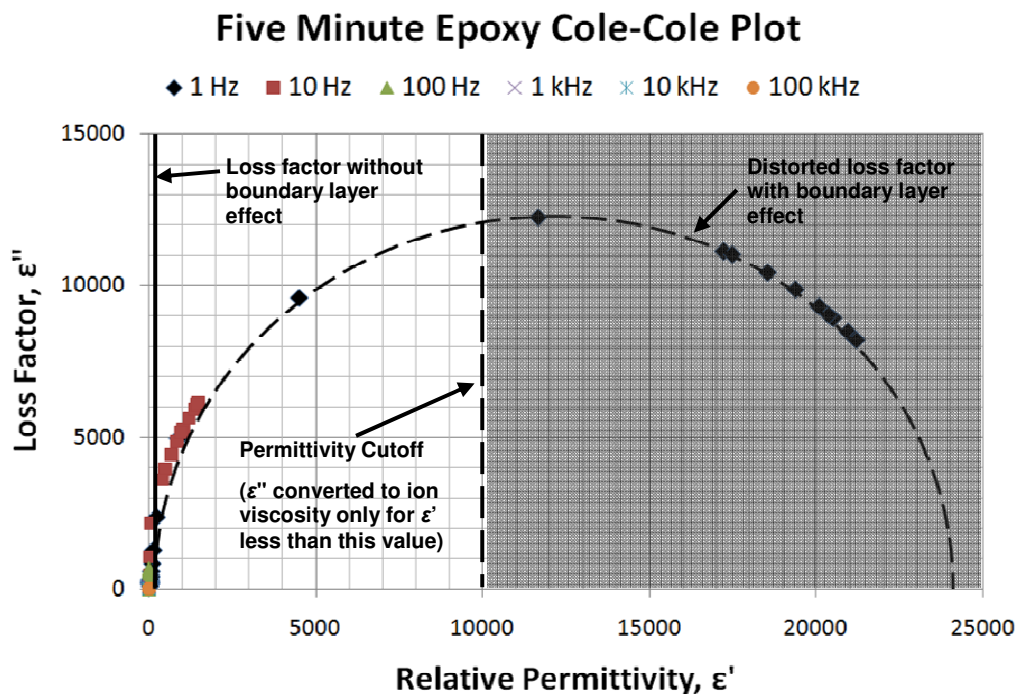Figure 18-8 shows the family of ion viscosity curves after using a reasonable Loss Factor Cutoff and Permittivity Cutoff. This plot now shows the progression of frequency independent resistivity and indicates the cure state of the material.
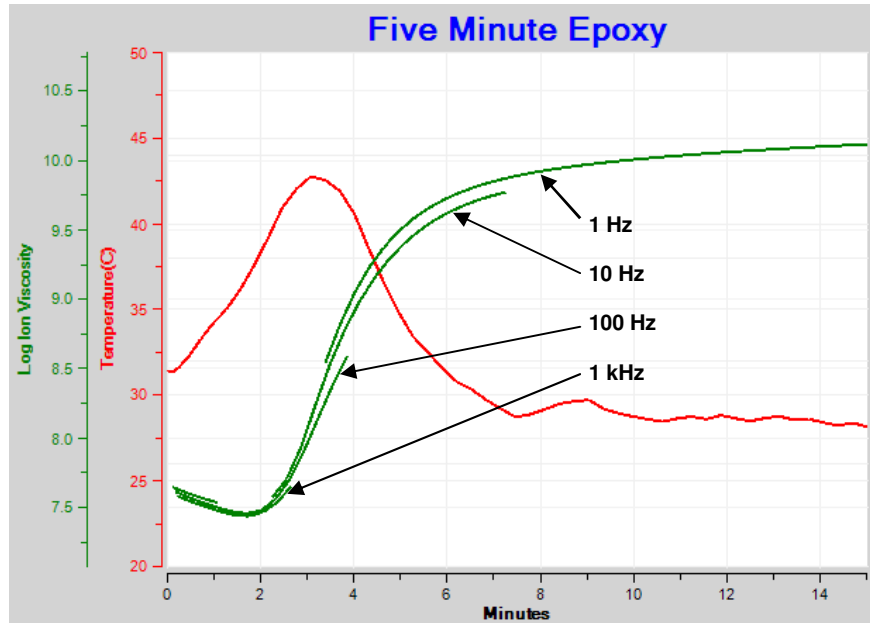

Figure 18-8
Ion viscosity with appropriate Loss Factor Cutoff and Permittivity Cutoff
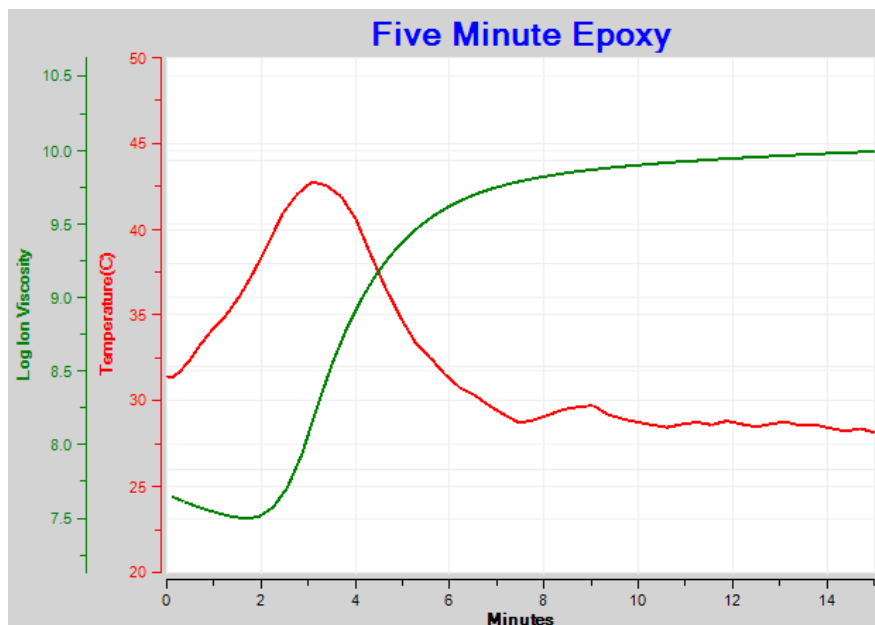

Figure 18-9
Ion viscosity for 10 Hz frequency only

To determine the time of maximum reaction rate or the time to end of cure, it is necessary to calculate the slope of log(ion viscosity), here simply called *slope* for brevity. Unfortunately, each of the multiple ion viscosity segments of Figure 18-8 would produce its own segment for slope. The result is a series of discontinuous and confusing slope curves. To avoid this problem, slope should be calculated using ion viscosity from a single low frequency, such as from the 10 Hz data of Figure 18-9. This simplification is possible because ion viscosity from a properly chosen frequency usually is very similar to the composite from multiple frequencies.

Figure 18-10 shows ion viscosity from 10 Hz data as well as the resulting single curve for slope. Now it is possible to clearly note the following events during cure:

- Critical Point 1—CP(1)—Onset of flow
    - Identified when ion viscosity passes a user defined level

- Critical Point 2—CP(2)—Viscosity minimum
    - Identified when ion viscosity reaches a minimum value

- Critical Point 3—CP(3)—Point of maximum reaction rate
    - Identified when slope reaches a maximum value

- Critical Point 4—CP(4)—End of cure
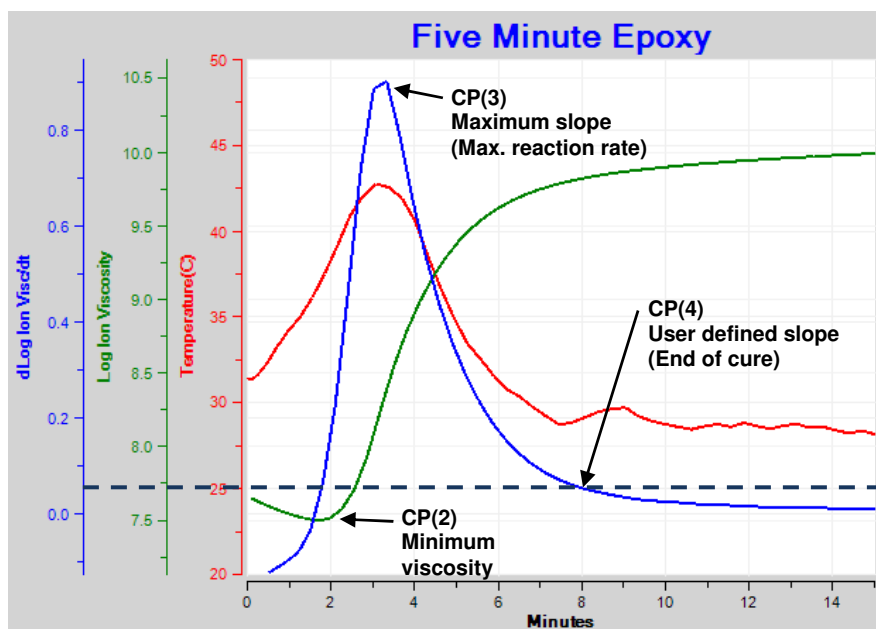   - Identified when slope reaches a user defined level

Figure 18-10
Ion viscosity and slope for 10 Hz frequency only

Electrode Polarization Correction

Electrode polarization occurs when the Material Under Test has a very high loss factor. Under this condition it is usually both highly fluid and highly conductive, and has an insulating boundary layer on the surface of the sensor electrodes. This boundary layer can distort permittivity and loss factor data as shown in the Cole-Cole plot of Figure 18-11 for the "Five Minute" epoxy data in this chapter. The arc of distorted data is a semi-circle with radius R. *Relaxed permittivity* ε'_r is relative permittivity toward the end of cure, or high frequency relative permittivity. *Maximum permittivity* ε'_{max} is the maximum value of relative permittivity when loss factor is zero as a result of boundary layers.
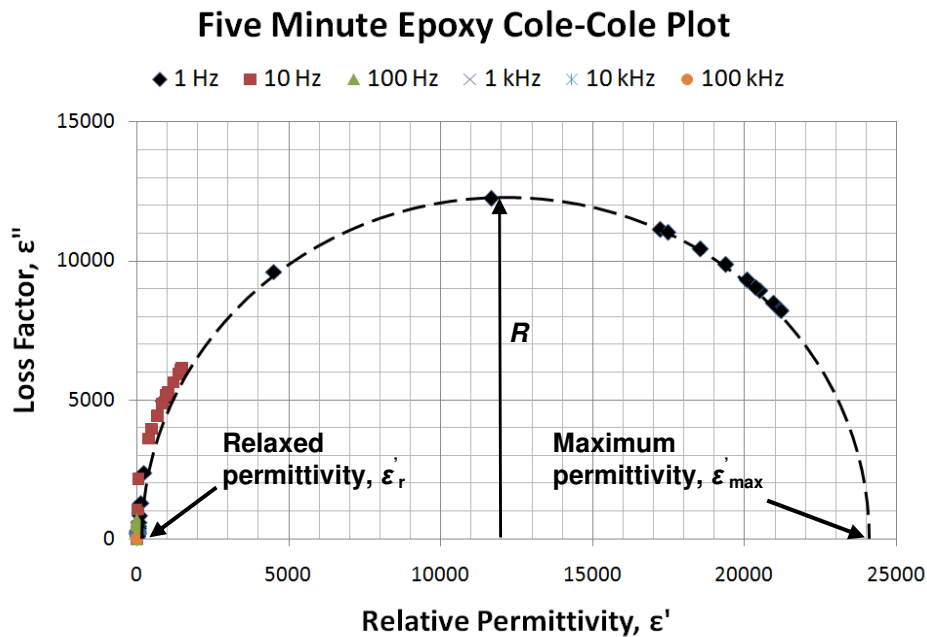
Figure 18-11
Cole-Cole plot of dielectric data distorted by electrode polarization

With a suitable choice of relaxed permittivity, it is possible to find an arc that fits the data and corrects the distortion caused by electrode polarization. This correction extends the measurement range for loss factor and resistivity, as shown in Figures 18-12 and 18-13. Refer to Chapters 16 and 17 for a complete treatment of the boundary layer effect and its correction.

Figure 18-12
Loss factor, showing distortion from boundary layer and correction of data

Figure 18-13
Resistivity, from loss factor data of Figure 18-12

Limitations of ion viscosity for measuring cure state

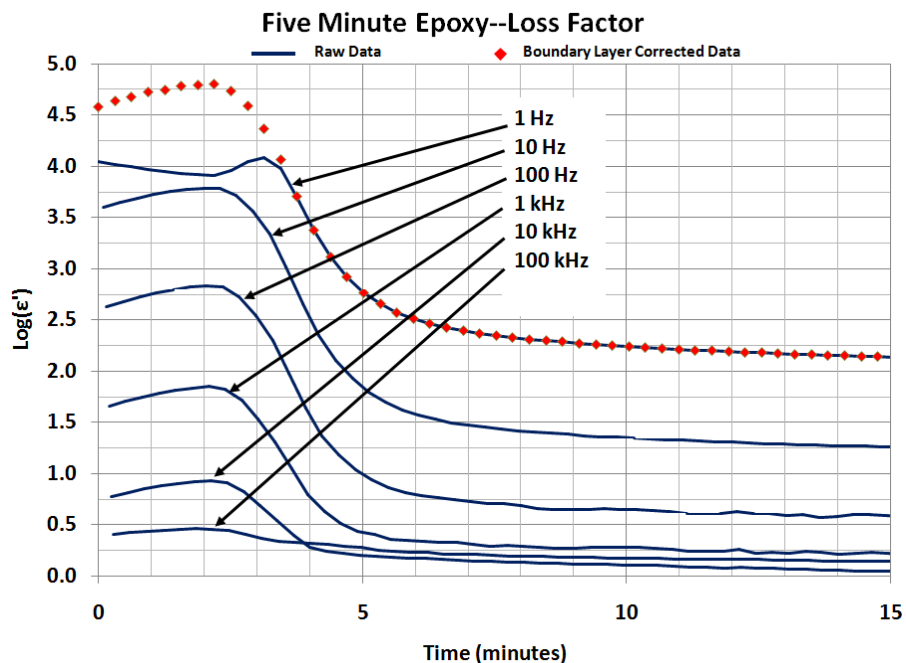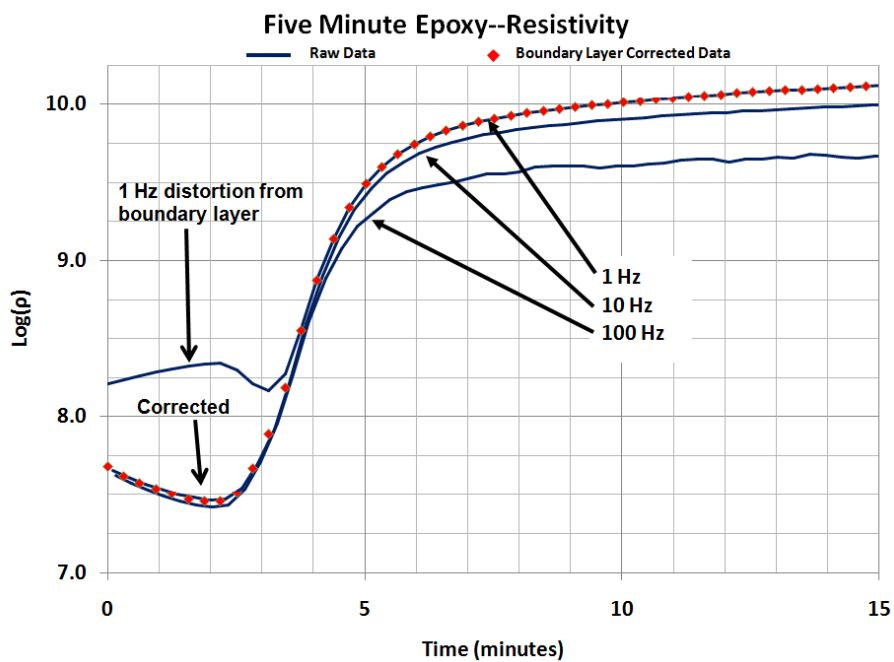To avoid misinterpreting dielectric measurements, it is important to understand the limitations of using ion viscosity. For the "Five-Minute" epoxy data at 1 Hz, frequency independent resistivity ρ_{DC} dominates dielectric response during the entire cure. As a result, ion viscosity (ρ_{DC}) is a valid measure of cure state throughout the test, indicating viscosity before gelation and modulus after gelation.

In situations when frequency independent resistivity does not dominate the entire cure, it is necessary to know when the influence of ρ_{DC} ends and the influence of dipolar relaxation begins. For example, Figure 18-14 shows data for the cure of a vinyl ester. Loss factor curves are inversely proportional to frequency—indicating frequency independent resistivity—only for early cure. At the end of cure, loss factor for all frequencies are very similar, a response caused by dipolar relaxation.
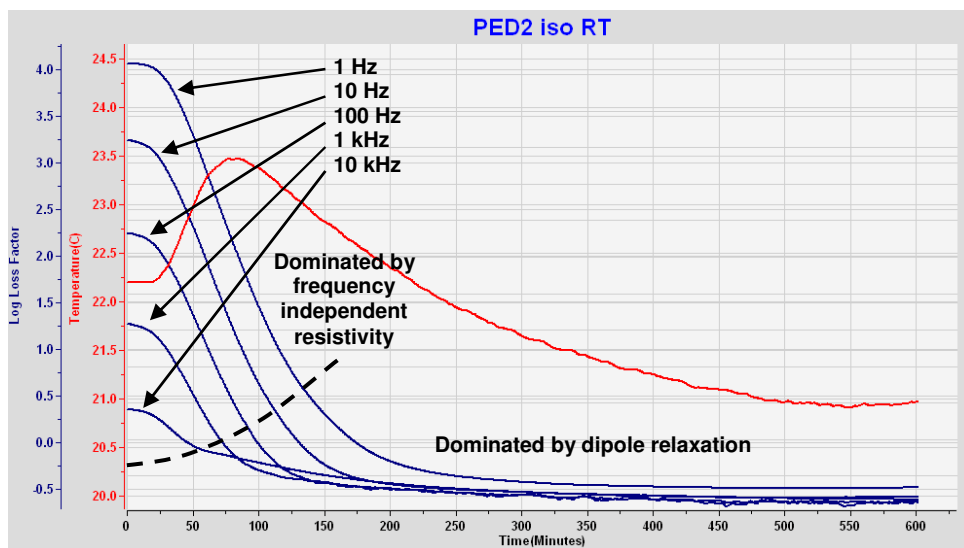
Figure 18-14
Loss factor for a vinyl ester cure

Figure 18-15 shows ion viscosity derived from the data of figure 18-14. For the frequencies used, resistivity curves overlap only for the first 125 minutes. After this time ion viscosity—that is, frequency *independent* resistivity—no longer applies and cannot be used to determine cure state. Cures near room temperature most often display this limitation. In contrast, because conductivity increases with temperature, cures at elevated temperatures are more likely to be dominated by frequency independent resistivity, and therefore ion viscosity, for the entire process.

Even when dipolar relaxation influences dielectric response, it is still possible to understand the progress of cure by observing loss factor. Loss factor is more useful in this case because the contributions of conductivity and dipole rotation are simply additive, and are easier to distinguish visually.

Figure 18-15
Ion viscosity and slope of ion viscosity for a vinyl ester cure

Summary

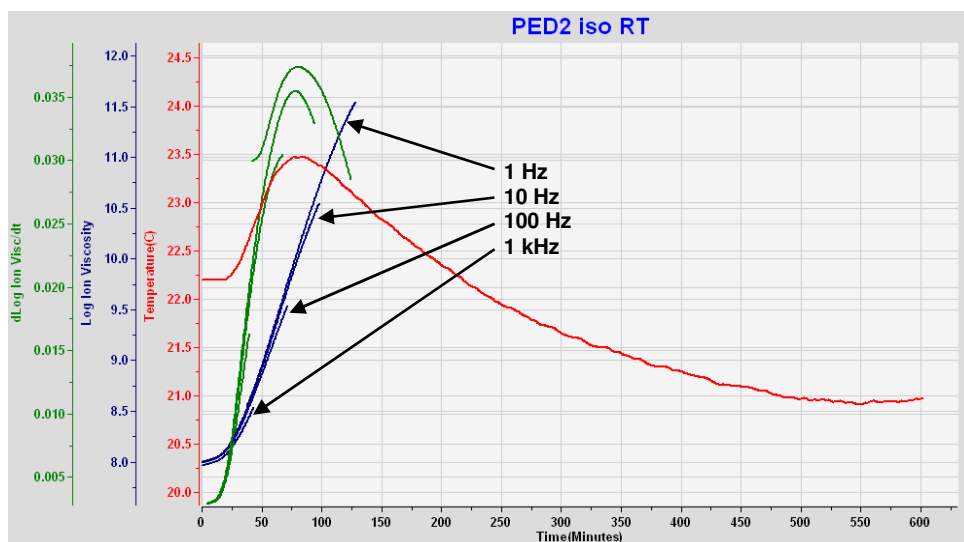Many factors can cause confusing interpretation of dielectric data. Selection of appropriate *Materials Properties* can guide data processing algorithms to remove artifacts caused by dipole relaxation or electrode polarization. The result, ideally, would be frequency independent resistivity, also known as *ion viscosity*, which correlates well with cure state. Table 18-1 summarizes the *Materials Properties* discussed in this chapter.

Table 18-1
***Material Properties* for converting loss factor to ion viscosity**

Material Property	Description
Loss Factor Cutoff	Allows conversion of data to ion viscosity for loss factors above the Loss Factor Cutoff
	Loss factors below Cutoff assumed to be dominated by AC conductivity
Permittivity Cutoff	Allows conversion data to ion viscosity when permittivity is below the Permittivity Cutoff
	Permittivities above Cutoff assumed to be distorted by electrode polarization
Relaxed Permittivity	Permittivity of material at end of cure or at high frequency
	Used for boundary layer correction
Maximum Permittivity	Maximum permittivity of material at zero loss factor due to electrode polarization
	Used for boundary layer correction
	May be determined mathematically from relaxed permittivity and distorted data

Chapter 19—Dielectric Cure Monitoring in Process Development and Manufacturing

Introduction

When working on a new thermoset, or a new formulation of a thermoset, the cure process is essentially unknown. When happens when the material is heated? When is the best time to apply pressure to squeeze out voids? How fast does the material react at different temperatures? Dielectric Analysis (DEA) complements more conventional thermal analysis techniques of differential scanning calorimetry (DSC) and dynamic mechanical analysis (DMA) to bridge the gap between laboratory and manufacturing environments.

Differential scanning calorimetry

Differential scanning calorimetry , one method for studying polymers, measures glass transition temperature T_g, which changes with cure state. For a particular epoxy, Figure 19-1 shows T_g measured with DSC and compared with results from dielectric cure monitoring. Each DSC data point requires curing the material to a chosen time, quenching the sample to stop cure and then performing the DSC analysis. This test must be repeated at multiple points during processing to obtain enough data to see the cure curve—a very tedious and repetitive task. In contrast, the cure curve from dielectric cure monitoring was obtained from a *single* test.
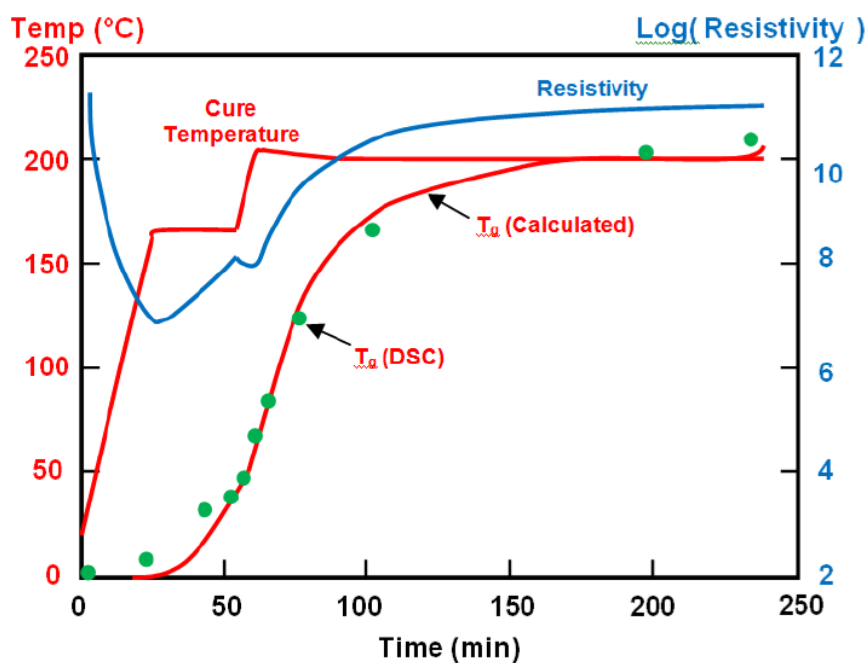

Figure 19-1
Data comparing DEA and DSC tests[1]

Glass transition temperatures from dielectric measurements come from a calculation that yields *Cure Index*, and in this case happen to overlay DSC data very well. Furthermore, the frequency independent resistivity—*ion viscosity*—provides information about viscosity and modulus, which DSC cannot do. Ion viscosity shows the time of minimum viscosity, the time of maximum reaction rate and the end of cure. All this information is available quickly and in real time, in contrast to the delay between process and test for DSC.

Even if DEA and DSC data do not superimpose as neatly as in Figure 19-1, a direct correspondence still exists between DEA and DSC measurements. One can use dielectric cure monitoring to very quickly evaluate the progress of cure under given conditions, change those conditions, observe the result and change conditions again as often as necessary. Sample preparation for DEA is very simple—apply material to a sensor and heat it. After using DEA for rapid iterations to reach a final formulation or process, *then* DSC can verify thermal-physical properties, saving time, effort and expense.

Dynamic mechanical analysis

Dynamic Mechanical Analysis is a second common technique for studying thermoset cure. Depending on the operating mode, DMA can measure certain moduli for either the early part of cure or the later part of cure. DMA is a direct measure of mechanical properties such as viscosity or modulus, but a single mode usually does not work for the entire cure. Furthermore, some DMA methods require careful sample preparation for consistent results.

Dielectric cure monitoring can supplement DMA because ion viscosity is often directly proportional to viscosity before gelation and to modulus after gelation. Note that DMA can detect gelation but DEA cannot. Gelation is a mechanical phenomenon due to the onset of crosslinking. Although a rapid increase in ion viscosity coincides with the increase in viscosity that accompanies crosslinking, no distinct electrical event at this time.

With proper frequency selection, DEA can measure electrical properties that directly relate to mechanical properties during the entire cure. In fact, the overlap between DEA and DMA data is generally recognized, and at least two major manufacturers of thermal analysis instruments offer combined DMA-DEA test cells. Simultaneous DMA-DEA tests extend the portion of cure during which mechanical properties can be measured or inferred.

Again, dielectric cure monitoring may be used to easily evaluate preliminary formulations or processes, allowing rapid iterations to achieve a desired result. At the end of development, DMA can then verify mechanical properties.

DEA in the process development cycle

DEA, DSC and DMA each measures different material properties. DEA does not replace either DSC or DMA, but instead compliments them. In R&D or process

development, DEA has the advantage of very simple sample preparation and the ability to make measurements during the entire cure in real time. Dielectric cure monitoring can accelerate R&D by deferring the need to make laborious DSC or DMA tests until near end of development.
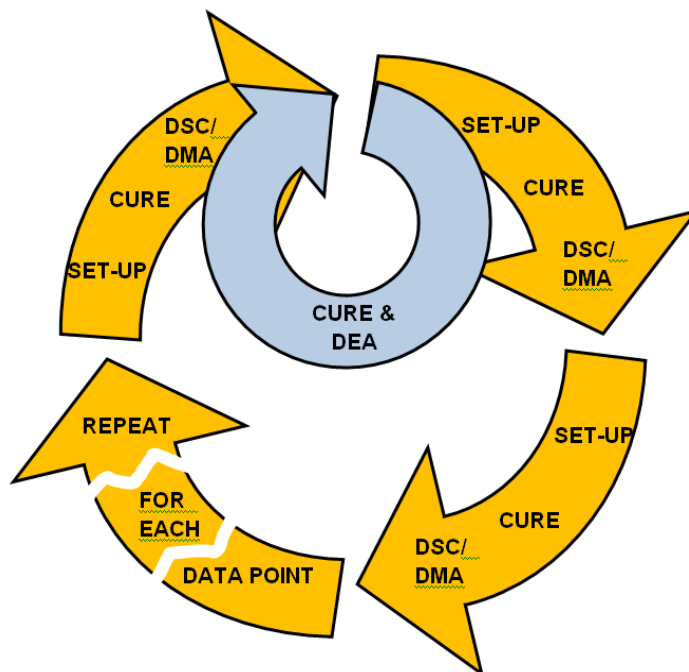

Figure 19-2
Dielectric Analysis (DEA) enables rapid feedback in the process development cycle

     Dielectric analysis or cure monitoring requires a sensor that is in good contact with the material under test. If the sensor is reusable, it is typically embedded in a platen or mold, which has the advantage of reducing long-term costs over many thousands of tests. If the sensor is disposable, the material is placed on the sensor and after the test everything is either stored for purposes of documentation or thrown away. After connecting the sensor to dielectric measurement instrumentation, software controls the measurement process—acquiring, storing and processing the data. If necessary, the material is compressed for good contact with the sensor and then heated to initiate cure.

     DEA has the advantage of allowing material tests in a wide variety of conditions, both in the laboratory, the QA/QC bench or the manufacturing floor. No other method has this versatility. Dielectric cure monitoring may be performed in an oven, on a hot plate, in a press or mold, in an autoclave or in an actual part being developed or manufactured. When embedded in a part or a large mass of material, the dielectric sensor can directly measure the effect of an exotherm on the rate of cure.

     In contrast, DMA is confined to a laboratory. If the sample is liquid, it must be tested in a special cell or impregnated in a matrix of some kind. If the sample is solid, it must be prepared with a specific geometric configuration. DSC is similarly limited to a laboratory, and the sample confined to a tiny DSC pan.

DEA in manufacturing

During the manufacture of composites, parts are typically cured using a fixed recipe for temperature and time. This process can be compared to baking a cake at 175 °C for 30 minutes—at the end of that time the cake might or might not be done. The baker must stick a toothpick into the cake to test it. If the cake is not done then it must stay in the oven and be tested again later. If testing the cake is not possible, the only choice is to bake it longer, maybe for 60 minutes—but then it might burn.

DEA is currently is most often used to confirm that parts are made consistently. For example, the nominal cure of an automobile body panel made of sheet molding compound (SMC) might look like Figure 19-3. By extracting and comparing Critical Points, the cure of every panel can be judged against this nominal curve. Results for each panel can be recorded for statistical quality control (SQC). Deviations beyond defined limits indicate that something in the curing process has drifted and information from the cure is available to correct the problem. Thus part quality is assured.
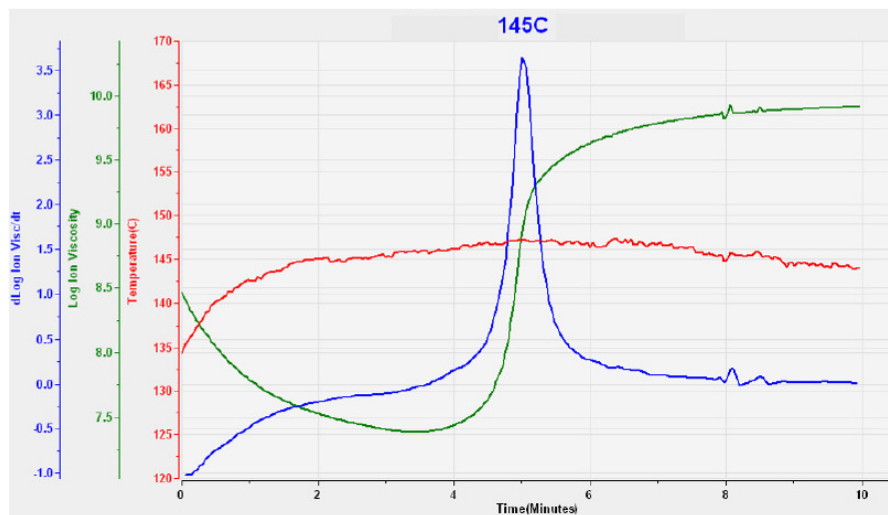

Figure 19-3
Typical sheet molding compound cure

Manufacturers of SMC products use timers to determine when to demold parts formed in their presses. This standard practice must allow for normal variation in process temperature and other factors that affect the rate of cure. To be conservative, demold time is chosen to guarantee that all parts reach a minimum cure state, with the result that some parts may be cured longer than necessary.

Some time ago the manufacturing engineer at one such company studied productivity when using dielectric measurements. In contrast to the timer that always opened the press at 70 seconds, dielectric cure monitoring equipment opened the press when each part reached a defined end of cure. As a result, DEA reduced average production cycle time by 10 seconds, an improvement that would have saved $70,000/year/press in labor costs alone.

For highly critical parts such as composite aircraft or spacecraft components, every step in manufacturing is documented, both to record that the part is made according to specification and for analysis in the event of failure. Many manufacturers measure temperature of the part as a very indirect and inaccurate way to infer the progress of cure. DEA, however, measures ion viscosity, which directly indicates cure state. So dielectric cure monitoring is valuable for documentation because no other technique can observe cure state in manufacturing and in real-time.

Productivity in manufacturing can benefit most immediately from dielectric cure monitoring, especially for high value components like wind turbine blades. These blades, often more than 50 meters long, are fabricated in a mold. The thickness of the blade, which affects the exotherm, and the rate of cure both vary along its length. Manufacturers use experience and guesswork to determine cure time before removing the blade from its mold. But removing a blade too soon can cause cracks because it is not stiff enough, and removing a blade later than necessary reduces throughput.

Dielectric sensors could be installed in the mold at strategic locations, or perhaps every five meters along its length, for example. Dielectric cure monitoring can determine when cure along the entire part has reached a desired point, and only at that time would the wind turbine blade be demolded. As a result, if a factory ships even as little as one or two more blades a week, profitability increases.

Related to productivity is the possibility of closed loop process control. Figure 19-4 shows how Critical Points vary with temperature for a particular sheet molding compound. As expected, the time to end of cure CP(4) decreases with increasing temperature, in this case a decrease of about 15% for a 10 °C increase in temperature.
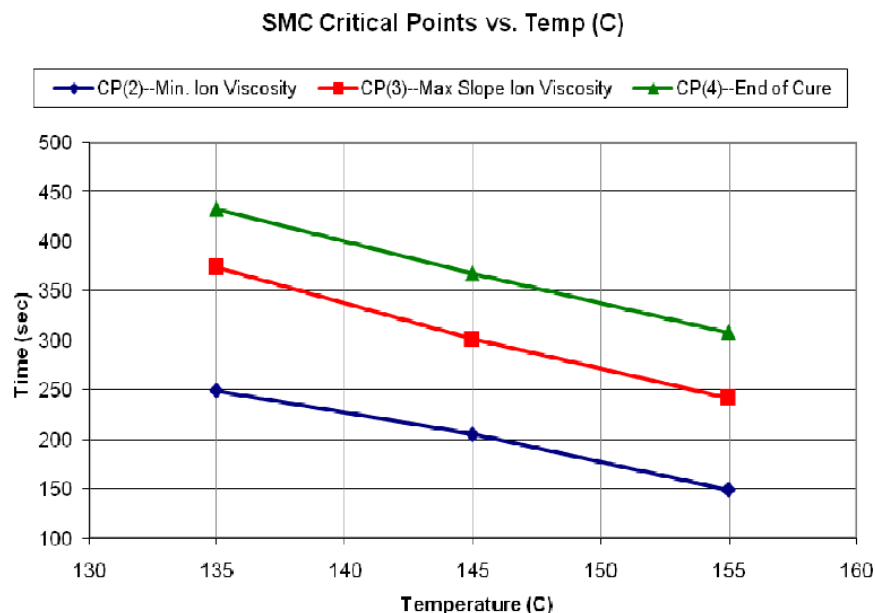

Figure 19-4
Variation of Critical Points with temperature

In large composite structures, such as a wind turbine blade, bridge beam or an aircraft fuselage, different locations cure at various rates because of differences in thickness and thermal environment. If sections of a large part have independent heaters, then dielectric measurements can provide feedback for a control system. This system can adjust temperatures so all sections cure at a uniform rate for optimum throughput.

Conclusion

Dielectric cure monitoring is a simple electrical measurement that requires minimal sample preparation or skill to perform. In addition, the same sensors and measurement techniques may be used in research, quality control and manufacturing environments. Dielectric analysis correlates with measurements from more conventional laboratory tests, such as differential scanning calorimetry or dynamic mechanical analysis. As a result, DEA can act as the "go between" that brings information from the research lab to the manufacturing floor, and from the manufacturing floor to the manager responsible for product quality.

References

1. Day, D.R., *Dielectric Properties of Polymeric Materials*, Micromet Instruments, (1988).
   (Figure has been redrawn for clarity)

Lambient Technologies
Sales and Service Offices

Western Hemisphere

United States:

Lambient Technologies LLC

649 Massachusetts Avenue

Cambridge, MA 02139

TEL: 857-242-3963

E-MAIL info@lambient.com

RT Instruments, Inc.
10 N. East Street, Suite 106 Woodland, CA 95776

 TEL (530) 666-6700
 FAX (530) 662-2875
  E-MAIL rtinstruments@sbcglobal.net

United Kingdom:

Nortest
Unit 3, Scrivens Yard
Castle Ashby
Northampton, U.K. NN7 1LF

TEL +44-1607-696270

E-MAIL techsales@nortest.co.uk

Europe:
(except U.K.)

Linseis Messgeräte GmbH
Vielitzerstrasse 43
D-95100 Selb, Germany

TEL +49-9287-880-0
FAX +49-9287-704-88
E-MAIL info@linseis.de

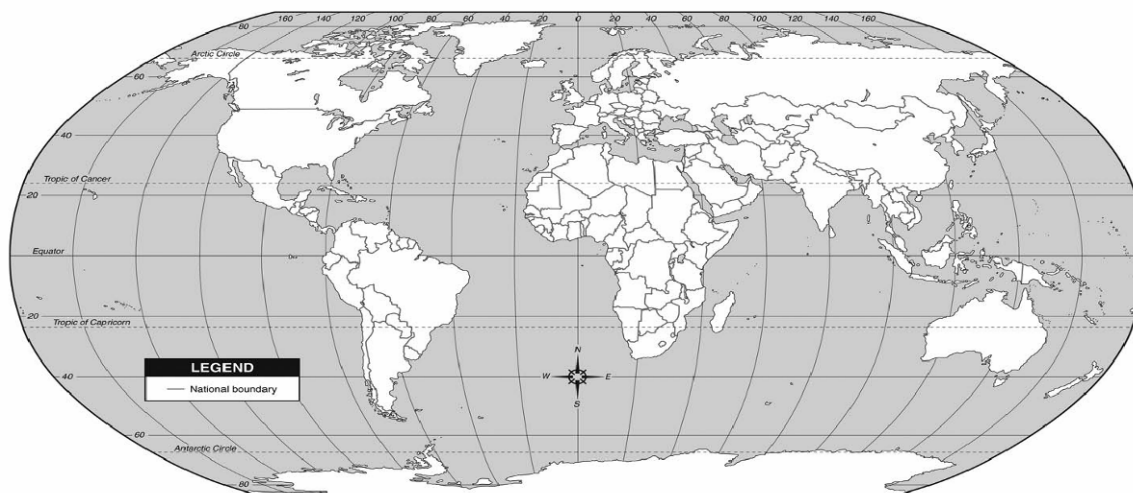
Fulltech Instruments S.r.l
Via del Fontanile Arenato, 200
00163 Roma, ITALY

TEL: +39.06.66152431
FAX: +39.06.6664325
Email: info@fulltech.it

Lambient Technologies
Sales and Service Offices

Eastern Hemisphere

Japan: **Syscom, Inc.**
Wada Bldg.
4-27-5 Ikebukuro
Toshima-ku
Tokyo 171-0014, Japan

TEL +81-3-6907-9105
FAX +81-3-6715-8740
E-MAIL morishita@syscom-inc.co.jp

Korea: **Yeonjin Corp.**
3rd Floor, Yeonjin B/D
32-141 4th Street
Dangsan-dong, Yeongdeungpo-gu
Seoul, 150-805, Korea

TEL +82-2-501-7990, +82-2-2675-0508
FAX +82-2-2675-0567
E-MAIL info@yeonjin.com

Taiwan : **Tien Shiang Trade & Engineering Co., Ltd.**
Room 807, 50 Lin Seng N.Rd.
Taipei, Taiwan, R.O.C.
NN7 1LF

TEL +886-2-25637871/2
FAX +886-2-25115760

EMAIL: tinshing@ms16.hinet.net

China: **Beijing Saisimeing Instruments, Inc.**
Rm A1805, Century Trade Bldg.
No. 72 North XiSanHuan Road
HaiDian District
Beijing 100037, China

TEL +86-10-5179-9159
FAX +86-10-5179-9160
E-MAIL zhang@Saisimeing.com.cn

New Zealand &
Australia: **Poly-Instruments Pty. Ltd.**
P.O. Box 519
South Melborne
Victoria 3205, Australia

TEL +61 (0) 3 95555020

E-MAIL sales@poly-instruments.com